isvr Institute of Sound and Vibration Research

Theory Manual For WANDS 2.1
Wave-Number-Domain FE-BE Software For Structures And Fluids

C-M. Nilsson and C.J.C Jones

ISVR Technical Memorandum No 975

August 2007

University of Southampton

SCIENTIFIC PUBLICATIONS BY THE ISVR

Technical Reports are published to promote timely dissemination of research results by ISVR personnel. This medium permits more detailed presentation than is usually acceptable for scientific journals. Responsibility for both the content and any opinions expressed rests entirely with the author(s).

Technical Memoranda are produced to enable the early or preliminary release of information by ISVR personnel where such release is deemed to the appropriate. Information contained in these memoranda may be incomplete, or form part of a continuing programme; this should be borne in mind when using or quoting from these documents.

Contract Reports are produced to record the results of scientific work carried out for sponsors, under contract. The ISVR treats these reports as confidential to sponsors and does not make them available for general circulation. Individual sponsors may, however, authorize subsequent release of the material.

UNIVERSITY OF SOUTHAMPTON

INSTITUTE OF SOUND AND VIBRATION RESEARCH

DYNAMICS GROUP

Theory Manual for WANDS 2.1 Wave-Number-Domain FE-BE Software for Structures and Fluids

by

C-M. Nilsson and C.J.C Jones

ISVR Technical Memorandum No: 975

August 2007

Authorised for issue by
Professor M.J. Brennan
Group Chairman

THEORY MANUAL FOR
WANDS 2.1
WAVE-NUMBER-DOMAIN FE-BE SOFTWARE FOR
STRUCTURES AND FLUIDS

Carl-Magnus Nilsson and Chris Jones

This page intentionally left blank

Contents

This page intentionally left blank

Chapter 1

Structure of the report

This report constitutes the theory manual of the WANDS software in the most current version. Since the software is bound to change over time, this report is also updated from time to time. For this reason, the chapters are separately dated. Each time a chapter is updated a new version of the contents list in chapter 1, *Introduction* is made. Terms with specific meaning for the context of WANDS are indicated by being printed in italics. A separate user manual for WANDS is also produced as an ISVR TM.

The first chapter of this report considers the way boundary conditions and (closely related) coupling conditions in FE and BE models are implemented.

The second chapter explains how the different coupling models are implemented in WANDS.

The third chapter briefly summarizes some of the most important subroutines in WANDS.

The following chapters details the theory for the different methods. This includes the theory of plate strip waveguide finite elements, solid waveguide finite elements and boundary elements. These chapters also give a few validation examples for the separate methods.

Chapter 2

Introduction

This report considers numerical methods for systems with uniform geometry and properties along one axis, as they are implemented in WANDS (WAve Number Domain Software). WANDS, as the name suggest, uses a fourier transform along the axis with uniform properties to describe this dependence in the wavenumber domain. The dependence with respect to the cross-sectional geometry is described with Finite Elements (FE) and/or Boundary Elements (BE). The FE models in the current version of WANDS describe structural models of plates, solids and beams, whereas the BE models describe fluids. Each type of FE or BE domain is termed a "*sub-model*". In addition, the coupling conditions implemented to join the different FE or BE models are also referred to as *sub-models* or *coupling sub-models.* Currently there is only one solution method implemented in WANDS. However, the output from WANDS gives *sub-model* matrices that can be loaded into numerical program packages such as MATLAB where other solution methods can be implemented.

WANDS is programmed with the intention that more domains and solution methods should be easily implemented in future versions. For instance this could be Biot equations for porous media and coupling between fluid FE and fluid BE models. In addition, there are several different solution methods that may be implemented. Some of these can be found in the introduction to reference [1], although that summary does not consider the implementation of BE models.

The possibility to add more *sub-models* and solution methods to WANDS means that a thorough understanding of both the theory and the structure of WANDS is needed for anyone who wants to expand the software. This report is primarily written for that person. Hence, this report can be considered largely as a *theory manual* for WANDS. Also for users of WANDS in its current version, a thorough understanding of the theory is very useful. As an example inspections of the system matrix, and the blockmatrices in it, is a very good way to find any errors in the input data file as well as in the WANDS code itself.

To handle a large number of sub-models in a consistent way, the coupling between the *sub-models* must also be handled in a consistent way. Here, each coupling between two different *sub-models* is seen as another type of *sub-model* in its own right. With the currently implemented coupling conditions there are therefore currently 17 different sub-models,(when beams are included), although some of the coupling sub-models are theoretically very simple. In addition beams may be coupled to either plate or solid FE submodels, these beam models are sometimes referred to as submodels of their own. Although, from a programming point of view, they are incorporated into the respective FE model.

2.1 Background

Propagation of mechanical waves in complex shaped systems are difficult to analyse in a single consistent way. The underlying problem is that the wavelengths get shorter as the frequencies increase.

At low frequencies the wavelengths are much longer than the length of any geometrical dimension or irregularity in the system, and simple analytical wave-propagation models can be used to give highly accurate solutions.

For problems at slightly higher frequencies the dimensions of the irregularities are of the same magnitude as the wavelength. For such problems numerical methods such as the conventional Finite Element method or the conventional Boundary Element method give reasonable computation times and can be used successfully.

At high frequencies the wavelength become much shorter than the geometrical dimensions and *high-frequency* methods considering reflecting waves (ray-tracing) or energy methods such as Statistical Energy Analysis (SEA) can be used,. Although there is still work to be done for improving these methods, they generally provide small equation systems and hence fast calculations.

Methods appropriate to the *mid-frequencies* have proved harder to find. This is largely because the low frequency methods become very costly in terms of the computations needed, whereas the high frequency models are too crude since they do not represent a good physical representation of the problem. Increasingly progress is being made for solving mid frequency problems. New numerical approaches based on using waves to approximate the field are applied and computing power is increased.

The above categorization of low, mid and high frequency methods is well understood and research effort is applied accordingly. However, an extra concern arises from the fact that many analyses to be tackled are of systems with very different dimensions along different axes. The dimensions then fall into different frequency range categories. For such systems it can be advantageous to employ special methods for solving for the wave propagation problem presented by the large dimensions while retaining the detailed numerical solution in the other domains. The main driver for developing such methods is that the computational effort required when applying conventional methods in all three dimensions would be to costly. However, at least for the methods considered here, the physical insight of the solutions that can be gained by treating problems in terms of wave-propagation is also attractive.

In the current work numerical methods for problems which have uniform properties along one axis are treated. Although these methods differ slightly, they all consider wave-propagation along the axis of uniform properties. Thus they are here termed *wave-domain methods*. There are numerous examples of systems for which these methods are advantageous, i.e. aluminium extrusions, pipes and ducts.

One large field is railway related applications, such as rails, extruded aluminium panels, tunnels, noise barriers and several bridges. Detection of cracks in rails, for which lowly damped *high-order* waves are used, is one application currently (2007) investigated. Noise from embedded rails is another application where *wave-domain methods* have been applied, since unlike conventional rails, 2D methods are not suitable, see [2]. Long extruded aluminium panels are common in the design of railway cars, and although they have advantages for crashworthiness and weight, they are poor sound insulators, see [3]. Analyses of ground vibration from tunnels are very costly in terms of the computer power needed and full scale models are obviously not possible, [4]. Yet another ongoing railway related research activity is railway bridges.

The need for the wave-approach in railway applications is the reason for deriving the WANDS software, although there are of course numerous other applications.

2.2 Current list of sub-models

The following *sub-models* are currently included in WANDS.

- Plate FE models (FEP models)
- Beams coupled to FEP models
- Solid FE models (FES models)
- Beams coupled to FES models
- Coupling between plate FE and solid FE models (FEP-FES models)
- Fluid FE models (FEF models)
- Coupling between plate FE and fluid FE (FEP-FEF models)
- Coupling between solid FE and fluid FE (FES-FEF models)
- Fluid BE models (BEF models)
- Coupling between fluid boundary element models (BEF-BEF models)
- Coupling between plate FE and fluid BE models (FEP-BEF models)
- Coupling between solid FE and fluid BE models (FES-BEF models)
- Solid BE models (BES models)
- Coupling between solid boundary element models (BES-BES models)
- Coupling between plate FE and fluid BE models (FEP-BES models)

- Coupling between solid FE and fluid BE models (FES-BEF models)
- Coupling between solid BE and fluid BE models (BES-BEF models)

The abbreviations above refer to names that are used internally in WANDS. As is seen in Chapter 14, this structuring into different models is somewhat arbitrary, since it does not always directly represent the mathematical representation of the problem. The beam models may thus be seen as optional features for the plate and solid FE models respectively. Hence beam models can not exist alone in WANDS and they do not need any special coupling models associated with them.

Also, the fluid BE formulation give rise to both a relation between the pressure and velocity due to the geometry of the fluid domain and a set of equations for the prescribed boundary conditions. Hence the fluid BE models might be seen as consisting of two separate models. Nevertheless the list given above gives an idea of how submodels are used both in this manual and as the interface to the user of WANDS.

Chapter 3

General description of boundary and coupling conditions in FE and BE models

3.1 Introduction

In WANDS several different finite element (FE) and boundary element (BE) models are coupled together. The models to be coupled as well as the coupling conditions it self are each called a ”sub-model”. If all existing FE/BE and coupling sub-model types are counted there are no less than 17 different sub-model types that must be handled. In future versions the number of sub-models may become even greater as more sub-model types are added to WANDS. In addition to this there are several matrices for each sub-model and an arbitrary number of different sub-models of the same type.

In this report FE models that consist of either plate or solid finite elements are considered. In addition beam finite elements may be connected to either of these model types. The beam equations just adds extra stiffnesses and masses to the plate and solid FE models. Thus, the stiffnesses and masses of the beam equations are simply added into the corresponding matrices of the plate and solid FE models respectively.

However, for other sub-model types the implementation is more complicated. There is a need to group these sub-model types and treat them in a generalized way in order to make their implementation more straightforward. Here the approach used in WANDS is described.

The first section in this chapter introduces the theory implemented in the derivation of the sub-models. The theory described here is given with very few details since the aim is to give an easy-to-follow overview. The theoretical details for each sub-model type are detailed throughout this report.

The second section of this chapter concentrates on how the sub-models are assembled in WANDS. This section is important to understand how WANDS can be amended with more sub-model types and/or solution methods.

3.2 Theory

In the this section, the theories for implementation of boundary conditions in FE and BE models are briefly outlined. The derivation of the BE models is based on ideas from the derivation of BE models for fluid equations. These ideas should however be applicable to other domain types with small alterations. Since the theory of coupling between different models is closely related to boundary conditions, the coupling models are treated simultaneously.

A most practical way to derive the coupling between different types of models is to use the same starting point for all models. Throughout this manual Hamilton's principle is used as this starting point. For linear systems and harmonic motion this principle may be stated as,

$$\delta(U-T)-\delta W=0 \tag{3.1}$$

Here, δ should be interpreted as, "the first variation of". U is the potential energy in the system, which for the systems here is the same as the strain energy, T is the kinetic energy and W is the virtual work on the system which includes both external forces as well as internal forces that give rise to losses in the system.

In addition to equation (3.1), *essential* or *Dirichlet* boundary conditions must also be fulfilled. For structures these boundary conditions impose constraints on the displacements. A second set of boundary conditions referred to as *natural* or *Neuman* boundary conditions are implicitly included in equation (3.1). For structures such boundary conditions prescribes the relationship between displacements and forces on the boundary.

By using expressions for the potential energy kinetic energy and the virtual work in equation (3.1) it can be taken one step further. The resulting expression is referred to as the *weak form* of the equation of motion. Here, this is a bilinear functional describing the system.

FE-model boundary conditions and coupling

In WANDS the FE model is derived by an approximation the *weak form* of the equation of motion for the domain. With this formulation the *natural* (or *Neuman*) boundary conditions never explicitly enter the equations.

However, *essential* (*Dirichlet*) boundary conditions must also be fulfilled. For a structural model these boundary conditions give constraints for the displacements. These constraints generally also exert forces onto the domain which must considered in addition to the essential boundary conditions. The coupling between plate and solid FE models is treated as a special case of such constraints.

BE-model boundary conditions

As the name suggest, a BE model is an approximation of an equation on the boundary. At least for fluids,this boundary equation can be derived from equation (3.1) by Greens formula, which can be seen as a 2 or 3D equivalence to integration by parts. Applying Greens formula splits an integral over a 2D domain into two new integrals. One is still over the 2D (or 3D) domain but the other is a line (or 2D) integral over the boundary.

The virtual work made on the boundary from external forces is added to the second integral. This then describes the natural (or *Neuman*) boundary condition. Thus, it prescribes relations between forces and displacements, (or pressures and particle velocities for fluids).

The integrand in the first integral contains the left hand side of the homogeneous wave equation for the domain.

In the BE formulation the first integral is satisfied exactly whereas the the solution appearing from the second integral is approximated with piecewise polynomials. Since the virtual work on the boundary is included in this integral there are no additional terms from external forces appearing in the boundary element formulation.

The essential (*Dirichlet*) boundary conditions on the boundary must also be fulfilled. This gives a second set of equations. To enable more general cases the essential boundary conditions can be replaced with *impedance* (or *Robin*) boundary conditions.

For coupling between two fluid BE models the essential boundary condition is simply that the displacements and pressures along the shared boundary must be the same in both models.

FE-BE coupling conditions

Subsequently couplings between FE and BE models are considered. These couplings are closely related to how boundary conditions in the respective models are treated. The equality of displacements on the boundary can be treated by stating their equality as extra equations in the system. As stated before, the Neuman boundary conditions are not needed in the BE formulation, whereas they are included as extra forces in the FE model. Thus equations that project pressures from the boundary of a fluid BE model onto the boundary of a solid FE model must be added.

3.2.1 FE model and boundary conditions

The equations of motion for a system may be derived from Hamilton's principle. For harmonic motion the variational or weak form of these equations may be written,

$$\int_\Omega L_1(\delta u, u)\mathrm{d}\Omega - \int_\Omega \delta u f \mathrm{d}\Omega = 0\,. \tag{3.2}$$

where L_1 is a bilinear functional of δu and u derived from expressions of the potential and kinetic energies. The second integral in equation (3.2) describes the virtual work on the model.

Examples of this equation can be found in Chapter 5, 4 and 8. In addition there are also essential boundary conditions associated with the model. These yield constraints on the boundary which may be written as,

$$L_2(u) = 0 \quad \text{on the boundary}\,\Gamma\,. \tag{3.3}$$

where $L_2(u)$ is a linear combination of the displacements u on the boundary. The Finite Element model derived for WANDS approximates equation (3.2) with piecewise polynomials in each element. This procedure is detailed in Chapter 5, 4 and 8. The result may be written as,

$$\mathbf{Du} = \mathbf{f}\,, \tag{3.4}$$

where, $\mathbf{D}$ is a dynamic stiffness matrix. $\mathbf{u}$ is a complex valued vector containing the displacements at the nodes of the FE-mesh and $\mathbf{f}$ is the corresponding vector describing the external forces. For the solution method implemented in WANDS, $\mathbf{D} = \mathbf{D}(\kappa, \omega)$ where κ is the wavenumber along the waveguide and ω is the frequency.

For the simple cases of a restrained boundary node n, such that,

$$u_n = 0 \tag{3.5}$$

the implementation of equation (3.3) is simplified by taking out the n:th row and the n:th column of $\mathbf{D}$ in equation (3.4). The reasons for this simple approach can be found in reference [5](Ch. 2.10). As for most FE softwares, WAFER and WANDS uses this approach for simple restrained degrees of freedom.

However this simple approach is not valid for all constraints. For a more general case, equation (3.3) is approximated at the nodes by,

$$\mathbf{Cu} - \mathbf{q} = \mathbf{0} \tag{3.6}$$

where, $\mathbf{q}$ is a set of imposed displacements and $\mathbf{C}$ is a matrix projecting the sought solution vector $\mathbf{u}$ onto $\mathbf{q}$.

These constraints generally introduce forces acting on the constrained degrees of freedom. These forces keep the structure together so that the prescribed constraints are fulfilled. They can be included into equation (3.2) as a term in the virtual work.

The forces due to the displacements in equation (3.6) can be shown to be,

$$\mathbf{f_c} = -\mathbf{C}^{\mathrm{T}}\mathbf{u} \tag{3.7}$$

Hence, by including this virtual work, equation (3.4) becomes,

$$\mathbf{D}\mathbf{u} + \mathbf{C}^{\mathrm{T}}\mathbf{f_c} = \mathbf{f} \tag{3.8}$$

In addition equation (3.6) must be included into the system. The system thus becomes,

$$\begin{bmatrix} \mathbf{D} & \mathbf{C}^{\mathrm{T}} \\ \mathbf{C} & \mathbf{0} \end{bmatrix} \begin{bmatrix} \mathbf{u} \\ -\mathbf{f}_c \end{bmatrix} = \begin{bmatrix} \mathbf{f} \\ \mathbf{q} \end{bmatrix} \tag{3.9}$$

A more mathematical approach to derive the same equation is to multiply equation (3.6) with Lagrange multipliers $\boldsymbol{\lambda}$ and add them to the energy that is to be minimized in be the FE formulation, see [5] (chapter 9.2) or Chapter 7 here. This yields,

$$\frac{1}{2}\mathbf{u}^{\mathrm{T}}\mathbf{D}\mathbf{u} - \mathbf{u}^{\mathrm{T}} + \boldsymbol{\lambda}^{\mathrm{T}}(\mathbf{C}\mathbf{u} - \mathbf{q}) = \mathbf{0} \tag{3.10}$$

After partial derivatives, first with respect to $\mathbf{u}$ and subsequently with respect to $\boldsymbol{\lambda}$, equation (3.9) is obtained with $\boldsymbol{\lambda} = -\mathbf{f_c}$.

In WANDS this method to implement constraints is used when solid and plate FE models are to be coupled. Then we have,

$$\mathbf{D} = \begin{bmatrix} \mathbf{D}_{plate} & \mathbf{0} \\ \mathbf{0} & \mathbf{D}_{solid} \end{bmatrix} \qquad \mathbf{C}^{\mathrm{T}} = \begin{bmatrix} \mathbf{C}^{\mathrm{T}}_{\mathbf{sp1}} \\ \mathbf{C}^{\mathrm{T}}_{\mathbf{sp2}} \end{bmatrix} \text{ and } \mathbf{q} = \mathbf{0} \tag{3.11}$$

and the coupled plate-FE to solid-FE system is written,

$$\begin{bmatrix} \mathbf{D}_{plate} & \mathbf{0} & \mathbf{C}_{sp1}{}^{\mathrm{T}} \\ \mathbf{0} & \mathbf{D}_{solid} & \mathbf{C}_{sp2}{}^{\mathrm{T}} \\ \mathbf{C}_{sp1} & \mathbf{C}_{sp2} & \mathbf{0} \end{bmatrix} \begin{bmatrix} \mathbf{u}_{plate} \\ \mathbf{u}_{solid} \\ -\mathbf{f}_c \end{bmatrix} = \begin{bmatrix} \mathbf{f}_{plate} \\ \mathbf{f}_{solid} \\ \mathbf{0} \end{bmatrix} \tag{3.12}$$

It is worth mentioning that there are other methods to implement constraints in FE models, as discussed in Chapter 7 and reference [5] (Chapter 9).

3.2.2 BE model and boundary conditions

For a Boundary Element (BE) model the starting point is once again equations (3.2) and (3.3). There is however an important difference in that the boundary element method only takes account of forces on the boundary, so that the second integral in equation (3.2) now is taken over the boundary Γ instead of the whole domain Ω. Integration by parts (or for 2- and 3-D cases applying Greens formula) on equation (3.2) yields,

$$\int_{\Omega} u L_3(\delta u) \mathrm{d}\Omega - \int_{\Gamma} L_4(\delta u, u, f) \mathrm{d}\Gamma = 0 \tag{3.13}$$

Before considering how this equation can be approximated with a BE model, it is useful to discuss it first. By comparing equations (3.2) and (3.13) it can be noted that L_4 includes a term coming from the integration by parts and also the virtual work on the boundary. Also, since the two integrals are over different domains (e.g. a fluid volume and its boundary) the sought solution is one that results from both integrals being zero.

For a non-trivial solution we require that the first integral is fulfilled for any u, hence,

$$L_3(\delta u) = 0 \, \text{in all of} \, \Omega \tag{3.14}$$

Equation (3.14) is the known as the *strong form* of the waveequation and it is the most commonly known form of the differential equation equation, e.g. for a rod equation with constant cross-section (3.14) is written as,

$$\frac{\partial^2 \delta v}{\partial x^2} - \frac{\omega^2}{c_L^2}\delta v = 0\,, \tag{3.15}$$

where c_L is the longitudinal wave–speed along the rods $x-$ coordinate and δv is the *virtual displacement* along the rod. Equations (3.14) and (3.15) are homogeneous since no forces acting inside of the domain Ω are permissible here.

If the second integral in equation (3.13) is set to zero the resulting equation is referred to as the *boundary integral equation.* Thus,

$$\int_\Gamma L_4(\delta u, u, f)\mathrm{d}\Gamma = 0 \tag{3.16}$$

For a fluid in a 2D region, the boundary integral equation takes the form,

$$\int_\Gamma \Psi\frac{\partial \delta\Psi^*}{\partial \mathbf{n}} - \delta\Psi^*\frac{\partial \Psi}{\partial \mathbf{n}}\mathrm{d}\Gamma = 0 \tag{3.17}$$

where, Ψ is the velocity potential, $\mathbf{n}$ is the unit normal out of the fluid domain. See 10.

Equations (3.16) and (3.17) are variational forms of the *Neuman* or *natural* boundary conditions. These type of boundary conditions relates derivatives of u to forces on the boundary and as already mentioned L_4 includes external forces on the boundary.

Hence, equation (3.13) is fulfilled if both of equations (3.14) and (3.16) are fulfilled. These two equations are normally the starting point for the derivation of the direct BE method implemented in WANDS (see e.g. [6])

BE formulation

In the BE formulation a number of solutions $u = G$ (*Green functions*) of equation (3.14) corresponding to sources at the node points on the boundary are used to span the solution of the system. The Greens function for each source point yields one equation in the equation system. The solutions on the boundary for δu are then approximated with piecewise polynomials known as *boundary elements.* These polynomials approximate both the primary variable, δu, and its derivative(s).

To make the system complete the essential boundary conditions $L_2(u) = 0$ from equation (3.3) must also be included, these may either be Dirichlet boundary conditions or Robin boundary conditions. The first of these merely states the displacements on the boundary, whereas the second type gives a local impedance, relating the displacement to the forces on the surface at each node.

In some BE models the essential boundary conditions are used to eliminate either δu or $\frac{\partial \delta u}{\partial n}$ before the system matrix equation is assembled, thus making the size of the system N x N rather than 2N x 2N (where, for a fluid, N is the number of nodes). Since the essential boundary conditions may consist of coupling to other models, this approach has not been used in WANDS.

So far in this section the description has been applicable to either fluid or solid elastic boundary elements. The following applies specifically to fluid BE models as detailed in Chapter 10

For an uncoupled fluid boundary element model we have,

$$\begin{bmatrix} \mu\mathbf{H} & -\mu\mathbf{G} \\ \mathbf{C}_b & -i\omega\rho\mathbf{C}_a \end{bmatrix} \begin{bmatrix} \frac{\partial \mathbf{\Psi}}{\partial n} \\ \mathbf{\Psi} \end{bmatrix} = \begin{bmatrix} \frac{\mathbf{p}_{in}}{i\omega\rho} \\ \mathbf{c}_c \end{bmatrix} \tag{3.18}$$

Here, $\mathbf{\Psi}$ is a velocity potential and the first row represents the BE approximation with possible incoming waves $\mathbf{p}_{in}$ on the right hand side. Further details of this system are explained in Chapter 10.

It is worth noting that there is a fundamental difference between the pressure $\mathbf{p}_{in}$ in equation (3.18) and the forces $\mathbf{f}$ introduced in equation (3.4). In equation (3.4) the forces are the total forces on the boundary, i.e. the forces corresponding to those that might be measured with suitable force transducer on a real system. Contrary, the $\mathbf{p}_{in}$ vector represents the pressure from incoming waves only, i.e. if these are impinging on a flat hard surface the true pressure on the surface (as hypothetically measured) would be $2\,\mathbf{p}_{in}$.

The second row in equation (3.18) represents the essential boundary conditions. Since these are local for each node, the matrices $\mathbf{C}_a$ and $\mathbf{C}_b$ each only have at most one entry on each row. A moving boundary may be represented by the vector $\mathbf{c}_c$.

WANDS does not require a specific number of boundary conditions, so the size of $\mathbf{C}_a$ and $\mathbf{C}_b$ is only determined by the number of boundary conditions specified by the user. This is because other boundary conditions may be added by the couplings to other models.

The coupling between two adjacent domains is treated similarly to the boundary conditions. Consider two adjacent fluid domains with all nodes shared between them. The $\mathbf{H}$ and $\mathbf{G}$ matrices for the respective model (subscripted 1 and 2) will represent the BE models. However the coupling between them will now represent the essential boundary conditions and thus replace the $\mathbf{C}_a$ and $\mathbf{C}_b$ matrices in equation (3.18). The total system will be,

$$\begin{bmatrix} \mu\mathbf{H}_1 & -\mu\mathbf{G}_2 & \mathbf{0} & \mathbf{0} \\ \mathbf{0} & \mathbf{0} & \mu\mathbf{H}_2 & -\mu\mathbf{G}_2 \\ \mathbf{A}_1 & \mathbf{A}_2 & \mathbf{B}_1 & \mathbf{B}_2 \end{bmatrix} \begin{bmatrix} \frac{\partial\mathbf{\Psi}_1}{\partial n} \\ \mathbf{\Psi}_1 \\ \frac{\partial\mathbf{\Psi}_2}{\partial n} \\ \mathbf{\Psi}_2 \end{bmatrix} = \begin{bmatrix} \frac{\mathbf{p}_{1in}}{i\omega\rho} \\ \mathbf{0} \\ \frac{\mathbf{p}_{2in}}{i\omega\rho} \\ \mathbf{0} \end{bmatrix} \tag{3.19}$$

Normally the $\mathbf{A}$ and $\mathbf{B}$ matrices in equation (3.19) will only represent the fact that the velocities and pressures on both boundaries are the same. Each matrix pair ($\mathbf{A}_1$ and $\mathbf{A}_2$ or $\mathbf{B}_1$ and $\mathbf{B}_2$) will then only have one non-zero entry on each row.

More complicated boundary conditions may be implemented, e.g. air-water coupling on a rough sea. If a moving boundary is requested, the zero vectors on the right hand side may also be replaced.

3.2.3 FE-BE coupling

The coupling between an FE model and a fluid BE model is explained here. As shown previously, the FE model must include components acting on its boundary. Here, these components will be due to the pressures in the BE model.

Contrary, in the BE model, there are no extra components for the first set of equations, which remain unaltered. However, the essential boundary conditions will change. For the coupled system these are due to the requirement that displacements on the boundary in the two models must be the same.

The pressure (i.e. the forces) on the boundary is directly related to the velocity potential, Ψ by, $p = i\omega\rho\mu\Psi$. Hence the pressure of the BE model is also given by piecewise polynomials (or boundary elements). For each element,

$$p = \mathbf{N_p}(\xi)^{\mathbf{T}}\hat{\mathbf{p}} \tag{3.20}$$

where $\hat{\mathbf{p}}$ is the pressure at the nodes in the element and $\mathbf{N_p}(\xi)$ are polynomials defined along the element's part of the boundary. Hence, an equivalent force will depend on the size of the element.

In the FE model the complex conjugate of the virtual work is likewise given by piecewise polynomials,

$$\delta u^* = \delta\mathbf{u}^{\mathrm{H}}\mathbf{N_u}(\xi) \tag{3.21}$$

Thus, the virtual work on the FE model from the fluid BE domain on a shared piece of boundary corresponding to one element is written,

$$\delta W = \int \delta u^* p \ \mathrm{ds} = \delta\mathbf{u}^{\mathrm{H}} \int \mathbf{N_u}(\xi)\mathbf{N_p}(\xi)^{\mathrm{T}} \mathrm{a}\, \mathrm{d}\xi \ \mathbf{p} \tag{3.22}$$

where the integration is carried out over the width $2a$ of the boundary element. The integrals over different elements results in element matrices that are assembled into a system matrix $\mathbf{C_1}$. The FE model is modified to include the pressures from the BE model, so that equation (3.4) becomes,

$$\mathbf{Du} - \mathbf{C_1p} = \mathbf{f}\,. \tag{3.23}$$

The BE model seen in equation (3.18) is almost unchanged. However, the boundary conditions on the second row in this equation will not include the boundary with the FE model. Instead, the essential boundary conditions on the shared boundary arise from the fact that the FE and the BE model have the same displacements. This can be expressed as,

$$i\omega\mathbf{C}_2\mathbf{u} - \mathbf{I}_2\mathbf{v}_n = \mathbf{0} \tag{3.24}$$

where $\mathbf{u}$ is the vector of displacements of the FE model and $\mathbf{v}_n$ is the normal velocity of the boundary element model, which is related to $\frac{\partial \Psi}{\partial n}$. If all of the boundary of the BE model is shared with the FE model, the coupled FE-BE system will be,

$$\begin{bmatrix} \mu\mathbf{H} & -\mu\mathbf{G} & \mathbf{0} \\ \mathbf{0} & -i\omega\rho\mu\mathbf{C_1} & \mathbf{D} \\ -\mu\mathbf{I}_2 & \mathbf{0} & i\omega\mathbf{C}_2 \end{bmatrix} \begin{bmatrix} \frac{\partial\mathbf{\Psi}}{\partial\mathbf{n}} \\ \mathbf{\Psi} \\ \mathbf{u} \end{bmatrix} = \begin{bmatrix} \mathbf{p}_{in} \\ \mathbf{f}_e \\ \mathbf{cc} \end{bmatrix} \tag{3.25}$$

3.2.4 EXAMPLE: ROD

As an example consider the longitudinal vibrations in a rod.

With the inclusions of external virtual work, Hamiltons principle states that,

$$\delta(\int_{t1}^{t2} U - T) - \delta W \, dt = 0 \tag{3.26}$$

where U is the potential energy, T is the kinetic energy and δW is the virtual work on the system. For the simple longitudinal motion the potential and kinetic energies are given by,

$$U = \int_{t1}^{t2} \int_{x1}^{x2} \frac{1}{2}(EA)(\frac{\partial u}{\partial x})^2 \, dx \, dt \tag{3.27}$$

and

$$T = \int_{t1}^{t2} \int_{x1}^{x2} \frac{1}{2}(A\rho)\dot{u}^2 dx \, dt \tag{3.28}$$

The virtual work from external forces may be written as,

$$\delta W = \int_{t1}^{t2} \int_{x1}^{x2} \delta u f dx \, dt \tag{3.29}$$

There may also be losses that would be modelled as virtual work made by internal forces. Here these losses are seen as an added imaginary part of the Young's modulus E.

The $\cdot$ denotes time derivative. Note that these expressions are defined in the time domain and that they are quadratic in u.

The variation means that a small perturbation is made such that one considers $U(u + \delta u) - U(u)$ instead of $U(u)$ and similarly for T. This is essentially the same as $\frac{\partial}{\partial u}U(u)\delta u$.

Now, by extending the time intervall to $\mp\infty$ and applying Parseval's theorem, the resulting expressions in the frequency domain may be written,

$$U = \int_{-\infty}^{+\infty} \int_{x1}^{x2} (\frac{\partial \delta \hat{u}}{\partial x})^{*}(EA)(\frac{\partial \hat{u}}{\partial x})\, dx\, d\omega \tag{3.30}$$

and

$$T = \int_{-\infty}^{+\infty} \int_{x1}^{x2} (i\omega\delta\hat{u})^{*}(A\rho)(i\omega\hat{u}) dx\, d\omega \tag{3.31}$$

It is very important to note that there are several assumptions that make this possible. Firstly it is assumed that the states of the system at $t1$ and $t2$ are irrelevant for the time when the system is actually viewed. Secondly the coefficients ρA and EA are time independent. This is the same as requiring the expressions U and T are quadratic, this is the reason why the frequency domain expressions have essentially the same form as the time domain expressions. It may also be noted that the expressions in the frequency domain involve the complex conjugate of $\hat{u}$. In the time domain u is always real, so there the formal distincion between u and u^{*} is irrelevant. Due to the linearity of the system different frequencies may be viewed independently.

If an infinite structure with constant material properties is to be considered, the procedure that takes the time domain to the frequency domain, could also be applied to take the x-domain to a wavenumber domain where different wavenumbers may be viewed independently.

Here, however, the x-domain is considered to be finite. The equation from Hamiltons principle then becomes,

$$\int_{-\infty}^{+\infty}\int_{x1}^{x2}(\frac{\partial\delta\hat{u}}{\partial x})^*(EA)(\frac{\partial\hat{u}}{\partial x})-(i\omega\delta\hat{u})^*(A\rho)(i\omega\hat{u})-\delta\hat{f}\hat{u}\,dx\,d\omega \tag{3.32}$$

This is the *weak form* of the equation of motion. In addition to this equation the displacements at $x1$ and $x2$ must be defined in some way. If only the displacements u but not their derivatives are involved these are called the *essential* or *Dirichlet* boundary conditions. If the impedance at the boundaries are given rather than a fixed value this is called a *Robin* or *impedance* boundary condition. There are several ways to solve the problem. One is to approximate $\hat{u}$ and $\delta\hat{u}$ with some functions and then minimize the functional. The ńormal' finite element approach is to chose the approximation space as piecewice polynomials. If both $\delta\hat{u}$ and $\hat{u}$ use the same approximation space, *e.g.* linear polynomials, this is equivalent to the *Galerkin* method. For the integrand to have any meaning, the numerical integration must converge, for the present example this will be true if piecewise linear polynomials are used.

A different way to find a solution is to integrate the first term, i.e. the term derived from the potential energy, in (3.32) by parts. This gives,

$$\left[\delta\hat{u}^*(EA)\frac{\partial\hat{u}}{\partial x}\right]_{x1}^{x2}-\int_{x1}^{x2}\delta\hat{u}^*(EA(\frac{\partial^2\hat{u}}{\partial x^2})dx+\omega^2(\rho A)\hat{u})dx-\int_{x1}^{x2}\delta\hat{u}^*\hat{f}dx=0 \tag{3.33}$$

To fulfill equation 3.33 for any choice of $\delta\hat{u}^*$, the integrand has to be zero, see *e.g.* [7]. This means that,

$$(EA(\frac{\partial^2\hat{u}}{\partial x^2})dx+\omega^2(\rho A)\hat{u})=\hat{f} \tag{3.34}$$

This is the strong form of the equation of motion. Furthermore there may be point forces at the boundaries, this then gives

$$(EA)\frac{\partial\hat{u}}{\partial x}|_{x=x1}=\hat{f}x=x1 \tag{3.35}$$

at $x=x1$ and similarly at $x=x2$. These boundary conditions are the *Neuman* or *natural* boundary conditions that must be fulfilled in addition to the *essential* or *impedance* boundary conditions.

By solving (3.34), exact wave solutions for the rod can be found. These solutions are however not fully determined in that the amplitudes of the waves must be found. By matching the essential and natural boundary conditions the complete solution can be described. If relations between values at the boundary relating to each other are expressed in a dynamic stiffness matrix, the method is known as the *dynamic stiffness* method.

It should be noticed that the integration by parts leading to equation (3.33) can be made for the adjoint system instead. Hence, in the absence of internal forces,

$$(EA(\frac{\partial^2 \delta\hat{u}^*}{\partial x^2})dx + \omega^2(\rho A)\delta\hat{u}^*) = 0 \tag{3.36}$$

and

$$\left[\hat{u}(EA)\frac{\partial\delta\hat{u}}{\partial x}\right]_{x1}^{x2} - \left[\delta\hat{u}^*\hat{f}\right]_{x1}^{x2} = 0 \tag{3.37}$$

By substituting from (3.35) we have,

$$\left[\hat{u}(EA)\frac{\partial\delta\hat{u}}{\partial x}\right]_{x1}^{x2} - \left[\delta\hat{u}^*(EA)\frac{\partial\hat{u}}{\partial x}\right]_{x1}^{x2} = 0 \tag{3.38}$$

This is the *reciprocity* relation for the rod. It can be noticed that the reciprocity is derived from the same boundary terms that give rise to the *Neuman* (or *natural*) boundary conditions. By using the exact wavesolutions for $\delta\hat{u}^*$ in the reciprocity relations we get a relation between $\hat{u}$ and $\frac{\partial\hat{u}}{\partial x}$ at the boundaries. The waves originating at $x1$ and travelling towards $x2$ give one relation and a second relation is found by the wave in the opposite direction. If in addition the *essential* or *impedance* boundary conditions are considered a fully determined system is found. This is the principle behind the boundary element method. It got its name because it is the values at the boundaries that is found.

Yet another method is to use the wave-solutions of the (3.34) as test(and trial) functions in the (3.32) rather than the piecewise polynomials. This method is referred to as the *spectral finite element* method.

Since the boundary element method, the spectral finite element method and the dynamic stiffness method all use the wave solutions and essential boundary conditions, they are bound to give the exact solution for the problem.

3.2.5 Summary

In WANDS there are essentially two different types of models. The first type comprise the FE and BE models, whereas the second type comprise the different coupling or boundary condition models.

Coupling and boundary conditions of BE-models are included as extra equations in a system matrix. These equations relate local pressures and displacements of the boundary nodes.

Coupling and boundary conditions of FE-models also need similar equations to describe constraints of local displacements on the boundary. However, FE-models must also include the forces due to these constraints.

3.3 Application

In this section main data structures used in the programming code of WANDS are described. The most important subroutines are also briefly explained.

Finally the sparsity pattern of the system matrix for a simple example of multidomain coupling is considered and the block matrices are related to the previous discussion.

3.3.1 Structures of sub-models

For each of the sub-models of a particular coupled model all the matrices needed are calculated by a subroutine for that sub-model type. The system matrix is then formed by writing all different sub model matrices into the system matrix. This is done in the following order:

1. All BE-sub-models are written. Only the BE formulation is written here, the

boundary conditions are written later. The matrices written are the **H** and **G** matrices given in the previous chapter. Also possible pressure input fields are written to the ”source” vector on the right hand side of the system equation.

2. For each plate model the dynamic stiffness matrix **D** is written. This matrix is formed by adding the FE matrices, $\mathbf{K}_i$ and **M**, with frequency and wavenumber coefficients. These have have in turn at this stage already been added with beam FE equations. Also possible forces are written to the ”source” vector.

3. All dynamic stiffness matrices for solid FE models are written, also with possible beam equations added.

4. The boundary conditions of the fluid BE models are written. There are two such matrices for each model, $\mathbf{C}_a$ and $\mathbf{C}_b$.

5. The coupling conditions between adjacent fluid BE models are written. This includes two different matrices one for each model. These matrices describe the condition that both pressure and velocities must comply at the shared boundary.

6. Coupling matrices between fluid BE models and plate FE models are written. This includes three different matrices. One matrix that describes the forces on the FE model from the fluid pressure and two matrices describing the condition that the displacements of both models must be the same at the boundary.

7. Coupling matrices between fluid BE models and solid FE models are written. The matrices included correspond to those for coupling between fluid BE and plate FE models.

8. Finally the matrices coupling plate and solid FE models are written. These couplings include four different matrices. The first, $\mathbf{C}_{sp1}^{\mathrm{T}}$, give the forces on the plate model. The second, $\mathbf{C}_{sp2}^{\mathrm{T}}$, gives the forces on the solid model. The third and the fourth gives the displacement constraints between the models and are the respective transposes of the first two.

Example

The procedure listed above may be best described by a simple example. The topology of this example is shown in the figure below.

The solid lines correspond to FE models. Top left is a plate FE model, P1, with two plate elements. Top right is a solid FE model, S1, made of two triangular elements. The two FE models are coupled at the third node of the plate. There are four fluid BE models in this system, numbered, F1 to F4, from the top down. The F1 BE model is coupled both the plate and the solid. The F2 and F3 models are coupled together. A wave is impinging on the F2 model at an angle of 45 degrees. Finally, the F4 model has a rigid boundary. The system matrix assembled from this model will look like this,

$$\begin{bmatrix}
\mathbf{H_{F1}} & -\mathbf{G_{F1}} & \mathbf{0} & \mathbf{0} & \mathbf{0} & \mathbf{0} & \mathbf{0} & \mathbf{0} & \mathbf{0} & \mathbf{0} & \mathbf{0} \\
\mathbf{0} & \mathbf{0} & \mathbf{H_{F2}} & -\mathbf{G_{F2}} & \mathbf{0} & \mathbf{0} & \mathbf{0} & \mathbf{0} & \mathbf{0} & \mathbf{0} & \mathbf{0} \\
\mathbf{0} & \mathbf{0} & \mathbf{0} & \mathbf{0} & \mathbf{H_{F3}} & -\mathbf{G_{F3}} & \mathbf{0} & \mathbf{0} & \mathbf{0} & \mathbf{0} & \mathbf{0} \\
\mathbf{0} & \mathbf{0} & \mathbf{0} & \mathbf{0} & \mathbf{0} & \mathbf{0} & \mathbf{H_{F4}} & -\mathbf{G_{F4}} & \mathbf{0} & \mathbf{0} & \mathbf{0} \\
i\omega\rho_1\mu_1\mathbf{C_{1P1}} & \mathbf{0} & \mathbf{0} & \mathbf{0} & \mathbf{0} & \mathbf{0} & \mathbf{0} & \mathbf{0} & \mathbf{D_{P1}} & \mathbf{0} & \mathbf{C_{sp1}^{T}} \\
i\omega\rho_1\mu_1\mathbf{C_{1S1}} & \mathbf{0} & \mathbf{0} & \mathbf{0} & \mathbf{0} & \mathbf{0} & \mathbf{0} & \mathbf{0} & \mathbf{0} & \mathbf{D_{S1}} & \mathbf{C_{sp2}^{T}} \\
\mathbf{0} & \mathbf{0} & \mathbf{0} & \mathbf{0} & \mathbf{0} & \mathbf{0} & \mathbf{0} & \mathbf{C_{bF4}} & \mathbf{0} & \mathbf{0} & \mathbf{0} \\
\mathbf{0} & \mathbf{0} & \mathbf{A_1} & \mathbf{A_2} & \mathbf{B_1} & \mathbf{B_2} & \mathbf{0} & \mathbf{0} & \mathbf{0} & \mathbf{0} & \mathbf{0} \\
\mathbf{0} & \mathbf{I_{2P1}} & \mathbf{0} & \mathbf{0} & \mathbf{0} & \mathbf{0} & \mathbf{0} & \mathbf{0} & \mathbf{C_{2P1}} & \mathbf{0} & \mathbf{0} \\
\mathbf{0} & \mathbf{I_{2S1}} & \mathbf{0} & \mathbf{0} & \mathbf{0} & \mathbf{0} & \mathbf{0} & \mathbf{0} & \mathbf{0} & \mathbf{C_{2S1}} & \mathbf{0}
\end{bmatrix} \tag{3.39}$$

More details on the programming are found in chapter 14

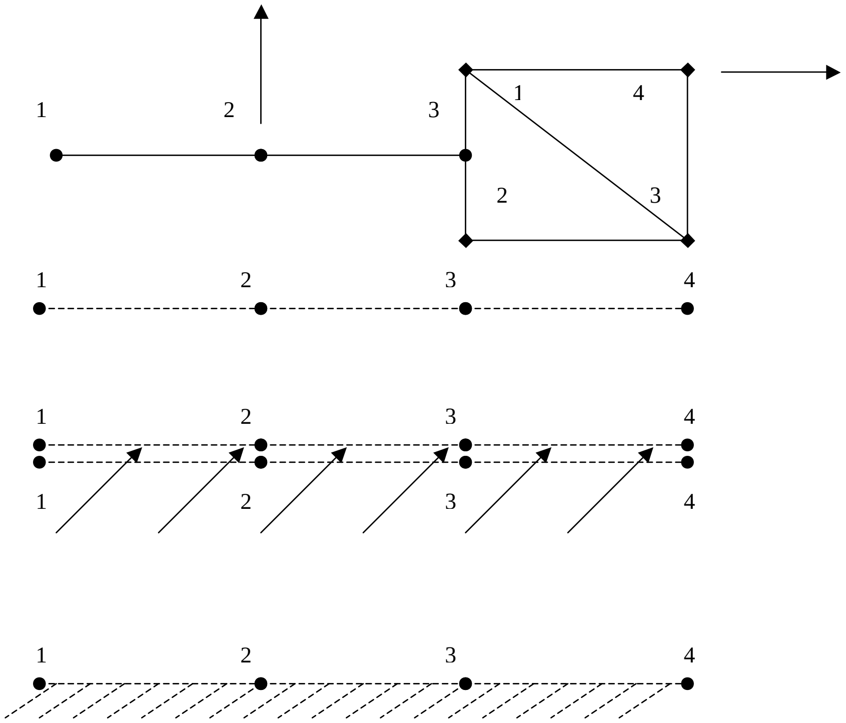

Figure 3.1: Simple example of multidomain coupling.

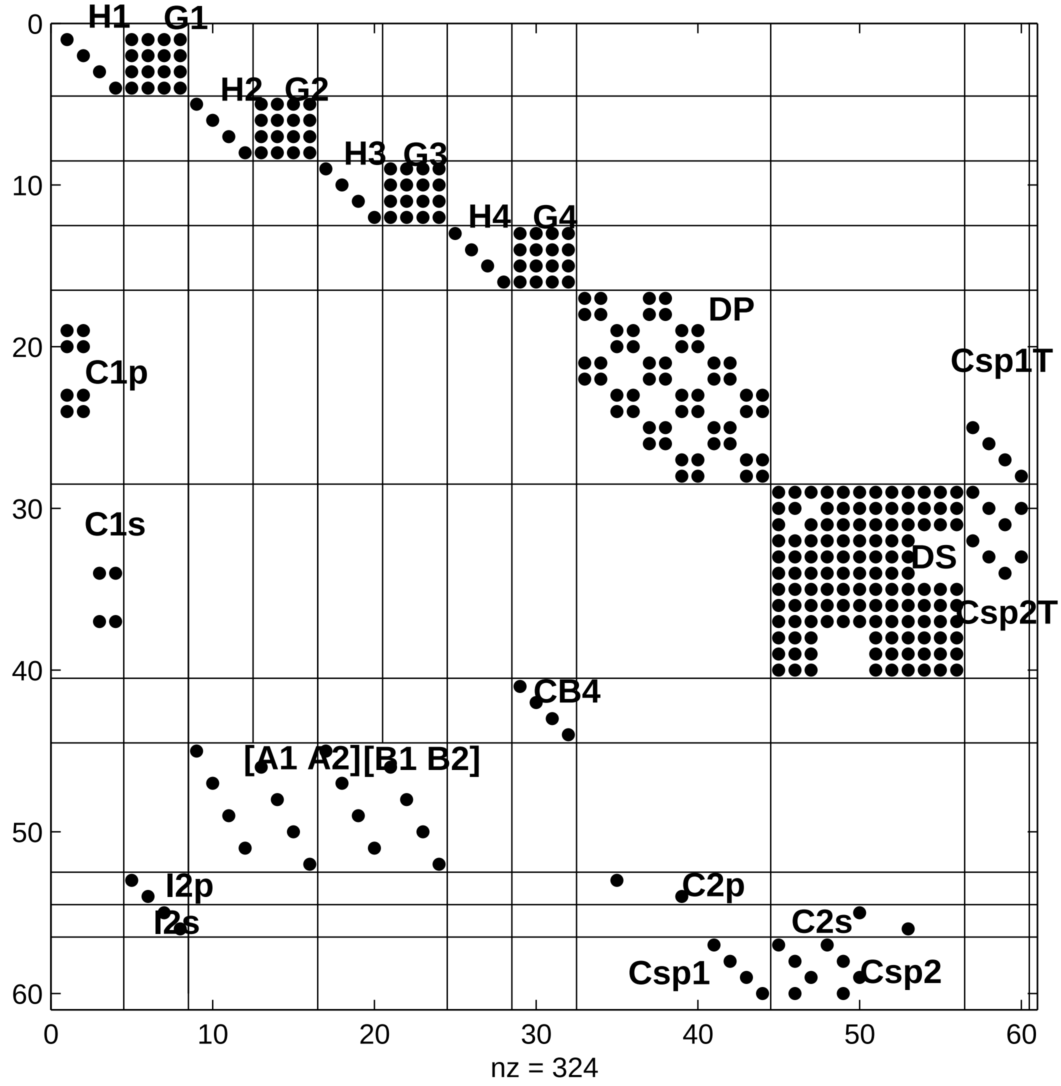

Figure 3.2: Simple example of multidomain coupling.

Chapter 4

Solid orthotropic waveguide finite elements

4.1 Theory

A variation of a Lagrangian, δL, for a solid is defined by,

$$\delta L = \int_{t_1}^{t_2} \delta \left(U - T \right) - \delta W \, dt \,, \tag{4.1}$$

where δ denotes first variation, t_1 and t_2 are the start and end times, U and T are the potential and kinetic energies and δW is the virtual work from external or internal (dissipative) forces. In the absence of other systems Hamilton's modified principle, [8], states that,

$$\delta L = 0 \,. \tag{4.2}$$

for any given t_1 and t_2. Here, the system state at t_1 and t_2 is irrelevant, given that harmonic motion over a long period of time is considered. Thus, t_2 and t_1 may tend to $\pm\infty$ respectively without any loss of information.

Parseval's identity for two real valued functions, $f\left(t\right)$ and $g\left(t\right)$ yields,

$$\int_{-\infty}^{+\infty} f(t)\; g(t)\; dt = \int_{-\infty}^{+\infty} \hat{f}(\omega)^{*}\; \hat{g}(\omega)\; d\omega\,, \tag{4.3}$$

where t is time, ω is angular frequency, $*$ denotes complex conjugate and $\hat{}$ denotes the Fourier transform defined by,

$$\hat{g}(\omega) = \frac{1}{\sqrt{2\pi}} \int_{-\infty}^{+\infty} g(t)\, e^{-i\omega t} dt\,. \tag{4.4}$$

Applying Parseval's identity on equation (4.1) gives,

$$\delta L(\omega) = \int_{-\infty}^{+\infty} \delta U(\omega) - \delta T(\omega) - \delta W(\omega)\; d\omega\,. \tag{4.5}$$

Calculated response at different frequencies are independent when linear systems are considered. Consequently, a variation formulation defined for each frequency is given by,

$$\delta L_{\omega} = \delta U(\omega) - \delta T(\omega) - \delta W(\omega)\;. \tag{4.6}$$

In the following, each of the terms on the right hand side of equation (8.6) are treated separately.

4.1.1 Potential energy

In the time domain the potential energy in a volume V may be written,

$$U = \frac{1}{2} \int_{V} \boldsymbol{\varepsilon}^{\mathrm{T}} \mathbf{D} \boldsymbol{\varepsilon}\, \mathrm{d}V \tag{4.7}$$

where, $\boldsymbol{\varepsilon} = \begin{bmatrix} \varepsilon_x & \varepsilon_y & \varepsilon_z & \gamma_{xy} & \gamma_{xz} & \gamma_{yz} \end{bmatrix}$ are the strains in the material and $\mathbf{D}$ is the material stress-strain matrix, which for orthotropic material may be written,

$$\mathbf{D} = \begin{bmatrix} E_{xx} & E_{xy} & E_{xz} & 0 & 0 & 0 \\ E_{xy} & E_{yy} & E_{yz} & 0 & 0 & 0 \\ E_{xz} & E_{yz} & E_{zz} & 0 & 0 & 0 \\ 0 & 0 & 0 & G_{xy} & 0 & 0 \\ 0 & 0 & 0 & 0 & G_{xz} & 0 \\ 0 & 0 & 0 & 0 & 0 & G_{yz} \end{bmatrix} \tag{4.8}$$

The first variation in the frequency domain of equation (4.9) is given by,

$$\delta U(\omega) = \int_V \delta\hat{\varepsilon}^{\mathrm{H}} \mathbf{D} \hat{\varepsilon} \, \mathrm{d}V \tag{4.9}$$

where, $^{\mathrm{H}}$ denotes the complex transpose. By convention, the dissipative virtual energy may now be approximated by letting the entries in **D** be amended by an imaginary part such that,

$$\mathbf{D} = \Re\{\mathbf{D}\} + i\Im\{\mathbf{D}\} \tag{4.10}$$

where $\Im\{\mathbf{D}\}$ also is symmetric and positive definite. For most problems it is sufficient to let,

$$\mathbf{D} = \Re\{\mathbf{D}\}(1 + i\eta) \tag{4.11}$$

where η is the 'normal' damping loss factor which may be given directly into the software. Inside the WANDS software the routines will be run twice if the more general damping is required (i.e. a damping that use different loss factors in different directions).

Strain–displacement relations

Linear strain–displacement relations are given by,

$$\boldsymbol{\varepsilon} = \begin{bmatrix} \varepsilon_x \\ \varepsilon_y \\ \varepsilon_z \\ \gamma_{xy} \\ \gamma_{xz} \\ \gamma_{yz} \end{bmatrix} = \begin{bmatrix} \frac{\partial u}{\partial x} \\ \frac{\partial v}{\partial y} \\ \frac{\partial w}{\partial z} \\ \frac{\partial u}{\partial y} + \frac{\partial v}{\partial x} \\ \frac{\partial u}{\partial z} + \frac{\partial w}{\partial x} \\ \frac{\partial v}{\partial z} + \frac{\partial w}{\partial y} \end{bmatrix} \tag{4.12}$$

which also may be written as,

$$\boldsymbol{\varepsilon} = \left[\mathbf{B}_0 + \frac{\partial}{\partial x}\mathbf{B}_1\right]\mathbf{u}\,, \tag{4.13}$$

where $\mathbf{u}^{\mathrm{T}} = \begin{bmatrix} u & v & w \end{bmatrix}$ are displacements in the x, y and z directions.

$$\mathbf{B}_0 = \begin{bmatrix} 0 & 0 & 0 \\ 0 & \frac{\partial}{\partial y} & 0 \\ 0 & 0 & \frac{\partial}{\partial z} \\ \frac{\partial}{\partial y} & 0 & 0 \\ \frac{\partial}{\partial z} & 0 & 0 \\ 0 & \frac{\partial}{\partial z} & \frac{\partial}{\partial y} \end{bmatrix} \quad \text{and} \quad \mathbf{B}_1 = \begin{bmatrix} 1 & 0 & 0 \\ 0 & 0 & 0 \\ 0 & 0 & 0 \\ 0 & 1 & 0 \\ 0 & 0 & 1 \end{bmatrix}\,. \tag{4.14}$$

FE–approximations

Consider a prismatic structure element with 'x' being the co–ordinate for which uniform properties exist and 'A' being the cross–sectional area. Approximate $\hat{\mathbf{u}}$ and $\delta\hat{\mathbf{u}}$ with,

$$\hat{\mathbf{u}} = \mathbf{N}(y,z)\tilde{\mathbf{u}}(x) \quad \text{and} \quad \delta\hat{\mathbf{u}} = \mathbf{N}(\mathrm{y},\mathrm{z})\delta\tilde{\mathbf{u}}(\mathrm{x}) \tag{4.15}$$

where, $\mathbf{N}(y,z)$ are 2D real valued FE–shape–functions and $\tilde{\mathbf{u}}$ and $\delta\tilde{\mathbf{u}}$ are real and virtual nodal displacements.

Inserting equation (4.13) into (4.10) then yields,

$$\delta U\left(\omega\right) = \int_x \frac{\partial^i \delta \tilde{\mathbf{u}}}{\partial x^i} \sum_{i=0}^{1} \sum_{j=0}^{1} \mathbf{a}_{ij} \frac{\partial^j \tilde{\mathbf{u}}}{\partial x^j} \mathrm{d}x \tag{4.16}$$

where,

$$\mathbf{a}_{ij} = \int_A \left[\mathbf{B}_i \mathbf{N}\right]^{\mathrm{T}} \mathbf{D} \left[\mathbf{B}_j \mathbf{N}\right] \mathrm{d}A\,. \tag{4.17}$$

It should be noted that,

$$\mathbf{a}_{01} = \mathbf{a}_{10}^{\mathrm{T}} \tag{4.18}$$

which may be seen directly from the definition in (4.17). This relation is utilized in the WANDS.

4.1.2 Kinetic energy

Kinetic energy in a volume V in the time domain is given by,

$$T = \frac{1}{2} \int_V \dot{\mathbf{u}}\, \mathbf{M}\, \dot{\mathbf{u}} \mathrm{d}V \tag{4.19}$$

where, $\dot{\mathbf{u}}$ represents the velocity of the displacements and $\mathbf{M}$ is a mass matrix defined by,

$$\mathbf{M} = \rho \begin{bmatrix} 1 & 0 & 0 \\ 0 & 1 & 0 \\ 0 & 0 & 1 \end{bmatrix} \tag{4.20}$$

where, ρ is the material density. Taking the first variation, transforming to the frequency domain and applying the FE–approximations in section (4.1.1) yields,

$$\delta T(\omega) = \omega^2 \int_x \delta \tilde{\mathbf{u}}^{\mathrm{H}} \left[\mathbf{m}_2\right] \tilde{\mathbf{u}} \mathrm{d}x \tag{4.21}$$

where,

$$\mathbf{m}_2 = \int_A \left[\mathbf{N}^{\mathrm{T}}\mathbf{M}\mathbf{N}\right] \mathrm{d}A\,. \tag{4.22}$$

4.1.3 External forces

The virtual energy, denoted with δW in equation, (4.1), is defined by,

$$\delta W = \int_V \delta \mathbf{u}^{\mathrm{T}} \mathbf{f} \mathrm{d}V \tag{4.23}$$

Thus, in the frequency domain, with the FE shape–function approximation from section 4.1.1, we have,

$$\delta W = \int_x \delta \tilde{\mathbf{u}}^{\mathrm{H}} \int_A \mathbf{N}^{\mathrm{T}} \hat{\mathbf{f}} \mathrm{d}A \mathrm{d}x = \int_x \delta \tilde{\mathbf{u}}^{\mathrm{H}} \tilde{\mathbf{f}}\, \mathrm{d}x \tag{4.24}$$

4.1.4 Waveguide finite element model

Inserting the expressions for δU, δT and δW, i.e. equations (5.16), (5.23) and (11.5), into equation (8.6), yields,

$$\delta L_\omega = \int_x \sum_{i=0}^{1} \sum_{j=0}^{1} \frac{\partial^i \delta \tilde{\mathbf{u}}}{\partial x^i} \mathbf{a}_{ij} \frac{\partial^j \tilde{\mathbf{u}}}{\partial x^j} - \omega^2 \delta \tilde{\mathbf{u}}^{\mathrm{H}} \left[\mathbf{m}_2\right] \tilde{\mathbf{u}} - \delta \tilde{\mathbf{u}}^{\mathrm{H}} \tilde{\mathbf{f}} \mathrm{d}x \tag{4.25}$$

This equation may be denoted as the 'weak form' of the waveguide–FE model.

The element matrices,$\mathbf{a}_{ij}$ and $\mathbf{m}_2$ must be evaluated for each different element. This evaluation, made with Gauss quadrature, also includes a co-ordinate transformation that enables deformed element shapes. This procedure is however better described in references to ordinary 2D-FE code e.g. [5].

Hamilton's principle, equation (8.2), integration by parts with respect to the x–co–ordinate and calculus of variation yields,

$$\left[\mathbf{k_2} \frac{\partial^2}{\partial x^2} + \mathbf{k_1} \frac{\partial^2}{\partial x^2} + \mathbf{k_0} - \omega^2 \mathbf{m_2}\right] \tilde{\mathbf{u}} - \tilde{\mathbf{f}} = \mathbf{0} \tag{4.26}$$

where, $\mathbf{k_0} = \mathbf{a}_{00}$, $\mathbf{k_1} = \mathbf{a}_{01} - \mathbf{a}_{10} =$ and $\mathbf{k_2} = -\mathbf{a}_{11}$.

Finite element assembling is carried out so that nodal displacements of nodes shared by several elements are set equal. The assembled matrices are denoted with capital letters, thus,

$$\left[\mathbf{K_2}\frac{\partial^2}{\partial x^2} + \mathbf{K_1}\frac{\partial^2}{\partial x^2} + \mathbf{K_0} - \omega^2\mathbf{M_2}\right]\tilde{\mathbf{U}} - \tilde{\mathbf{F}} = \mathbf{0} \tag{4.27}$$

4.1.5 Remarks

Remark 1

The calculation of the $\mathbf{a}_{11}$ matrix is simplified by performing the multiplication,

$$[\mathbf{B}_1]^{\mathrm{T}}\,\mathbf{D}\,[\mathbf{B}_1] = \begin{bmatrix} E_{xx} & 0 & 0 \\ 0 & G_{xy} & 0 \\ 0 & 0 & G_{xz} \end{bmatrix} \tag{4.28}$$

which then may be interpreted as a smaller stiffness matrix (denoted as $[B]_4$ by Sheng, [4])

Remark 2

A weak form of the wave–equation will result by assembling the $\mathbf{a}_{ij}$ matrices rather than the $\mathbf{k}_i$ matrices. This form implicitly contain information about natural boundary conditions and is therefore essential when general finite length problems are considered. An application utilizing the equivalent form of equation (4.25) for thin plate elements is found in reference [9]. The inclusion of the weak form into the software requires storing non symmetric matrices since $\mathbf{a}_{01}$ is neither symmetric nor antisymmetric.

Remark 3

For a moving load on an infinite length waveguide the following analysis may be made. Instead of utilizing Parseval's identity directly we keep the time integral in equation (4.1). The analysis leading to equation (4.25) will then instead be written,

$$\delta L = \int_{-\infty}^{+\infty} \int_{-\infty}^{+\infty} \sum_{i=0}^{1} \sum_{j=0}^{1} \frac{\partial^{i} \delta \tilde{\mathbf{u}}}{\partial x^{i}} \mathbf{a}_{ij} \frac{\partial^{j} \tilde{\mathbf{u}}}{\partial x^{j}} - \delta \dot{\tilde{\mathbf{u}}}^{\mathrm{T}} \left[\mathbf{m}_2\right] \dot{\tilde{\mathbf{u}}} - \delta \tilde{\mathbf{u}}^{\mathrm{T}} \tilde{\mathbf{f}} \mathrm{d}x \mathrm{d}t \tag{4.29}$$

Now, from Parseval's identity, the double integrals in equation (4.30) are equivalent to integrals of the twice Fourier transformed functions, here denoted by $\hat{\hat{}}$, i.e.

$$\delta L = \int_{-\infty}^{+\infty} \int_{-\infty}^{+\infty} \sum_{i=0}^{1} \sum_{j=0}^{1} \frac{\partial^{i} \delta \hat{\hat{\mathbf{u}}}^{T}}{\partial x^{i}} \mathbf{a}_{ij} \frac{\partial^{j} \hat{\hat{\mathbf{u}}}}{\partial x^{j}} - \delta \dot{\hat{\hat{\mathbf{u}}}}^{\mathrm{T}} \left[\mathbf{m}_2\right] \dot{\hat{\hat{\mathbf{u}}}} - \delta \tilde{\mathbf{u}}^{\mathrm{T}} \hat{\hat{\mathbf{f}}} \mathrm{d}\kappa \mathrm{d}\omega \tag{4.30}$$

Now, assuming a force travelling at speed c, i.e. $\tilde{\mathbf{f}} = \tilde{\mathbf{f}}\,(x - ct, t)$ it may be favourable to consider a solution $\tilde{\mathbf{u}} = \tilde{\mathbf{u}}\,(x - ct, t)$.

For any function $f(x - ct, t)$, the Fourier transform, $\mathcal{F}_{x \to \kappa}$, from $x \to \kappa$ yields,

$$\mathcal{F}_{x \to \kappa}\{f(x - ct, t)\} = e^{-i\kappa ct} \hat{f}(\kappa, t) \tag{4.31}$$

The second transform, $\mathcal{F}_{t \to \omega}$ from $t \to \omega$, then yields,

$$\mathcal{F}_{t \to \omega}\{e^{-i\kappa ct} \hat{f}(x, t)\} = \hat{\hat{f}}(\kappa, \omega + \kappa c) \tag{4.32}$$

The corresponding transform of the velocity is,

$$\mathcal{F}_{t \to \omega}\{\frac{\partial}{\partial t}(e^{-i\kappa ct} \hat{f}(\kappa, t))\} = i\omega \hat{\hat{f}}(\kappa, \omega + \kappa c) \tag{4.33}$$

which is proven in the Appendix to this chapter.

Considering independence of separate values of κ and ω, the integrations may be omitted and the final variational statement of motion becomes,

$$\delta L = \sum_{i=0}^{1} \sum_{j=0}^{1} \frac{\partial^{i} \delta \hat{\hat{\mathbf{u}}}^{\mathrm{H}}}{\partial x^{i}} \mathbf{a}_{ij} \frac{\partial^{j} \hat{\hat{\mathbf{u}}}}{\partial x^{j}} - \omega^{2} \delta \hat{\hat{\mathbf{u}}}^{\mathrm{H}} \left[\mathbf{m}_2\right] \hat{\hat{\mathbf{u}}} - \delta \tilde{\mathbf{u}}^{\mathrm{H}} \hat{\hat{\mathbf{f}}} \mathrm{d} \tag{4.34}$$

where, $\hat{\hat{\mathbf{u}}} = \hat{\hat{\mathbf{u}}}(\kappa, \overline{\omega})$, $\hat{\hat{\mathbf{f}}} = \hat{\hat{\mathbf{f}}}(\kappa, \overline{\omega})$ and $\overline{\omega} = \omega + \kappa c$.

This does not comply with the results given by Sheng [4] (page 12.) where instead, $\overline{\omega} = \omega - \kappa c$ is derived and also used in front of the kinetic term (the mass matrix). This discrepancy should be checked further.

Remark 3

External forces, in the weighted form seen in equation (11.5), are not included in the software. Implementation of such forces may be included, but it is usually sufficient to apply concentrated forces to the nodal degrees of freedom directly.

4.2 Validation

The validations are made by considering 8–node quadrilateral elements.

4.2.1 Convergence

Two meshes, with 9 and 25 elements respectively, of the same square are considered. The 25 element mesh is seen in Figure 4.1.

The convergence for an isotropic material (here steel is used) is seen in Figure 4.2.

The results in Figure 4.2 indicate that the convergence is as expected. For lower order waves, those branches to the left in Figure 4.2, the two meshes yields almost identical results. This is expected since both meshes should be able to resolve the corresponding, relatively simple, cross–sectional shapes. Also, as expected, there is discrepancy in the results between the two meshes for higher wave orders. Furthermore, the 25 element mesh gives lower frequencies for the same wavenumber. This is explained with the fact that the stiffness matrices includes derivatives with respect to the cross–sectional coordinates and thus include larger errors than the mass matrix. Such discretization errors tend to overestimate the exact potential and kinetic energies, and thus the resulting frequencies will be overestimated.

The rate of convergence for eigenfrequencies for ordinary finite elements is further discussed in [10]. However, at the moment such convergence studies are outside the scope of this project.

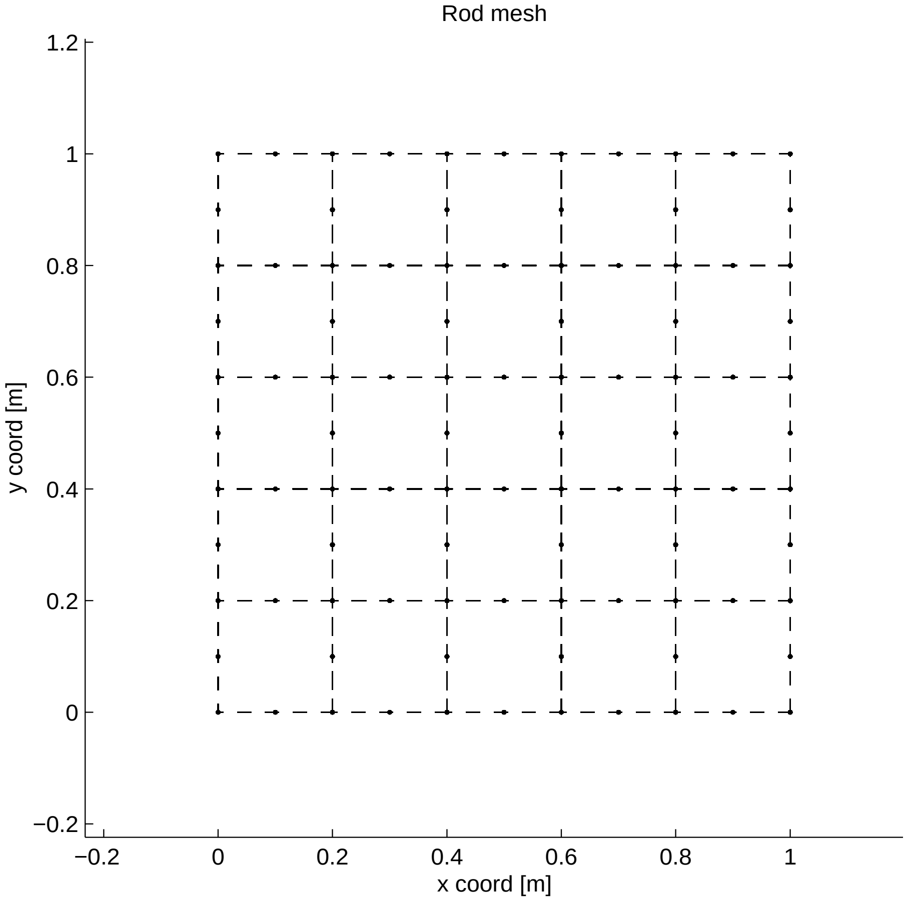

Figure 4.1: 25 element mesh

4.2.2 Isotropic rod

Alaami, reference [11], made studies of rectangular rods with a method similar to that presented here. Alaami's elements have triangular cross-section (and presumably linear shape–functions). Also, since there are no meshes given in [11], the exact values from Alaami's analysis are of less importance. Also by comparing with analytical results for a cylinder, Alaami claims to have a discrepancy of about 2% for 100 elements. Plotting tabulated values from [11] and the present analysis results in Figure 3, where the non dimensional frequency, Ω, is defined by,

$$\Omega = \omega/\omega_s \quad ; \quad \omega_s^2 = G/(\rho l^2)\,, \tag{4.35}$$

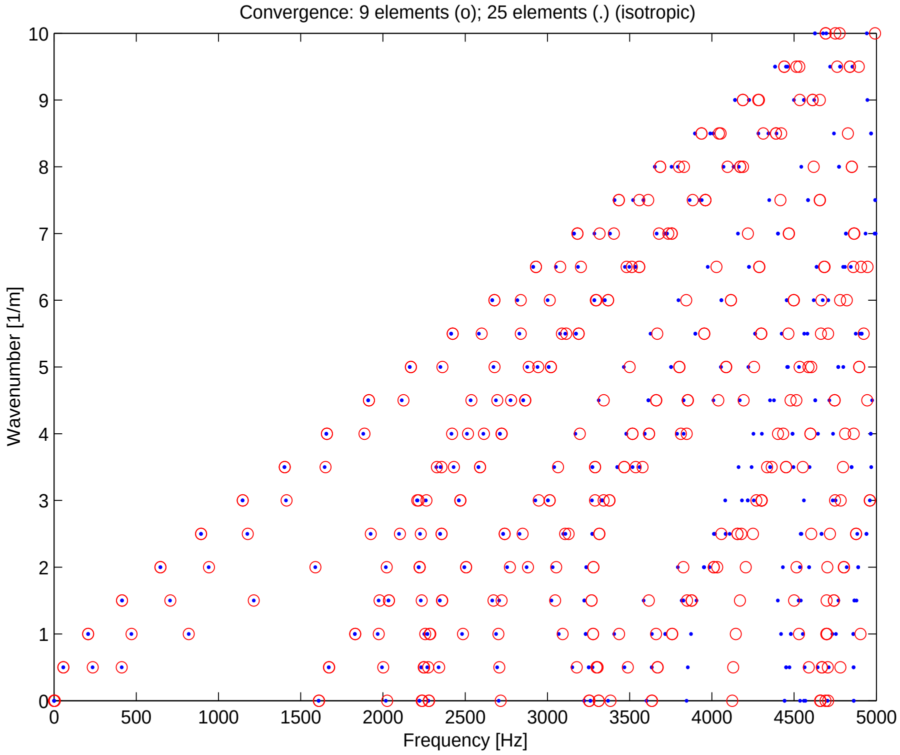

Figure 4.2: Rings=9–element mesh; Dots=25–element mesh

where G is the shear modulus and l is the side length. Poisson's ratio $\nu = 0.3$.

The results indicate a satisfactory agreement. The small discrepancies might be explained by a lack of convergence in Alaami's study, this would also explain the fact that the frequencies for the present study are generally lower.

4.2.3 Orthotropic rod

The dispersion relations for the orthotropic case is calculated for topaz, (How much would a topaz rod with 1 by 1 metre cross–section cost?). The material properties for the material used are given in Table 4.1.

Since non–dimensional frequencies are used, the density could take any reasonable value, the value in Table 4.1 is however typical of topaz.

The non dimensional frequency, Ω, is here defined by,

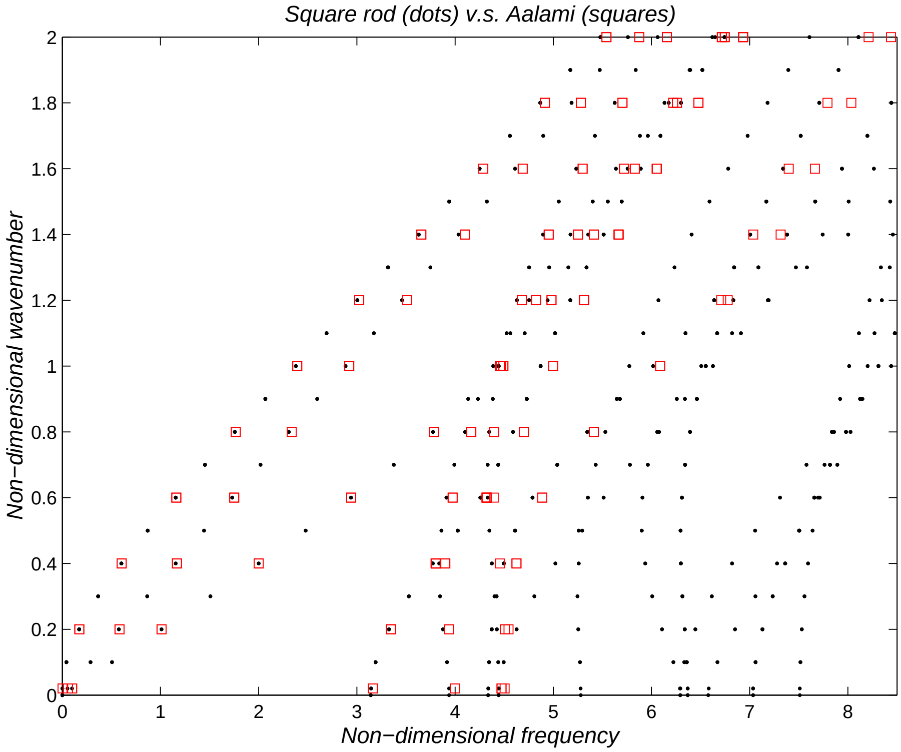

Figure 4.3: Dispersion relations for isotropic rod; Squares=Alaami's results; Dots=25–element mesh

$$\Omega = \omega/\omega_s \quad ; \quad \omega_s^2 = G_{yz}/(\rho l^2)\,, \tag{4.36}$$

As can be seen, there are no apparent discrepancies between the orthotropic results shown in 4.4 compared to the isotropic case shown in 4.3.

4.2.4 Analytical solution

Due to the relatively small differences between elasticities in different directions for topaz and the need for future validation cases, for instance for pre–stress, an analytical solution would be quite valuable. One such solution might be obtained for an rectangular rod with constrained boundaries. Assuming trigonometric cross–sectional displacements that are zero on the boundaries might then yield an analytical solution. So far no successfull solution for this problem has been found. However it

Side length:	l	1 m
Young's modulus x–direction:	E_{xx}	294 GPa
Young's modulus y–direction:	E_{yy}	349 GPa
Young's modulus z–direction:	E_{zz}	281 GPa
Young's modulus xy–direction:	E_{xy}	88 GPa
Young's modulus yz–direction:	E_{xz}	84 GPa
Young's modulus yz–direction:	E_{yz}	126 GPa
Shear modulus xy–direction:	G_{xy}	131 GPa
Shear modulus yz–direction:	G_{xz}	132 GPa
Shear modulus yz–direction:	G_{yz}	108 GPa
Density:	ρ	3550 kg/m^3

Table 4.1: Parameters for orthotropic rod

might be something to come back to.

4.3 Appendix

Theorem:

$$\mathcal{F}_{t\rightarrow\omega}\{\frac{\partial}{\partial t}(e^{-i\kappa ct}\hat{f}(\kappa,t))\} = i\omega\hat{\hat{f}}(\kappa,\omega+\kappa c) \tag{4.37}$$

Proof:

$$\begin{aligned}\mathcal{F}_{t\rightarrow\omega}\{\frac{\partial}{\partial t}(e^{-i\kappa ct}\hat{f}(\kappa,t))\} &= \int_{-\infty}^{+\infty}\frac{\partial}{\partial t}\left(e^{-i(\kappa ct)}\hat{f}\right)e^{-i\omega t}\mathrm{d}t \\ = -i\kappa c\int_{-\infty}^{+\infty}\hat{f}(\kappa,t)e^{-i(\omega+\kappa c)t}\mathrm{d}t &+ \int_{-\infty}^{+\infty}e^{-i(\kappa ct)}\frac{\partial}{\partial t}\left(\hat{f}(\kappa,t)\right)e^{-i\omega t}\mathrm{d}t \end{aligned} \tag{4.38}$$

The first term on the bottom line of equation (4.38) is here denoted I_1 and the second is denoted I_2. I_1 is recognized as,

$$I_1 = -i\kappa c\hat{\hat{f}}(\kappa,\omega+\kappa c) \tag{4.39}$$

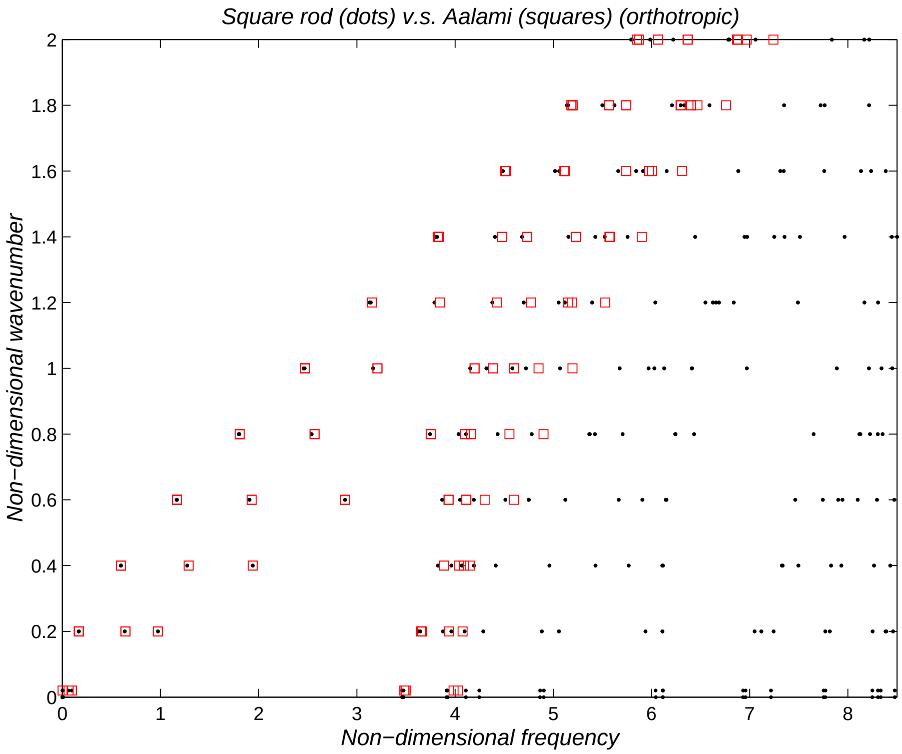

Figure 4.4: Dispersion relations for orthotropic rod; Squares=Alaami's results; Dots=25–element mesh

I_2 is evaluated with integration by parts as,

$$I_2 = \left[\hat{f}(\kappa, t)e^{-i(\omega+\kappa c)t}\right]_{-\infty}^{+\infty} - \int_{-\infty}^{+\infty} -i\left(\omega+\kappa c\right)e^{-i(\omega+\kappa c)t}\hat{f}(\kappa, t)\mathrm{d}t \tag{4.40}$$

For the Fourier transform to exist, the bracketed expression must equal zero, whereas the integral is recognized as,

$$\int_{-\infty}^{+\infty} i\left(\omega+\kappa c\right)e^{-i(\omega+\kappa c)t}\hat{f}(\kappa, t)\mathrm{d}t = i\left(\omega+\kappa c\right)\hat{\hat{f}}(\kappa, \omega+\kappa c) \tag{4.41}$$

Thus after summing I_1 and I_2 we have,

$$\mathcal{F}_{t\to\omega}\{\frac{\partial}{\partial t}(e^{-i\kappa ct}\hat{f}(\kappa, t))\} = i\omega\hat{\hat{f}}(\kappa, \omega+\kappa c) \tag{4.42}$$

which is the same as equation (4.37). QED.

Chapter 5

Orthotropic plate strip finite elements

5.1 Theory

The analysis based on Hamilton's principle in the beginning of Chapter 4 can be used as a starting point for the derivation of the plate elements as well. The main difference compared to the solid elements is the expression for the potential energy and the following treatment of this expression.

5.1.1 Potential energy

Following thin plate theory and considering the frequency domain, see [1], the first variation of potential energy in an area A for an orthotropic plate may be written,

$$\delta U = \int_A \left[\begin{array}{cc} \delta \boldsymbol{\varepsilon}^{\mathrm{H}} & \delta \boldsymbol{\kappa}^{\mathrm{H}} \end{array} \right] \mathbf{D} \left[\begin{array}{c} \boldsymbol{\varepsilon} \\ \boldsymbol{\kappa} \end{array} \right] \mathrm{d}A \tag{5.1}$$

where,

$$\begin{bmatrix} \boldsymbol{\varepsilon} \\ \boldsymbol{\varkappa} \end{bmatrix} = \begin{bmatrix} \varepsilon_x \\ \varepsilon_y \\ \gamma_{xy} \\ \kappa_x \\ \kappa_y \\ \kappa_{xy} \end{bmatrix} \tag{5.2}$$

and

$$\mathbf{D}_0 = \begin{bmatrix} h\left[\mathbf{D}_0\right] & \\ & \frac{h^3}{12}\left[\mathbf{D}_0\right] \end{bmatrix}, \tag{5.3}$$

where, h is the plate thickness and

$$\mathbf{D}_0 = \frac{1}{1-\nu_x\nu_y}\begin{bmatrix} E_x & E_x\nu_y & \\ E_y\nu_x & E_y & \\ 0 & 0 & G_{xy} \end{bmatrix}. \tag{5.4}$$

The strains, $\boldsymbol{\varepsilon}$, and the curvatures, $\boldsymbol{\kappa}$ are given by,

$$\begin{bmatrix} \varepsilon_x \\ \varepsilon_y \\ \gamma_{xy} \\ \kappa_x \\ \kappa_y \\ \kappa_{xy} \end{bmatrix} = \begin{bmatrix} \frac{\partial u}{\partial x} \\ \frac{\partial v}{\partial y} \\ \frac{\partial u}{\partial y} + \frac{\partial v}{\partial x} \\ \frac{\partial^2 w}{\partial x^2} \\ \frac{\partial^2 w}{\partial y^2} \\ \frac{\partial^2 w}{\partial x \partial y} \end{bmatrix} \tag{5.5}$$

Which may also be written,

$$\begin{bmatrix} \boldsymbol{\varepsilon} \\ \boldsymbol{\varkappa} \end{bmatrix} = \left[\mathbf{B}_0 + \frac{\partial}{\partial x}\mathbf{B}_1 + \frac{\partial^2}{\partial x^2}\mathbf{B}_2\right]\begin{bmatrix} u \\ v \\ w \end{bmatrix} \tag{5.6}$$

where the operators $\mathbf{B}_0$, $\mathbf{B}_1$ and $\mathbf{B}_2$ are given by,

$$\mathbf{B}_0 = \begin{bmatrix} 0 & 0 & 0 \\ 0 & \frac{\partial}{\partial y} & 0 \\ \frac{\partial}{\partial y} & 0 & 0 \\ 0 & 0 & 0 \\ 0 & 0 & \frac{\partial^2}{\partial y^2} \\ 0 & 0 & 0 \end{bmatrix}, \quad \mathbf{B}_1 = \begin{bmatrix} 1 & 0 & 0 \\ 0 & 0 & 0 \\ 0 & 1 & 0 \\ 0 & 0 & 0 \\ 0 & 0 & 0 \\ 0 & 0 & \frac{\partial}{\partial y} \end{bmatrix} \text{ and } \mathbf{B}_2 = \begin{bmatrix} 0 & 0 & 0 \\ 0 & 0 & 0 \\ 0 & 0 & 0 \\ 0 & 0 & 1 \\ 0 & 0 & 0 \\ 0 & 0 & 0 \end{bmatrix} \tag{5.7}$$

Now, shape–functions, $\boldsymbol{\Psi}_{ip}(y)$ and $\boldsymbol{\Psi}_b(y)$ are introduced. Here, $\boldsymbol{\Psi}_{ip}$ are linear functions and $\boldsymbol{\Psi}_b$ are cubic Hermite polynomials. Upon replacing the y–coordinate with the non–dimensional coordinate, $\xi = \frac{y-y_m}{L/2}$, where y_m is the mid y–coordinate of the element, the shape–functions are defined by,

$$\boldsymbol{\Psi}_{ip}(y) = [N_{1ip} \quad N_{2ip}] \tag{5.8}$$

$$= [\frac{1}{2}(1-\xi) \quad \frac{1}{2}(1+\xi)] \tag{5.9}$$

$$\boldsymbol{\Psi}_b(y) = [N_{1b} \quad N_{2b} \quad N_{1b} \quad N_{2b}] \tag{5.10}$$

$$= [\frac{1}{4}(2-3\xi+\xi^3) \quad \frac{L}{8}(1-\xi-\xi^2+\xi^3) \tag{5.11}$$

$$\frac{1}{4}(2+3\xi-\xi^3) \quad \frac{L}{8}(-1-\xi+\xi^2+\xi^3)] \tag{5.12}$$

for the in—plane and out–of–plane motions respectively. L is the width of the element.

The displacements are approximated as,

$$\begin{bmatrix} u \\ v \\ w \end{bmatrix} = \boldsymbol{\Psi}(y)\tilde{\mathbf{u}}(x)\,. \tag{5.13}$$

where,

$$\boldsymbol{\Psi} = \begin{bmatrix} N_{1ip} & 0 & 0 & 0 & N_{2ip} & 0 & 0 & 0 \\ 0 & N_{1ip} & 0 & 0 & 0 & N_{2ip} & 0 & 0 \\ 0 & 0 & N_{1b} & N_{2b} & 0 & 0 & N_{3b} & N_{4b} \end{bmatrix}, \tag{5.14}$$

for the nodal displacements partitioned as,

$$\tilde{\mathbf{u}}(x) = \left[\begin{array}{cccccccc} u_1 & v_1 & w_1 & \phi_1 & u_2 & v_2 & w_2 & \phi_2 \end{array} \right]^{\mathrm{T}} \tag{5.15}$$

Upon substituting equation (5.13) into equation (5.6) and the result subsequently into equation (5.21), the potential energy is approximated as,

$$\int \sum_{i=0}^{2} \sum_{j=0}^{2} \frac{\partial^i \delta \tilde{\mathbf{u}}^{\mathrm{H}}}{\partial x^i} \mathbf{a}_{ij} \frac{\partial^j \tilde{\mathbf{u}}}{\partial x^j} \mathrm{d}x \tag{5.16}$$

where

$$\mathbf{a}_{ij} = \int \left[\mathbf{B}_i \boldsymbol{\Psi}\right]^{\mathrm{T}} \left[\mathbf{D}\right] \left[\mathbf{B}_j \boldsymbol{\Psi}\right] \mathrm{d}y \tag{5.17}$$

To evaluate $\mathbf{a}_{ij}$, we start with the terms $[\mathbf{B}_j \boldsymbol{\Psi}]$. Multiplication, (here using MAPLE to avoid mistakes), yields,

$$[\mathbf{B}_0\mathbf{\Psi}] = \begin{bmatrix} 0 & 0 & 0 & 0 & 0 & 0 & 0 & 0 \\ 0 & \frac{\partial N_{1ip}}{\partial y} & 0 & 0 & 0 & \frac{\partial N_{2ip}}{\partial y} & 0 & 0 \\ \frac{\partial N_{1ip}}{\partial y} & 0 & 0 & 0 & \frac{\partial N_{2ip}}{\partial y} & 0 & 0 & 0 \\ 0 & 0 & 0 & 0 & 0 & 0 & 0 & 0 \\ 0 & 0 & \frac{\partial^2 N_{1b}}{\partial y^2} & \frac{\partial^2 N_{2b}}{\partial y^2} & 0 & 0 & \frac{\partial^2 N_{3b}}{\partial y^2} & \frac{\partial^2 N_{4b}}{\partial y^2} \\ 0 & 0 & 0 & 0 & 0 & 0 & 0 & 0 \end{bmatrix} \tag{5.18}$$

$$[\mathbf{B}_1\mathbf{\Psi}] = \begin{bmatrix} N_{1ip} & 0 & 0 & 0 & N_{2ip} & 0 & 0 & 0 \\ 0 & 0 & 0 & 0 & 0 & 0 & 0 & 0 \\ 0 & N_{1ip} & 0 & 0 & 0 & N_{2ip} & 0 & 0 \\ 0 & 0 & 0 & 0 & 0 & 0 & 0 & 0 \\ 0 & 0 & 0 & 0 & 0 & 0 & 0 & 0 \\ 0 & 0 & \frac{\partial N_{1b}}{\partial y} & \frac{\partial N_{2b}}{\partial y} & 0 & 0 & \frac{\partial N_{3b}}{\partial y} & \frac{\partial N_{4b}}{\partial y} \end{bmatrix} \tag{5.19}$$

$$[\mathbf{B}_2\mathbf{\Psi}] = \begin{bmatrix} 0 & 0 & 0 & 0 & 0 & 0 & 0 & 0 \\ 0 & 0 & 0 & 0 & 0 & 0 & 0 & 0 \\ 0 & 0 & 0 & 0 & 0 & 0 & 0 & 0 \\ 0 & 0 & N_{1b} & N_{2b} & 0 & 0 & N_{3b} & N_{4b} \\ 0 & 0 & 0 & 0 & 0 & 0 & 0 & 0 \\ 0 & 0 & 0 & 0 & 0 & 0 & 0 & 0 \end{bmatrix} \tag{5.20}$$

These matrices may be evaluated for any value of y or ξ. The inner integral in equation (5.16) is thus made from $\xi = -1$ to $\xi = +1$ and $\mathrm{d}y = (L/2)\mathrm{d}\xi$. Thus $L/2$ is the Jacobian of the 1D coordinate transform.

Equation (5.21) may be seen as a weak form equation for the potential energy.

5.1.2 Kinetic energy

The first variation of the kinetic energy in the frequency domain, is written,

$$\delta T = \int_A \rho h \begin{bmatrix} \delta u^* & \delta v^* & \delta w^* \end{bmatrix} \begin{bmatrix} u \\ v \\ w \end{bmatrix} \mathrm{d}A \tag{5.21}$$

where ρ is the plate density.

With the same approximations as in the previous section we have,

$$\delta T = \int_x \delta \tilde{\mathbf{u}}^{\mathrm{H}} \, \mathbf{m}_2 \, \tilde{\mathbf{u}} \, \mathrm{d}x \tag{5.22}$$

where,

$$\mathbf{m}_2 = \int_y \rho h \boldsymbol{\Psi}^{\mathrm{T}} \boldsymbol{\Psi} \mathrm{d}y \tag{5.23}$$

is evaluated as discussed in the previous section.

5.1.3 External forces

Distribution of external forces may be included into the formulation as shown in reference [1], by considering the virtual work. Normally it is sufficient to include point forces at the nodes only and, as for the solid elements, this is the way forces on plate elements are included in WANDS.

5.1.4 Element formulation

Inserting variations of potential and kinetic energies into Hamilton's principle, followed by integration by parts while neglecting boundary terms of the ends of the waveguide and subsequently applying calculus of variation yields,

$$\left[\mathbf{k_4} \frac{\partial^4}{\partial x^4} + \mathbf{k_2} \frac{\partial^2}{\partial x^2} + \mathbf{k_1} \frac{\partial^2}{\partial x^2} + \mathbf{k_0} - \omega^2 \mathbf{m}_2 \right] \tilde{\mathbf{u}} - \tilde{\mathbf{f}} = \mathbf{0} \tag{5.24}$$

where, $\mathbf{k}_0 = \mathbf{a}_{00}$, $\mathbf{k}_1 = \mathbf{a}_{01} - \mathbf{a}_{10}$, $\mathbf{k}_2 = \mathbf{a}_{02} + \mathbf{a}_{20} - \mathbf{a}_{11}$ and $\mathbf{k}_4 = \mathbf{a}_{22}$.

5.1.5 Co-ordinate transformation and assembling

Now the 1D cross-section of the element must be projected on the 2D cross-section of the assembled model. This is made by introducing the coordinate transforms $\mathbf{T}$. Consider an element rotated by the angle α and nodes given by the position vectors,

$\mathbf{r}_1$ and $\mathbf{r}_2$. The unit vector along the element is given by $\frac{\mathbf{r}_2-\mathbf{r}_1}{\|\mathbf{r}_2-\mathbf{r}_1\|}$. By taking the scalar vector product with the unit vector along the y–direction and applying the identity $\mathbf{a} \bullet \mathbf{b} = \|\mathbf{a}\|\|\mathbf{b}\|\mathbf{cos}(\alpha)$ for scalar vector products, it may be shown that

$$\cos(\alpha) = \frac{y_2 - y_1}{\|\mathbf{r}_2 - \mathbf{r}_1\|} \tag{5.25}$$

By applying the vector, '×', product and its interpretation in a similar way it may be shown that,

$$\sin(\alpha) = \frac{z_2 - z_1}{\|\mathbf{r}_2 - \mathbf{r}_1\|} \tag{5.26}$$

From Figure 5.1, the transformation from the local co–ordinates of the rotated element displacements to those in the global co–ordinate system, the latter indicated with the subindex 'g', is given by,

$$\begin{bmatrix} u_{1g} \\ v_{1g} \\ w_{1g} \\ \phi_{1g} \\ u_{2g} \\ v_{2g} \\ w_{2g} \\ \phi_{2g} \end{bmatrix} = \begin{bmatrix} 1 & 0 & 0 & 0 & 0 & 0 & 0 & 0 \\ 0 & \cos(\alpha) & -\sin(\alpha) & 0 & 0 & 0 & 0 & 0 \\ 0 & \sin(\alpha) & \cos(\alpha) & 0 & 0 & 0 & 0 & 0 \\ 0 & 0 & 0 & 1 & 0 & 0 & 0 & 0 \\ 0 & 0 & 0 & 0 & 1 & 0 & 0 & 0 \\ 0 & 0 & 0 & 0 & 0 & \cos(\alpha) & -\sin(\alpha) & 0 \\ 0 & 0 & 0 & 0 & 0 & \sin(\alpha) & \cos(\alpha) & 0 \\ 0 & 0 & 0 & 0 & 0 & 0 & 0 & 1 \end{bmatrix} \begin{bmatrix} u_1 \\ v_1 \\ w_1 \\ \phi_1 \\ u_2 \\ v_2 \\ w_2 \\ \phi_2 \end{bmatrix} \tag{5.27}$$

The opposite transformation from the global coordinates to the local coordinate are sought and these are given by the inverse of the matrix in equation (5.27). Luckily, since these sort of transformation matrices are orthonormal, the inverse is simply given by the transpose. The transpose of the matrix in equation (5.27) is denoted by $\mathbf{T}$. Transformation of each of the stiffness matrices in equation (5.24) is made by,

$$\mathbf{k}_{ig} = \mathbf{T}^{\mathrm{T}}\mathbf{k}_i\mathbf{T} \tag{5.28}$$

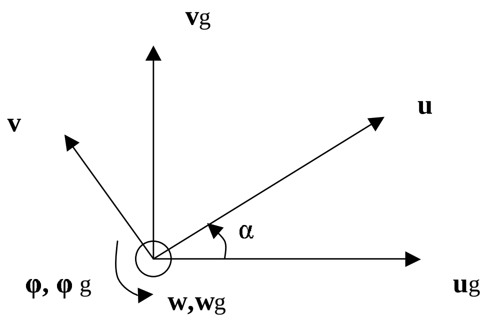

Figure 5.1: Co-ordinate rotation .

and the transformation of the mass matrix is similar. The reason for using the transformation on both sides of the original matrix is clear from considering the weak form expressions.

Assembling of the element matrices yields the equation for the whole system as,

$$\left[\mathbf{K_4}\frac{\partial^4}{\partial x^4} + \mathbf{K_2}\frac{\partial^2}{\partial x^2} + \mathbf{K_1}\frac{\partial^2}{\partial x^2} + \mathbf{K_0} - \omega^2\mathbf{M}_2\right]\tilde{\mathbf{U}} = \tilde{\mathbf{F}} \tag{5.29}$$

5.2 Validations

The first validation is made by comparing the current software package with a model made by a package developed by Svante Finnveden at KTH. A Y-shaped profile is considered. The profile is seen in Figure 5.2 and thought to be made of 1 mm thick steel. The eigenvalues of each of the matrices in equation (5.29) are considered. An error estimate for each matrix is calculated as,

$$\frac{\max|\lambda_f - \lambda_s|}{\max|\lambda_s|} \tag{5.30}$$

where, λ_f and λ_s are the eigenvalues for the WANDS and the KTH model respectively. The largest error found is $2.3 \cdot 10^{-6}$.

Secondly, a steel-pipe is considered. The pipe model is made of 40 elements of equal length. The pipe is 1 mm thick and has 0.1 m radius. The comparison is made with a semi-analytic solution as presented in [12]. The dispersion relation is plotted in Figure 5.3.

The straight line without rings in Figure 5.3 represents a fluid wave in the air inside the pipe. An inconsistency can be seen about 100 Hz where the WFE–model have a cut on. This cut on will be at a lower frequency for a model with 20 elements than for the model with 40 elements. For a model with 80 elements the situation is again better although for 160 elements it becomes worse. This behaviour is likely to indicate a numerical problem. Another indication of this problem as that each semi–analytic dispersion curve displays two FE-solutions, which indicates that the geometrical symmetry of the pipe is not handled properly. Internally the plate–strip

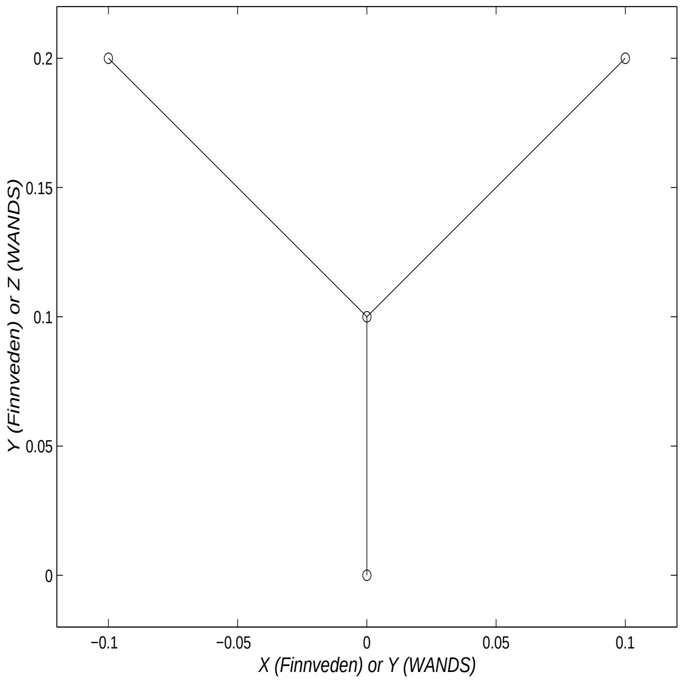

Figure 5.2: Y–beam mesh

program is now changed to 'doubleprecision' for all but the input variables. The output still is now also written with double precision. However, for some problems, it has been found that the output matrices are not quite symmetric or antisymmetric. For these cases better results in calculations are obtained if they are forced to be symmetric or antisymmetric. Another reason for numerical instability comes from the entries in the **D** matrix of equation (5.3), these might have very large differences in magnitude when using SI–units since the thickness usually is much less than unity. An attempt to implement this by using a length scale in dm rather than m is seen in Figure 5.4.

This is clearly better, but a length scale in cm again makes correspondence less accurate (for even lower frequencies). Letting the outputs be written with 10 decimals yields much better results as seen in Figure 5.5

Thirdly, an orthotropic plate strip with hinged sides is considered, for this case an analytical solution exists, see [1]. Here, the thickness is $1\,mm$ and the width of the plate is $1\,m$. The Young's modulus in the x- and y-directions are 200 and

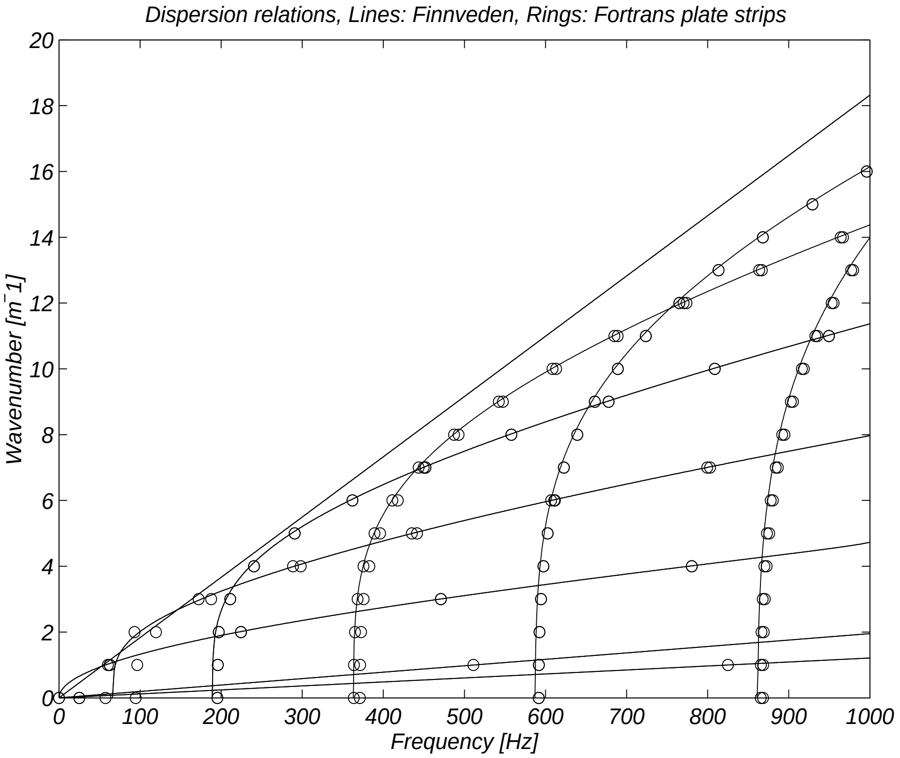

Figure 5.3: Dispersion relations for steel pipe; Lines=Finnveden; Rings=40–element mesh

50 GPa respectively. The Poisson's ratio in the x-direction is 0.3. The out-of-plane dispersion relations for a ten element model compared to the analytical solution is seen in Figure 5.6

The discrepancies in Figure 5.6 are of order and type expected from the FE–approximation. The results indicated by Figure 5.6 are good, but this case only considers out-of-plane motion, thus validation for in-plane motion is not given here.

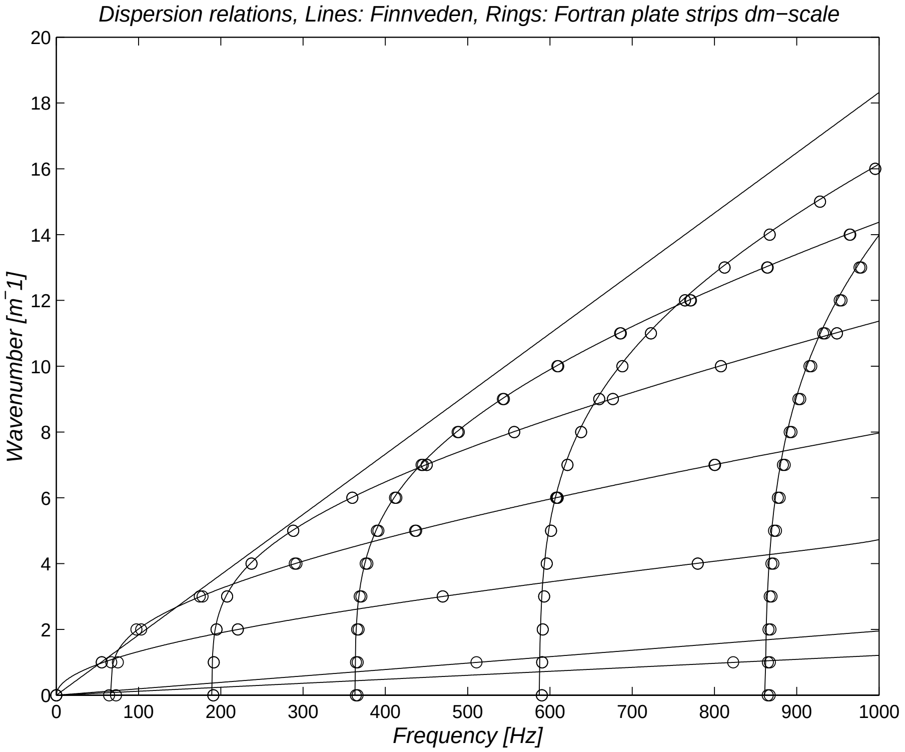

Figure 5.4: Dispersion relations for steel pipe; Lines=Finnveden; Rings=40–element mesh (using dm scale)

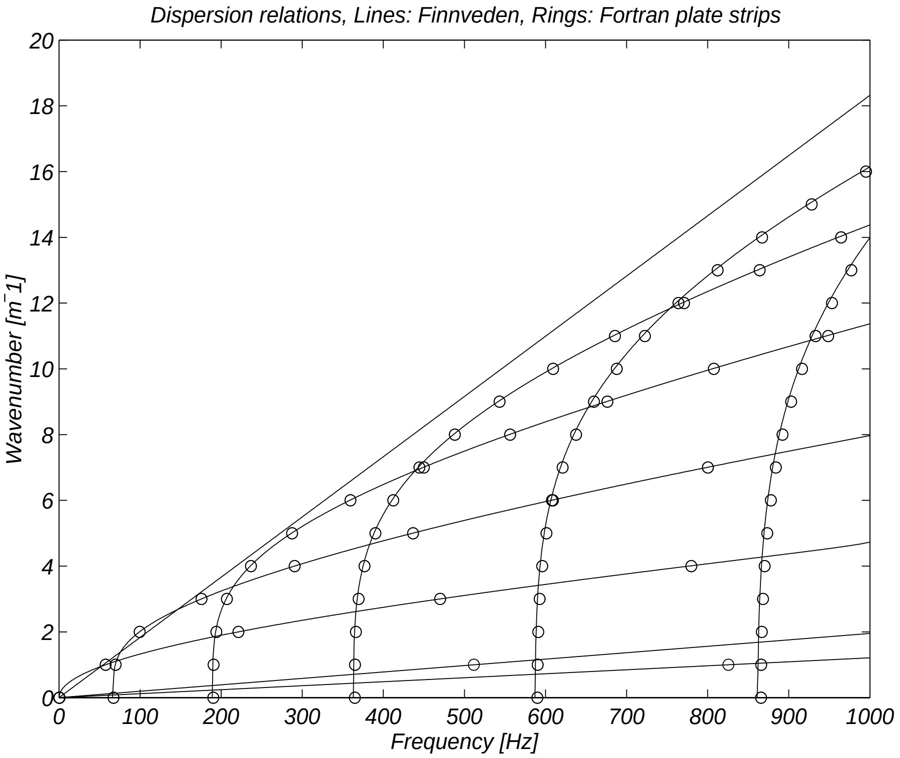

Figure 5.5: Dispersion relations for steel pipe; Lines=Finnveden; Rings=40–element mesh

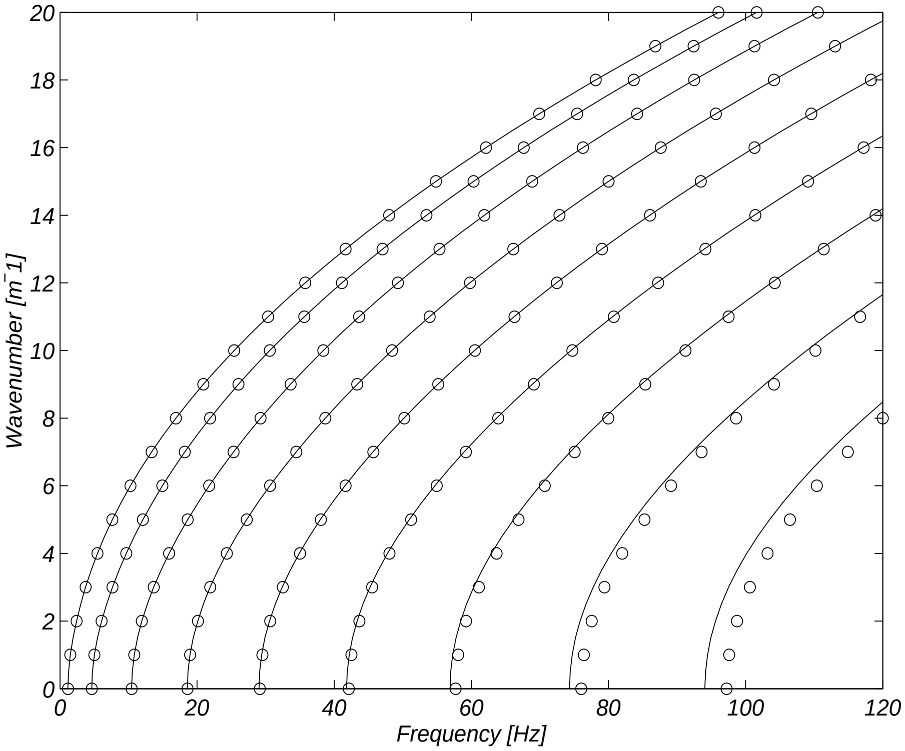

Figure 5.6: Dispersion relations for orthotropic plate, Lines=analytic solution, Rings=WFE solution.

Chapter 6

Beam elements

6.1 Introduction

Beam elements along the ‘extrusion’ are included in the FE code and described in this chapter. The beam elements restrain motion in the x-, y- and z-directions as well as rotations. Thus a single beam element describes longitudinal, flexural and torsional motion. Moreover the flexural motions may be coupled when the y- and z-axes do not coincide with the beam symmetry-axis and similar coupling may also occur between longitudinal and rotational coupling. Flexural motions are described with Euler theory, i.e. stiffnesses proportional to the fourth derivative with respect to the direction of propagation. Longitudinal and torsional stiffnesses are proportional to the second derivatives with respect to the direction of propagation.

6.2 Theory

A beam is here seen as having four different types of waves, flexural motion in the, y- and z- directions, longitudinal motion in the x- direction and rotation about the x- direction.

6.2.1 Flexural motion

Uncoupled flexural motion

First, consider a beam such that no coupling between any two motions is present. A wave equations for a beams flexural motion about the y-axis may then be written, see e.g. [13].

$$D_z \frac{\partial^4 w}{\partial x^4} - \omega^2 m_a \, w = F_z \tag{6.1}$$

For displacements, w, in the z- direction. D_z is the flexural rigidity for bending about the y-axis, as found in many books on structural mechanics. For reference D_z is calculated as the integral,

$$D_z = \int_A E_x(y,z) z^2 dA \,, \tag{6.2}$$

over the cross–section area, A. For constant isotropic material, $E_x(y,z) = E$ simplifies to,

$$D_z = E \, I_y \,. \tag{6.3}$$

m_a is the mass per unit length in the x-direction,

$$m_a = \int_A \rho(y,z) \, dA \,. \tag{6.4}$$

Similarly, the flexural equation for motion about the z-axis, i.e. in the y-direction, is written as,

$$D_y \frac{\partial^4 v}{\partial x^4} - \omega^2 m_a v = F_y \,. \tag{6.5}$$

Coupled flexural motion

If there is flexural motion the two displacements, v and w will be coupled. The coupling results in the system,

$$\left(\begin{bmatrix} D_y & -D_{yz} \\ -D_{yz} & D_{zz} \end{bmatrix} \tfrac{\partial^4}{\partial x^4} - \omega^2 \begin{bmatrix} m_a & 0 \\ 0 & m_a \end{bmatrix} \right) \begin{bmatrix} v \\ w \end{bmatrix} = \begin{bmatrix} F_y \\ F_z \end{bmatrix} \tag{6.6}$$

where,

$$D_{yz} = \int_A E_x(y,z)\, yz \, \mathrm{dA} \tag{6.7}$$

The minus sign in equation 6.6 is due to the convention of defining moments as positive when they cause positive rotation about the y- or z- axis.

6.2.2 Longitudinal and torsional motion

Uncoupled motion

The equation for the longitudinal motion, u, in the x-direction is written as,

$$D_l \frac{\partial^2 u}{\partial x^2} - \omega^2 m_a \, u = F_x \tag{6.8}$$

where, D_x, is given as,

$$D_l = \int_A E_x(y,z) dA \tag{6.9}$$

which may be simplified to,

$$D_l = A E_x \,, \tag{6.10}$$

when $E_x(y,z)$ is constant.

The equation for the rotation of the beam is written as,

$$D_t \frac{\partial^2 \phi}{\partial x^2} - \omega^2 J_a \, \phi = F_r \,, \tag{6.11}$$

where, J_a is the cross–sections moment of inertia and D_r is the torsional rigidity, which for a circular cross-section with inner and outer radius, r_i and r_o is given by,

$$D_t = \frac{\pi}{2} G(r_o^4 - r_i^4), \tag{6.12}$$

where, G is the (constant) shear modulus, [13]. Generally the torsional rigidity is much more difficult to calculate. One method to establish, D_r is to make a waveguide FE model of it. This is explained in the following section.

Coupled motion

As for the flexural motion, coupling may also exist between longitudinal and torsional motion. This coupling is generally referred to as *warping*, and explained in e.g. reference [14].

The ẃarping’ coupling is highly dependent on the position at which a beam couples to the surrounding structure. Thus, it must be evaluated at this position. The coupled matrix equation is written,

$$\left(-\begin{bmatrix} D_l & D_{tl} \\ D_{tl} & D_t \end{bmatrix} \frac{\partial^2}{\partial x^2} - \omega^2 \begin{bmatrix} m_a & 0 \\ 0 & J_a \end{bmatrix} \right) \begin{bmatrix} u \\ \phi \end{bmatrix} = \begin{bmatrix} F_x \\ M_x \end{bmatrix} \tag{6.13}$$

For more information about ’warping’ in thin–walled beams see [15]. Generally the analytical calculation of the warping is cumbersome. Also, the approximation in equation (6.13) may be very crude. For instance, consider two circular beams of different diameter connected with a thin plate–strip, as presented in Figure 6.1.

With reference to Figure 6.1, the torsional motion is a linear combination of the beams flexural motion. Thus it is proportional to κ^4, furthermore there is a strong coupling between the flexural and torsional motion. One way to overcome the problem of giving correct input data for a beam might be to make a waveguide finite element model and subsequently perform a modal condensation only to have the first four waves in the model. This, however, has not yet been tested.

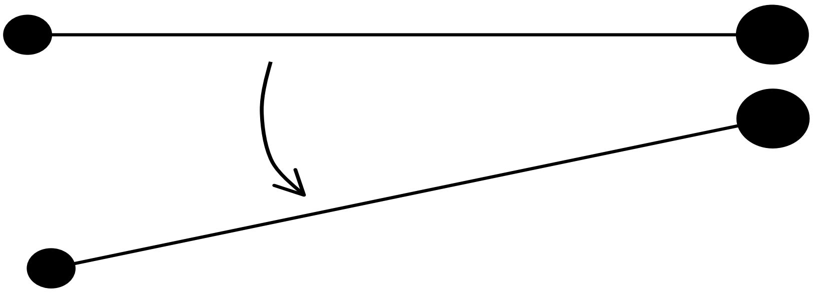

Figure 6.1: Rotation of a beam made of two circular beams and a plate

6.3 Coupling of beams to surrounding models

The implemented beam elements do not define any new nodes. Instead the beams couple to already existing nodes in the plate and solid models.

6.3.1 Plate connected beams

For the plate models all four degrees of freedom exist for each node. Thus it is easy to add the extra rigidities,D_y, D_z, D_l and D_t and corresponding masses to each node. In WANDS these parameters are formed in extra matrices, K_{4bp}, K_{2bp} and M_{bp}. Thus the complete plate system is given by,

$$\left[(\mathbf{K}_{p4} + \mathbf{K}_{bp4}) \frac{\partial^4}{\partial x^4} + (\mathbf{K}_{p2} + \mathbf{K}_{bp2}) \frac{\partial^2}{\partial x^2} + \mathbf{K}_{p1} \frac{\partial^2}{\partial x^2} + \mathbf{K}_{p0} - \omega^2 (\mathbf{M_p} + \mathbf{M_{bp}}) \right] \tilde{\mathbf{W}}(x) = \tilde{\mathbf{F}}_p(x) \tag{6.14}$$

where $\tilde{\mathbf{F}}_p(x)$ is the force vector of the model.

6.3.2 Solid connected beams

For the solid model the rotation is unspecified at the nodes. However, it may be specified as a linear combination of two nodal displacements. The linear combination is best specified at a position between two nodes. By following the theory and notations made in Chapter 7, the four degrees of freedom are given by,

$$\begin{bmatrix} u_b \\ v_b \\ w_b \\ \phi_b \end{bmatrix} = \begin{bmatrix} \frac{1}{2}(1-\zeta) & 0 & 0 & \frac{1}{2}(1+\zeta) & 0 & 0 \\ 0 & \frac{1}{2}(1-\zeta) & 0 & 0 & \frac{1}{2}(1+\zeta) & 0 \\ 0 & 0 & \frac{1}{2}(1-\zeta) & 0 & 0 & \frac{1}{2}(1+\zeta) \\ 0 & \frac{1}{2}r_{dz} & -\frac{1}{2}r_{dy} & 0 & -\frac{1}{2}r_{dz} & \frac{1}{2}r_{dy} \end{bmatrix} \begin{bmatrix} u_{s1} \\ v_{s1} \\ w_{s1} \\ u_{s2} \\ v_{s2} \\ w_{s2} \end{bmatrix} \tag{6.15}$$

where, u_b , v_b , w_b , ϕ_b are the displacements and rotation at the position of the beam. u_{s1} , v_{s1} , w_{s1} are the displacements of the first coupling node in the solid model and u_{s2} , v_{s2} , w_{s2} are the displacements of the second. The beam's position between the two solid nodes is given by the non-dimensional coordinate ζ with a value between -1 and $+1$, (note at -1 and $+1$ the rotation is undefined at the solid model nodes).

With this information the beam stiffness matrices is distributed to the solid element degrees of freedom. This is done by seeing the matrix in equation (6.15) as a transformation matrix, T. Denoting $\begin{bmatrix} u_b & v_b & w_b & \phi_b \end{bmatrix} = \mathbf{u}_b$ and the vector $\begin{bmatrix} u_{s1} & v_{s1} & w_{s1} & u_{s2} & v_{s3} & w_{s2} \end{bmatrix} = \mathbf{u}_s$, the energies corresponding to the beam stiffnesses and mass are given by,

$$\begin{aligned} &\mathbf{u}_b^{\mathrm{H}}[\mathbf{K}_{4b}]\frac{\partial^4 \mathbf{u}_b}{\partial x^4} = \mathbf{u}_s^{\mathrm{H}}[\mathbf{T}]^{\mathbf{T}}[\mathbf{K}_{4b}][\mathbf{T}]\frac{\partial^4 \mathbf{u}_s}{\partial x^4} \\ &\mathbf{u}_b^{\mathrm{H}}[\mathbf{K}_{2b}]\frac{\partial^2 \mathbf{u}_b}{\partial x^2} = \mathbf{u}_s^{\mathrm{H}}[\mathbf{T}]^{\mathbf{T}}[\mathbf{K}_{2b}][\mathbf{T}]\frac{\partial^2 \mathbf{u}_s}{\partial x^2} \\ &\text{and} \\ &\mathbf{u}_b^{\mathrm{H}}[\mathbf{M}_b]\mathbf{u}_b = \mathbf{u}_s^{\mathrm{H}}[\mathbf{T}]^{\mathbf{T}}[\mathbf{M}_b][\mathbf{T}]\mathbf{u}_s \end{aligned} \tag{6.16}$$

Thus, the stiffness and mass matrices for the solid coupled beam are,

$$
\begin{aligned}
&[\mathbf{K}_{4sb}] = [\mathbf{T}]^{\mathbf{T}}[\mathbf{K}_{4b}][\mathbf{T}] \\
&[\mathbf{K}_{2sb}] = [\mathbf{T}]^{\mathbf{T}}[\mathbf{K}_{2b}][\mathbf{T}] \\
&\text{and} \\
&[\mathbf{M}_{sb}] = [\mathbf{T}]^{\mathbf{T}}[\mathbf{M}_{b}][\mathbf{T}]
\end{aligned}
\tag{6.17}
$$

The matrices for the solid coupled beams are assembled into separate matrices and the whole solid and beam model is formed by,

$$
\left[(\mathbf{K}_{bs4})\frac{\partial^4}{\partial x^4} + (\mathbf{K}_{s2} + \mathbf{K}_{bs2})\frac{\partial^2}{\partial x^2} + \mathbf{K}_{s1}\frac{\partial^2}{\partial x^2} + \mathbf{K}_{s0} - \omega^2(\mathbf{M_s} + \mathbf{M_{bs}})\right]\tilde{\mathbf{W}}(x) = \tilde{\mathbf{F}}_s(x) \tag{6.18}
$$

where $\tilde{\mathbf{F}}_s(x)$ is the force vector of the model.

6.4 Validation

The validation is made in two stages. First the validation of a beam coupled to the middle of a plate model is made. This validation is very simple, since the beam model outputs may be checked directly. Hence, it is only required to check that the input data parameters are written at the correct positions in the output data matrices, $\mathbf{K}_{4bp}$, $\mathbf{K}_{2bp}$ and $\mathbf{M}_{bp}$.

Secondly a similar model, but with solid elements (8-noded quadrilaterals) and a solid coupled beam is made. The dispersion relations for the two models are then compared. Also, to ensure that the effect of the beam is significant a model without the beam is also considered. The dispersion relations for the cases without and with beams can be seen in Figures 6.2 and 6.3.

The models represents simply supported plate strips with or without a beam placed at the middle.

The following parameters are used,

Width of plate: $= 1\,m$,

Thickness of plate: $= 0.02\,m$,

Young's modulus $= 210\,GPa$,

Poisson's ratio: 0.3.

Plate density: $\rho = 7800 kg/m^3$

Masses:

$M_a = 500 kg/m, J_a = M_t = 2.5 kgm$

Longitudinal and torsional rigidities:

$D_l = 750\,Nm^2$, $D_t = 1 \cdot 10^7\,Nm^2$, $D_{tl} = 75\,Nm^2$

Flexural rigidities:

$D_{fy} = 20 \cdot 10^6\,Nm^2, D_{fz} = 30 \cdot 10^6\,Nm^2, D_{fyz} = -2 \cdot 10^6\,Nm^2$

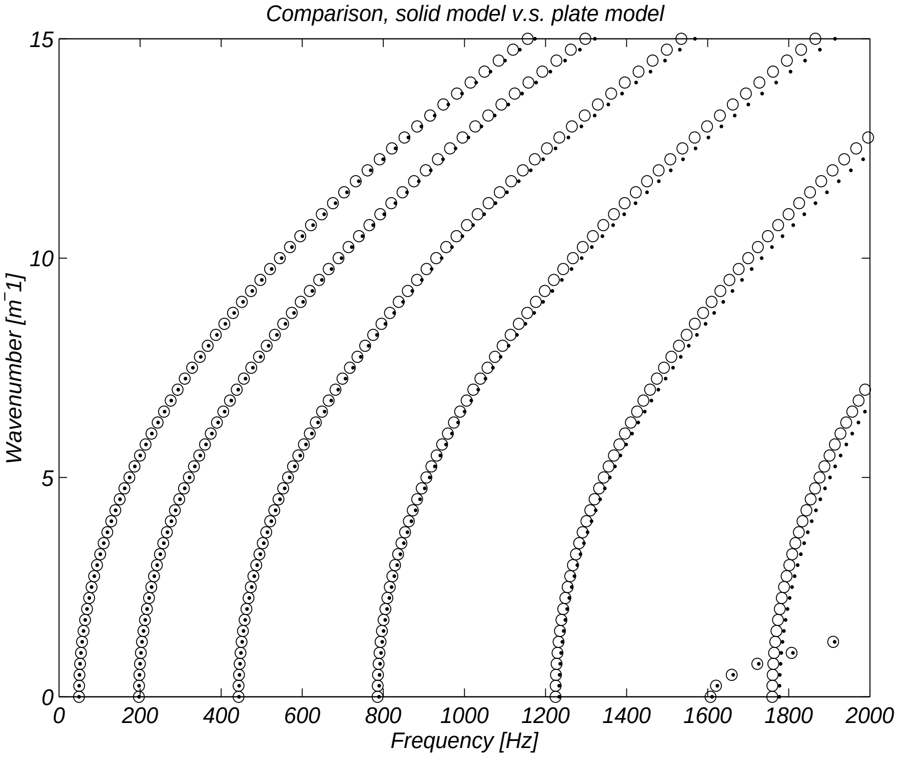

Figure 6.2: Dispersion relations for simply supported plate without beam; Solid elements (●); Plate elements (○).

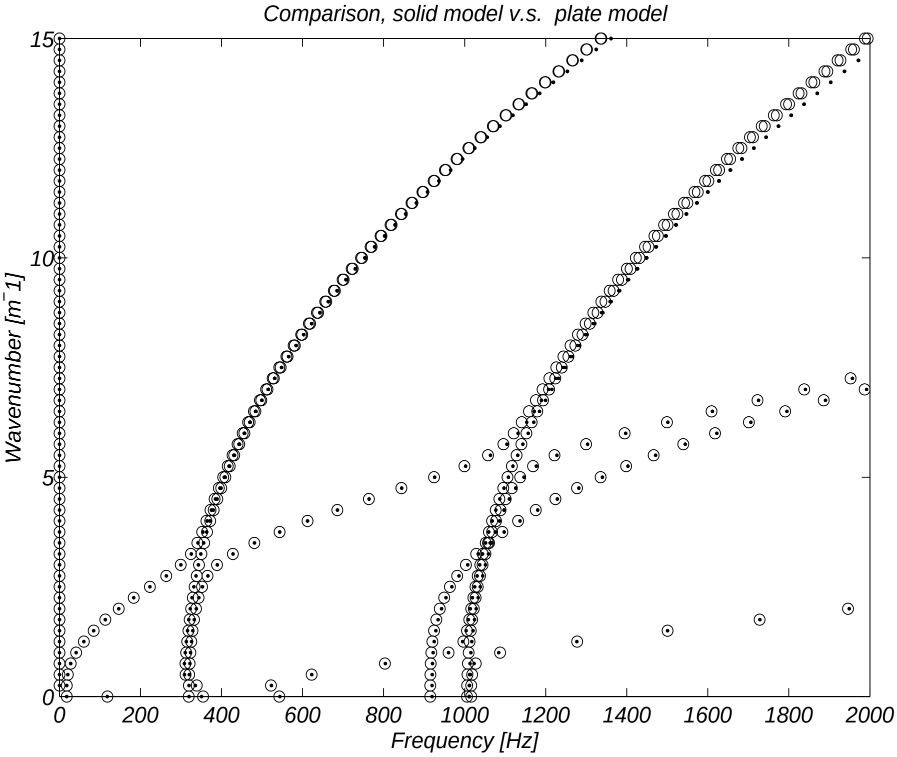

Figure 6.3: Dispersion relations for simply supported plate with beam; Solid elements (•); Plate elements (○).

Chapter 7

FE-solid to FE-plate coupling

7.1 Introduction

To couple a plate element with a solid element requires a way to couple the rotational d.o.f. of the plate to the solid. In this chapter, methods to accomplish this coupling is examined.

The main reference throughout this section is the book 'Concepts and Applications of Finite Element Analysis', by Cook et.al. [5].

There are, in principle, two separate ways to include rotational coupling into the WFE software.

The first option is to rewrite the solid elements so that their nodal degrees of freedom include rotation. The coupling condition is then included by requiring the rotation of a plate element and a solid element to equal where they share the same node.

The second option is to let the rotation of the plate be constrained by neighboring nodes of the solid. This is most easily implemented if the plate node is placed on a boundary of the solid element but **not** sharing one of its nodes. The implementation of this second option may be made in several different ways. In WANDS these constraints are implemented with Lagrange multipliers.

7.2 Rotational degrees of freedom in solid elements

7.2.1 Assembling

If rotational degrees of freedom were to be implemented in the software the rotations at each node with at least one plate element joined to it, should assemble both displacement d.o.f. as well as the rotation. Rotation at nodes shared by solid elements only should not be assembled, since this would introduce an unnecessary constraint not needed in the C^0 continuity of solid elements. This means that the assembling algorithm must keep track of two separate node types both appearing for the solid elements.

7.2.2 Solid elements

Solid elements may be formed either ny introducing new shape functions or by transforming shape functions of existing elements, see p. 237-238 in [5]. In both ways care must also be taken when transforming the coordinates from the original 'type' elements to other geometries, i.e. dealing with Jacobians etc.

Another reported problem is that, if all nodes have the same rotation, no deformation of the element is possible, see p. 238 in [5]. This may be handled by introducing an additional energy into the elements for the difference between the midpoint rotation and the nodal rotations. One example of this is given in [16].

7.2.3 Conclusion

The many problems prevent this method from being used for coupling plate rotations to solids. In fact the only given rationale for introducing rotations into elements is for 2D plates. Also, at least in 3D, the problem above still seems to be the subject of research activity.

7.3 Rotational coupling by restraints

7.3.1 Restraints for rotational coupling

Consider two nodes, '1' and '2', of an element with linear interpolation (i.e. linear shape–functions). Any point 'p' on the element boundary joining the two nodes has the co-ordinates,

$$\mathbf{r}_p(\xi_p) = \mathbf{r}_m + \mathbf{r}_d\xi_p \tag{7.1}$$

where, $\xi_p \in [-1, 1]$ is the non–dimensional co-ordinate describing the position between the two nodes, (e.g. $\xi_p = 0$ is the midpoint between the nodes). $\mathbf{r}_m$ is the position vector for the midpoint and $\mathbf{r}_d$ is the unit directive vector.

$$\mathbf{r}_m = \frac{\mathbf{r}_2 + \mathbf{r}_1}{2} \tag{7.2}$$

and

$$\mathbf{r}_d = \frac{\mathbf{r}_2 - \mathbf{r}_1}{\|\mathbf{r}_2 - \mathbf{r}_1\|} \,. \tag{7.3}$$

where, $\| \cdot \|$ denotes the Euclidian norm.

For linear interpolating shape–functions, given the two displacement vectors, $\mathbf{u}_1 = \begin{bmatrix} u_1 & v_1 & w_1 \end{bmatrix}$ and $\mathbf{u}_2 = \begin{bmatrix} u_2 & v_2 & w_2 \end{bmatrix}$ of the respective node, the displacement at 'p' may be written as,

$$\mathbf{u}_p^{\mathrm{T}} = \mathbf{N}(\xi_p) \begin{bmatrix} \mathbf{u}_1^{\mathrm{T}} \\ \mathbf{u}_2^{\mathrm{T}} \end{bmatrix} \tag{7.4}$$

where, $\mathbf{N}(\xi) = \begin{bmatrix} \frac{1}{2}(1-\xi) & \frac{1}{2}(1+\xi) \end{bmatrix}$.

A small rotation at 'p' is given by,

$$\boldsymbol{\theta}_p = \nabla \times \mathbf{u}_p \tag{7.5}$$

Here, only the x component of $\boldsymbol{\theta}_p$ is sought. By using the chain rule of differentiation, this component is given by,

$$\theta_{px} = \frac{\partial w}{\partial \xi}\frac{\partial \xi}{\partial y} - \frac{\partial v}{\partial \xi}\frac{\partial \xi}{\partial z} \tag{7.6}$$

The differentiations, $\frac{\partial \xi}{\partial y}$ and $\frac{\partial \xi}{\partial z}$ may now be recognized as the the y and z components of the directive vector $\mathbf{r}_d$. The differentiations, $\frac{\partial w}{\partial \xi}$ and $\frac{\partial v}{\partial \xi}$ may be evaluated directly from equation (7.4). Consequently,

$$\theta_{px} = \frac{1}{2}(w_2 - w_1)r_{dy} - \frac{1}{2}(v_2 - v_1)r_{dz} \tag{7.7}$$

Equations, (7.4) and (7.7), gives constraints for any plate element node at the point 'p' as function of the position and displacements of nodes 1 and 2. **The derivation assumes that the node of the plate element is on the boundary of the solid element.** These constraints may be implemented in the FE–code in different ways as discussed in the following. To do so and to follow the notation in Cook these equations are rewritten as,

$$[\mathbf{C}]\mathbf{D} = \mathbf{0} \tag{7.8}$$

where $[\mathbf{C}]$ is known as the constraint matrix and $\mathbf{D}$ is the vector of degrees of freedom either involved in the restraints or of the whole system.

If node number 1 of the plate model is to be connected to nodes 1 and 2 of the solid model, $[\mathbf{C}]\mathbf{D}$ will be:

$$[\mathbf{C}]\mathbf{D} = \begin{bmatrix} \frac{1}{2}(1-\zeta) & 0 & 0 & \frac{1}{2}(1+\zeta) & 0 & 0 & -1 & 0 & 0 & 0 \\ 0 & \frac{1}{2}(1-\zeta) & 0 & 0 & \frac{1}{2}(1+\zeta) & 0 & 0 & -1 & 0 & 0 \\ 0 & 0 & \frac{1}{2}(1-\zeta) & 0 & 0 & \frac{1}{2}(1+\zeta) & 0 & 0 & -1 & 0 \\ 0 & \frac{1}{2}r_{dz} & -\frac{1}{2}r_{dy} & 0 & -\frac{1}{2}r_{dz} & \frac{1}{2}r_{dy} & 0 & 0 & 0 & -1 \end{bmatrix} \begin{bmatrix} u_{s1} \\ v_{s1} \\ w_{s1} \\ u_{s2} \\ v_{s2} \\ w_{s2} \\ u_{p1} \\ v_{p1} \\ w_{p1} \\ \phi_{p1} \end{bmatrix} \tag{7.9}$$

where subscripts s and p refer to 'solid' and 'plate' nodes respectively and columns of zeros are added for the dof's not included in the constraints.

7.3.2 Constraint implementation by transformation

Equation (7.8) may be rewritten to, see pages 272-273 in [5] for details.

$$\begin{bmatrix} \mathbf{D}_r \\ \mathbf{D}_c \end{bmatrix} = [\mathbf{T}]\mathbf{D}_r \tag{7.10}$$

where, $\mathbf{D}_r$ are the d.o.f. to be retained and $\mathbf{D}_c$ are those to be condensed out, (i.e. removed) and $[\mathbf{T}]$ is a transformation matrix. For the new system, for each of the system matrices, $\mathbf{K}_j$ and $\mathbf{M}_2$ we have,

$$\mathbf{K}_{new} = \mathbf{T}^{\mathrm{T}}\mathbf{K}_{old}\mathbf{T} \tag{7.11}$$

and

$$\mathbf{F}_{new} = \mathbf{T}^{\mathrm{T}}\mathbf{F}_{old} \tag{7.12}$$

for the forces. The new system then becomes singular and must be partitioned and rewritten into a a smaller system. Consequently there are many manipulations needed for creating the new system. Manipulations of smaller systems will appear if subsystems of the elements of concern are considered. Also there is a possibility not to partition and rewrite the equations, but this will result in singular matrices, reference [17].

Due to the many matrix manipulations the above method to implement constraints makes it less attractive.

7.3.3 Constraint implementation by Lagrange multipliers

This is the way the constraints are implemented in WANDS. Lagrange multipliers are introduced in the Lagrangian for Hamilton's principle by adding,

$$\boldsymbol{\lambda}^{\mathrm{T}}[\mathbf{C}]\mathbf{D}\,. \tag{7.13}$$

After applying calculus of variations, the new system then becomes,

$$\begin{bmatrix} \mathbf{K}(\kappa) - \omega^2\mathbf{M}_2 & \mathbf{C}^T \\ \mathbf{C} & \mathbf{0} \end{bmatrix} \begin{bmatrix} \mathbf{D} \\ \boldsymbol{\lambda} \end{bmatrix} = \begin{bmatrix} \mathbf{F} \\ \mathbf{0} \end{bmatrix} \tag{7.14}$$

Physically the Lagrangian multipliers $\boldsymbol{\lambda}$ can be seen as forces keeping the constrained d.o.f. in their correct position.

Two minor drawbacks will arise from the present method. Additional d.o.f. will be added to the system rather than condensed out. Furthermore there will be a larger bandwidth of the matrices. Since the problems at hand will have few constraints (i.e. points where plate elements meet solid elements) the added d.o.f. are not a big problem. The larger bandwidth may cause some problems when solving the complete system for each wave number and frequency with Gaussian elimination or LU factorization (as made in WANDS). However, an iterative solver is probably better, since the start vector may be taken as the solution of the last wavenumber calculated and thus yield a very fast convergence. For an iterative solver the bandwidth is of less importance.

The main advantage of Lagrange multipliers is that the method is simple to implement. Especially, the implementation can be made after assembling the two separate systems for the solid and the plate elements. The constraints may then be formulated and added to join the two systems. Of course the node numbers and involved d.o.f. must be handled, but the original systems does not change. Further information is found on p. 275-276 in [5].

7.3.4 Constraint implementation by penalty method

This method is somewhat similar to the Lagrange multiplier method, but instead of adding Lagrange multipliers a penalty function is added to the Lagrangian. Thus, the energy,

$$\frac{1}{2}\mathbf{D}^{\mathrm{T}}[\mathbf{K}_c]\mathbf{D} \tag{7.15}$$

is added, where,

$$[\mathbf{K}_c] = [\mathbf{C}]^{\mathrm{T}}[\boldsymbol{\alpha}][\mathbf{C}] \tag{7.16}$$

and $[\boldsymbol{\alpha}]$ is a diagonal matrix, with entries of large magnitude that must be chosen in some way. By substituting equation (7.16) into equation (7.15) it is seen that the penalty function becomes zero if the constraints, $[\mathbf{C}]\mathbf{D} = 0$ are met.

Physically the penalty matrix, $[\mathbf{K}_c]$, can be interpreted as springs holding the constraints in their right position. The implementation of the method seem to be the easiest of all methods explored here, since no new d.o.f. are introduced, though the bandwidth will generally still increase. The main drawback of the method is the way in which $[\boldsymbol{\alpha}]$ is to be chosen. If the entries in $[\boldsymbol{\alpha}]$ are too small the constraints will have no effect, whereas if they are too large numerical cancellation problems may occur.Further information is found on p. 276-278 in [5].

7.3.5 Conclusions

The 'Lagrange multiplier method' and the 'penalty method' are the two methods favoured by the author. This is mostly due to their simplicity, that enables the constraints to be added after forming unconstrained systems for the solid and plate elements. The penalty method has advantages in its simplicity, symmetry and physical interpretation. But the drawback is possible numerical problems. Thus the Lagrange multiplier method has been chosen for WANDS.

7.4 Validations

Two validations are considered. A model with simply supported sides is examined and compared with an analytical solution. Also, a beam with a triangular cross-section is modelled both with plate strip elements only and with one side modelled with solid elements. The results given in this section are for the Lagrange multiplier method.

7.4.1 Plate strip model

A model of a plate strip with simply supported edges is made. Sections 1 and 3 are modelled with plate strip elements whereas section 2 is modelled with 8–node solid elements. The rotation of the side of the solid elements is given by two of its corners. The reason for choosing 8-node elements is that 4-node elements use linear shape functions over its cross–section. These linear shape functions can not approximate thin plate bending within one element.

The plate strip is subdivided in three sections, section 1 with coordinates (0,0.25) section 2 with coordinates (0.25,0.75) and section 3 with coordinates (0.75,1). Each finite element has a width of 0.05 m. The material is steel and the thickness is 0.02 m.

7.4.2 Triangle model

Two triangle beams are modelled. One with plate strip elements only and one with one side modelled with solid 8-node elements.

The triangle has co–ordinates $(0, 0)$,$(0, 1)$ and $(0.5, -0.5)$. For the plate–strip model each side is divided into 9 equally spaced elements. For the plate–solid model, the

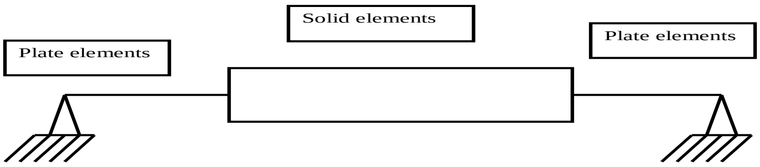

Figure 7.1: Plate strip

longest side is replaced with 30 solid elements. The material is steel and the thickness is 0.02 m.

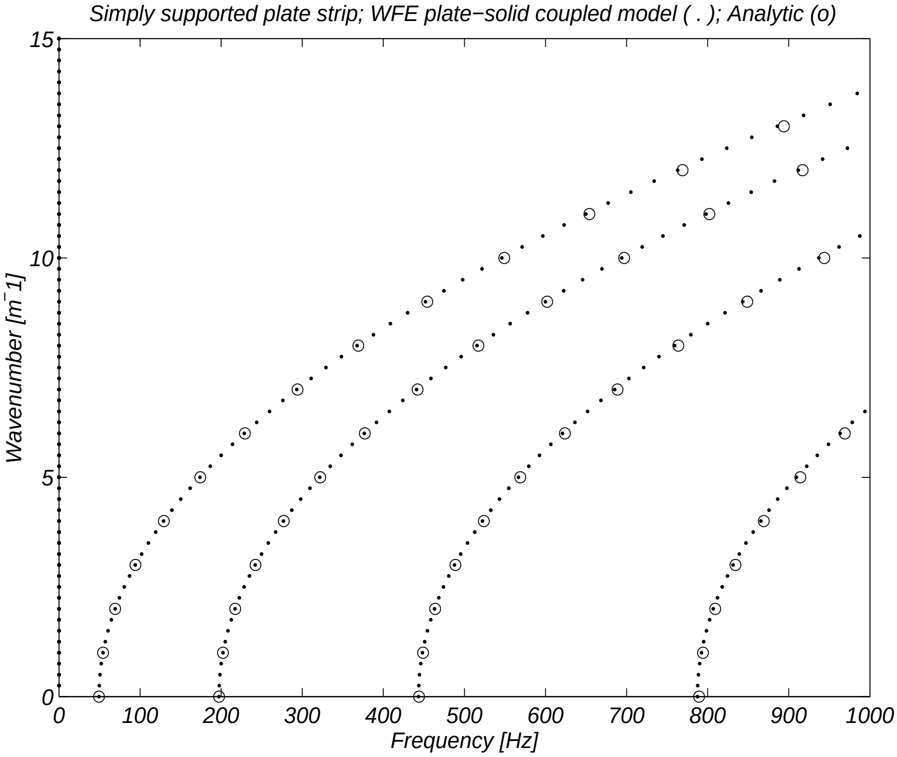

Figure 7.2: Dispersion relations for plate strip

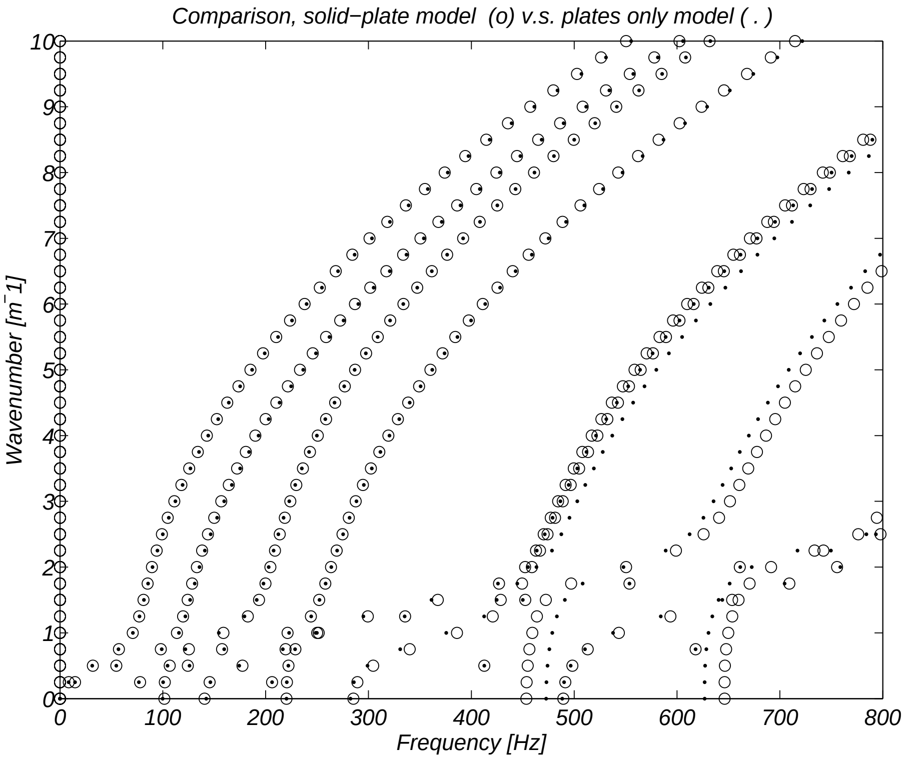

Figure 7.3: Dispersion relations for 'delta' beam

Chapter 8

Fluid finite elements

8.1 Frequency domain Lagrangian

The variation of a fluid Lagrangian, δL_f, may be defined by, [1].

$$\delta L_f = -\int_{t_1}^{t_2} \delta \left(U_f - T_f\right) - \delta W_{f,loss} \, dt \, , \tag{8.1}$$

where δ denotes first variation, t_1 and t_2 are the start and end times, U_f and T_f are the fluid potential and kinetic energy and $\delta W_{f,loss}$ is the virtual work from dissipative forces. In the absence of fluid–shell coupling, e.g. for rigid walls,

$$\delta L_f = 0 \, . \tag{8.2}$$

All terms in equation (8.1) are here required to be bilinear or quadratic functionals. This restriction is necessary since linear differential equations are sought. Furthermore, the system state at t_1 and t_2 is irrelevant, given that harmonic motion over a long period of time is considered. Thus, t_2 and t_1 may tend to $\pm\infty$ respectively without any loss of information.

Parseval's identity for two real valued functions, $f\left(t\right)$ and $g\left(t\right)$ yields,

$$\int_{-\infty}^{+\infty} f(t)\, g(t)\, dt = \int_{-\infty}^{+\infty} \hat{f}(\omega)^{*}\, \hat{g}(\omega)\, d\omega\,, \tag{8.3}$$

where t is time, ω is angular frequency, $*$ denotes complex conjugate and $\hat{}$ denotes the Fourier transform defined by,

$$\hat{g}(\omega) = \frac{1}{\sqrt{2\pi}} \int_{-\infty}^{+\infty} g(t)\, e^{-i\omega t} dt\,. \tag{8.4}$$

Applying Parseval's identity on equation (8.1) gives,

$$\delta L_f(\omega) = -\int_{-\infty}^{+\infty} \delta U_f(\omega) - \delta T_f(\omega) - \delta W_{f,loss}(\omega)\, d\omega\,. \tag{8.5}$$

Calculated response at different frequencies are independent when linear systems are considered. Consequently, a variational formulation defined for each frequency is given by,

$$\delta L_{f\omega}(\omega) = \delta T_f(\omega) - \delta U_f(\omega) + \delta W_{f,loss}(\omega)\;. \tag{8.6}$$

In the following $\delta L_{f\omega}$ is referred to as the fluid 'Lagrangian variation'. Each of the terms on the right hand side of equation (8.6) are treated independently in Section 8.2.

8.2 The fluid Lagrangian variation

In this thesis the fluid is considered to be 'ideal' or close to 'ideal', i.e. the fluid has low viscosity and low heat conductivity.

8.2.1 Velocity potential

Acoustic pressure, p, the change of density due to acoustic pressure, ρ_a and the fluid particle displacement, $\mathbf{u}_f$ in an ideal, undamped, fluid are related through the velocity potential ψ, such that, [18],

$$\frac{\partial \mathbf{u}_f}{\partial t} = -\mu \nabla \psi \,, \tag{8.7}$$

$$\rho_a = \mu \frac{\rho_f}{{c_f}^2} \frac{\partial \psi}{\partial t} \,, \tag{8.8}$$

and

$$p = \rho_f \, \mu \frac{\partial \psi}{\partial t} \,, \tag{8.9}$$

ρ_f is the fluid density at equilibrium, c_f is the sound velocity in an unbounded fluid and μ is a scaling constant introduced to enhance numerical stability in fluid–structure coupled systems.

8.2.2 Potential energy

From Temkin [18, Chapter 2.7], the acoustic potential energy per unit volume, $U_f^{'''}$ in an ideal fluid is given by,

$$U_f^{'''} = \frac{1}{2} \frac{c_f^2}{\rho_f} {\rho_a}^2 \tag{8.10}$$

Combining equation (8.10) with equation (8.8), and taking the first variation of $U_f^{'''}$ and applying the transformation to the frequency domain according to Section 1 yields the expression,

$$\delta U_f = \int \delta U_f^{'''} dV = \omega^2 \int \mu^2 \frac{\rho_f}{c_f^2} \, \delta \hat{\psi}^* \hat{\psi} \, dV \tag{8.11}$$

where V is the volume of the fluid and * denotes complex conjugate.

8.2.3 Kinetic energy

Also from [18], the kinetic acoustic energy, $T_f^{'''}$ per unit volume in an ideal fluid is given by,

$$T_f''' = \frac{1}{2}\rho_f \left\| \frac{\partial \mathbf{u}_f}{\partial t} \right\|^2 , \tag{8.12}$$

where, $\|\ldots\|$ symbolises the Euclidean norm. Combining Equation (8.12) with Equation (9.2), taking the first variation of T_f''' and applying the transformation to the frequency domain according to Section 1 yields,

$$\delta T_f = \int \delta T_f''' \, dV = \int \mu^2 \rho_f \, \nabla \delta \hat{\psi}^{\mathrm{H}} \nabla \hat{\psi} \, dV \, , \tag{8.13}$$

where, $^{\mathrm{H}}$ symbolises the conjugate transpose, i.e. $^{*\mathrm{T}}$.

8.2.4 Virtual work from dissipative forces

The virtual work from dissipative forces are treated similarly to those for structures. Consequently, it is found that dissipative forces can be accounted for by adding imaginary parts to the coefficients in δU_f and δT_f, i.e. to '$\mu^2 \frac{\rho_f}{c_f^2}$' and '$\mu^2 \rho_f$'. Hence, the coefficients, '$\mu^2 \frac{\rho_f}{c_f^2}$' and '$\mu^2 \rho_f$' in equations (8.11) and (8.13) are replaced by,

$$\mu^2 \rho_f \left(1 + i\eta_v\right) \quad \text{and} \quad \mu^2 \frac{\rho_f}{c_f^2} \left(1 - i\eta_e\right) \, , \tag{8.14}$$

where $\eta_v \geq 0$ and $\eta_e \geq 0$ are, the generally frequency dependent, damping coefficients.

Note that, the existence of a velocity potential, ψ, is valid since $\mathbf{u}_f$ is irrotational in ideal conditions. In practice, dissipative forces in fluids are commonly due to shear viscosity. This viscosity may cause a rotational velocity field. Thus, an introduction of dissipative forces due to shear viscosity may violate the assumptions leading to equations (8.11) and (8.13). However, if shear forces are small compared to the acoustic pressure the assumption of an 'ideal fluid' is still valid in practice.

8.2.5 Lagrangian variational statement

The Lagrangian variation for the fluid is now given by combining equations (8.6), (8.11), (8.13) and (8.14). The result is simply stated here:

$$\delta L_f = \mu^2 \int \rho_f(1+i\eta_v)\nabla\delta\hat{\psi}^{\mathrm{H}}\,\nabla\hat{\psi} - \omega^2(1-i\eta_e)\frac{\rho_f}{c_f^2}\;\delta\hat{\psi}^*\hat{\psi}\,dV \tag{8.15}$$

In the succeeding sections the coefficients, ρ_f and c_f are considered to be constant within each waveguide finite element. The scaling constant, μ, is required to be constant within the entire fluid.

8.3 Waveguide finite elements

8.3.1 Shape functions and cross section geometry

The waveguide finite element method yields wave equations along the waveguide. The dependence, with respect to the cross–section of a fluid element, is approximated with test- and shape-functions for the variation term and the velocity potential, respectively.

Assume that the velocity potential can be written with the śhape'-functions $\mathbf{N}_f$ as.

$$\hat{\Psi} = \mathbf{N}_f^{\mathrm{T}}\hat{\boldsymbol{\psi}}(x) \tag{8.16}$$

and similarly for $\delta\hat{\Psi}$. Then equation (8.15) can be rewritten with the aid of,

$$\int \nabla\delta\hat{\psi}\nabla\hat{\psi}\mathrm{dV} = \int\int \delta\boldsymbol{\psi}^{\mathrm{H}}\frac{\partial\mathbf{N}_{\mathrm{f}}}{\partial\mathrm{y}}\frac{\partial\mathbf{N}_{\mathrm{f}}^{\mathrm{T}}}{\partial\mathrm{y}}\hat{\boldsymbol{\psi}} + \delta\boldsymbol{\psi}^{\mathrm{H}}\frac{\partial\boldsymbol{N}_{\mathrm{f}}}{\partial\mathrm{z}}\frac{\partial\mathbf{N}_{\mathrm{f}}^{\mathrm{T}}}{\partial\mathrm{z}}\hat{\boldsymbol{\psi}} + \frac{\partial\delta\hat{\boldsymbol{\psi}}^{\mathrm{H}}}{\partial\mathrm{x}}\mathbf{N}_{\mathrm{f}}\mathbf{N}_{\mathrm{f}}^{\mathrm{T}}\frac{\partial\hat{\boldsymbol{\psi}}}{\partial\mathrm{x}}\mathrm{dAdx} \tag{8.17}$$

and

$$\int \delta\hat{\boldsymbol{\psi}}\hat{\psi}\mathrm{d}V = \int\int \delta\hat{\boldsymbol{\psi}}^{\mathrm{H}}\mathbf{N}_f\mathbf{N}_f^{\mathrm{T}}\hat{\boldsymbol{\psi}}\mathrm{d}A\mathrm{d}x \tag{8.18}$$

The routines used for integration over the cross section of solid elements can be used for the fluid finite elements as well. The resulting equation of motion for a single fluid element is,

$$\delta L_f = \int \delta\hat{\boldsymbol{\psi}}^{\mathrm{H}}\mathbf{b}_{00}\hat{\boldsymbol{\psi}} + \frac{\partial\delta\hat{\boldsymbol{\psi}}^{\mathrm{H}}}{\partial x}\mathbf{b}_{11}\frac{\partial\hat{\boldsymbol{\psi}}}{\partial x} - \omega^2\delta\hat{\boldsymbol{\psi}}^{\mathrm{H}}\mathbf{n}_2\hat{\boldsymbol{\psi}}\mathrm{d}x \tag{8.19}$$

Note that the potential energy here gives the term proportional to ω^2 whereas the kinetic energy gives the terms proportional to the derivatives with respect to the x-axis. This is the reason for the minus sign in equation (8.1).

The assembling of the fluid elements is carried out as for solid and plate elements, the resulting equation in the absence of coupling is thus written as,

$$\int \delta\hat{\boldsymbol{\Psi}}^{\mathrm{H}}\mathbf{B}_{00}\hat{\boldsymbol{\Psi}} + \frac{\partial\delta\hat{\boldsymbol{\Psi}}^{\mathrm{H}}}{\partial x}\mathbf{B}_{11}\frac{\partial\hat{\boldsymbol{\Psi}}}{\partial x} - \omega^2\delta\hat{\boldsymbol{\Psi}}^{\mathrm{H}}\mathbf{N}_2\hat{\boldsymbol{\Psi}}\mathrm{d}x = \mathbf{0} \tag{8.20}$$

The zero right hand side of this equation is because there are no external sources implemented in WANDS, although this could easily be implemented. The weak form of equation (8.21) can be integrated by parts as for solid and plate elements to give the strong form,

$$-\mathbf{B}_{11}\frac{\partial^2\hat{\boldsymbol{\Psi}}}{\partial x^2} + \mathbf{B}_{00}\hat{\boldsymbol{\Psi}} - \omega^2\mathbf{N}_2\hat{\boldsymbol{\Psi}} = \mathbf{0} \tag{8.21}$$

which is the waveguide FE model for a fluid.

Chapter 9

Fluid FE coupling to Plate FE and Solid FE

The coupling between fluid finite elements and plate finite element is in theory virtually the same as that between fluid finite elements and solid finite elements. Hence, this chapter is focused on the derivation of the coupling between fluid and plate elements. The small differences are noted in section 9.5.

9.1 Frequency domain coupling functional

From Chapter 1 in [1] a functional describing coupling between a fluid and a shell over a wetted surface S, is given by,

$$\delta B_c = -\int\limits_S \rho_f \, \mu \int\limits_{t_1}^{t_2} \frac{\partial \delta\psi}{\partial t} \, w + \delta w \, \frac{\partial \psi}{\partial t} \, dt \, dS \,, \tag{9.1}$$

where, t denotes time, ρ_f is the fluid density at equilibrium, μ is a positive scaling constant, δ denotes first variation, w is the shell normal displacement into the fluid and ψ is the fluids velocity potential defined by,

$$\frac{\partial \mathbf{u}_f}{\partial t} = -\mu \nabla \psi \,, \tag{9.2}$$

where, $\mathbf{u}_f$ is the fluid particle displacement. The first term in equation (9.1) is the virtual work from the plate on the fluid and the second term is the virtual work from the fluid on the plate.

The system state at t_1 and t_2 is irrelevant, given that harmonic motion over a long period of time is considered. Thus, t_2 and t_1 may tend to ±∞ respectively without any loss of information.

Parseval's identity for two real valued functions, $f(t)$ and $g(t)$ yields,

$$\int\limits_{-\infty}^{+\infty} f(t)\; g(t)\; dt = \int\limits_{-\infty}^{+\infty} \hat{f}(\omega)^{*}\; \hat{g}(\omega)\; d\omega\,, \tag{9.3}$$

where t is time, ω is angular frequency, $*$ denotes complex conjugate and ^ denotes the Fourier transform defined by,

$$\hat{g}(\omega) = \frac{1}{\sqrt{2\pi}} \int\limits_{-\infty}^{+\infty} g(t)\, e^{-i\omega t} dt\,. \tag{9.4}$$

Letting t_1 and t_2 tend to ±∞ and applying Parseval's identity to equation (9.1) gives,

$$\delta B_c(\omega) = i\omega \int\limits_{S} \rho_f\, \mu \int\limits_{-\infty}^{\infty} \delta\hat{\psi}^{*}\, \hat{w} - \delta\hat{w}^{*}\, \hat{\psi}\, d\omega\, dS\,. \tag{9.5}$$

Calculations of the response at different frequencies are independent when linear systems are considered. Consequently, a variational formulation defined for each frequency is given by,

$$\delta B_c(\omega) = i\omega\, \mu \int\limits_{S} \rho_f \left(\delta\hat{\psi}^{*}\, \hat{w} - \delta\hat{w}^{*}\, \hat{\psi}\right)\, dS\,, \tag{9.6}$$

where, μ is taken out of the integral since it is required to be constant throughout the fluid.

9.2 Fluid shell coupling elements

9.2.1 Sign convention

Equation (9.1) and consequently equation (9.5) are defined so that a positive value of the shell displacement, w, corresponds to displacement into the fluid. This fact must be considered when fluid–shell coupling is introduced into the waveguide finite element model. In WANDS a coordinate interior to the fluid must be specified. Two vectors are then formed. The first, $\mathbf{r_{12}}$, is between the first and second local nodes of the wetted edge of the element (assuming that this is the same for both elements). The second,$\mathbf{r_{10}}$, is between the first local element node and the interior node in the fluid. The sign of the cross product between the two vectors, i.e.

$$sign(\mathbf{r}_{12} \times \mathbf{r}_{10}) \tag{9.7}$$

then gives the direction of the displacement. Figure 9.1 shows two adjoining fluid and plate elements. If the node numbering of the coupled elements differs, the sign is switched.

The co-ordinates for the two nodes 'i' and 'l' coincide. Similarly, nodes 'j' and 'm' also coincide. Node 'k' is an internal node in the fluid, not to be connected to a shell element. Upon requesting that the local z-coordinate of the shell element points into the fluid, a positive out-of-plane displacement, w, corresponds to displacement into the fluid. The node numbering is then chosen such that,

Node 'i' is the local node 1 or 2 of the fluid element.

Node 'l' is the local node 1 of the plate element.

Node 'j' is the local node 2 or 3 of the fluid element.

Node 'm' is the local node 2 of the plate element.

9.2.2 Shape–functions

Trial and test-functions are chosen equal in the following description and referred to as 'shape–functions'. The shape-functions for the velocity potential, $\hat{\psi}$ and the plate

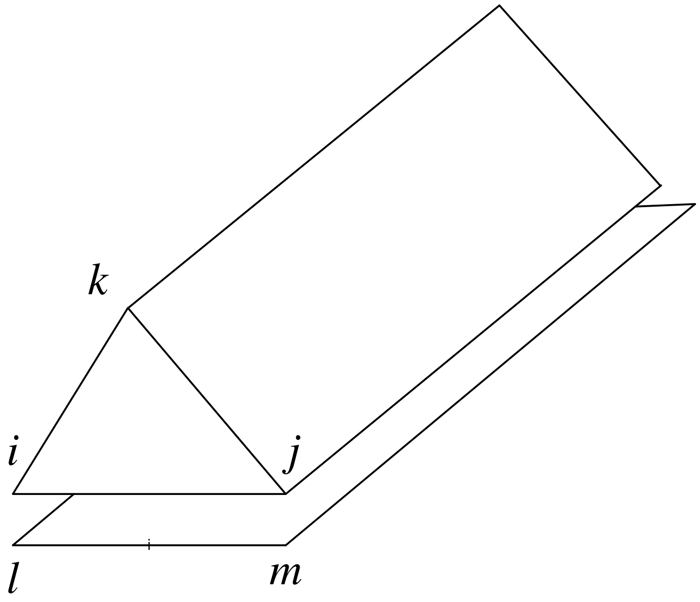

Figure 9.1: Plate and fluid element

or shells out of plane displacement $\hat{w}$ are described in Chapter 8 and 5 respectively.

Shape functions for plate

From Chapter 5, the out-of-plane displacement of the plate is denoted $\hat{w}$. The element interpolation of $\hat{w}$ and $\delta\hat{w}$ is written,

$$\hat{w} = \mathbf{N}_b^{\mathrm{T}}\left(\vartheta\right)\hat{\mathbf{w}}\left(\mathbf{x}\right) \qquad \delta\hat{w}^* = \delta\hat{\mathbf{w}}\left(\mathbf{x}\right)^{\mathrm{H}}\mathbf{N}_b\left(\vartheta\right)\ , \tag{9.8}$$

where

$$\hat{\mathbf{w}} = \left[\begin{array}{cccc} \hat{w}_1 & \hat{\phi}_1 & \hat{w}_2 & \hat{\phi}_2 \end{array}\right]^{\mathrm{T}} \quad , \quad \delta\hat{\mathbf{w}} = \left[\begin{array}{cccc} \delta\hat{w}_1 & \delta\hat{\phi}_1 & \delta\hat{w}_2 & \delta\hat{\phi}_2 \end{array}\right]^{\mathrm{T}}, \tag{9.9}$$

and

$$\mathbf{N}_b(\vartheta) = \begin{bmatrix} \frac{1}{4}\left(2 - 3\vartheta + \vartheta^3\right) \\ \frac{a}{4}\left(1 - \vartheta - \vartheta^2 + \vartheta^3\right) \\ \frac{1}{4}\left(2 + 3\vartheta - \vartheta^3\right) \\ \frac{a}{4}\left(-1 - \vartheta + \vartheta^2 + \vartheta^3\right) \end{bmatrix}. \tag{9.10}$$

w_1, w_2 θ_1 and θ_2 are the displacements and rotations about the x-axis for the respective nodes.

Shape functions for fluid

For linear elements, the interpolation of $\hat{\psi}$ on the wetted surface between nodes 1 and 2 is written,

$$\hat{\psi} = \begin{bmatrix} \xi_1 & \xi_2 \end{bmatrix} \begin{bmatrix} \hat{\psi}_1(z) \\ \hat{\psi}_2(z) \end{bmatrix} \tag{9.11}$$

where,$\hat{\psi}_1(z)$ is the value of $\hat{\psi}$ at node 1 and $\hat{\psi}_2(z)$ is the value of $\hat{\psi}$ at node 2. The triangular co–ordinates ξ_1 and ξ_2 vary linearly between node 1 and node 2. At node 1,

$$\begin{bmatrix} \xi_1 & \xi_2 \end{bmatrix} = \begin{bmatrix} 1 & 0 \end{bmatrix} \tag{9.12}$$

and at node 2,

$$\begin{bmatrix} \xi_1 & \xi_2 \end{bmatrix} = \begin{bmatrix} 0 & 1 \end{bmatrix} \tag{9.13}$$

Thus, on the wetted surface, the relation between ξ_1, ξ_2 and ϑ is,

$$\xi_1 = \frac{1}{2}(1 - \vartheta) \text{ and } \xi_2 = \frac{1}{2}(1 + \vartheta) \tag{9.14}$$

Consequently, the shape functions for $\hat{\psi}$ along the wetted surface are the same as those for the linearly dependent in–plane displacements of a plate strip, i.e. $\hat{u}$ and $\hat{v}$, see Chapter 5. Hence, following the notations there, $\mathbf{N}_p$ is now defined as,

$$\mathbf{N}_p = \begin{bmatrix} \xi_1 & \xi_2 \end{bmatrix}^{\mathrm{T}} \tag{9.15}$$

.

Similar expressions are given for quadratic and cubic fluid elements.

9.2.3 coupling element

In Cartesian co–ordinates a small wetted surface area element is, dS = dx dy. Consequently, with the interpolations for $\hat{\psi}$ and $\hat{w}$ given above, the sought coupling element is described by,

$$\delta B_{fc,\omega} = i\omega \int \begin{bmatrix} \delta\hat{\boldsymbol{\psi}}^{\mathrm{H}} & \delta\hat{\mathbf{w}}^{\mathrm{H}} \end{bmatrix} \mathbf{m}_1 \begin{bmatrix} \hat{\boldsymbol{\psi}} \\ \hat{\mathbf{w}} \end{bmatrix} \mathrm{dx} \tag{9.16}$$

where,

$$\mathbf{m}_1 = \rho_f\, \mu \begin{bmatrix} & \mathbf{I}_1 \\ -\mathbf{I}_1{}^{\mathrm{T}} & \end{bmatrix}, \tag{9.17}$$

and

$$\mathbf{I}_1 = a \int\limits_{-1}^{+1} \mathbf{N}_p\,(\vartheta)\, \mathbf{N}_b^{\mathrm{T}}\,(\vartheta)\, \mathrm{d}\vartheta\,, \tag{9.18}$$

This integral is evaluated analytically. The matrices $\mathbf{I_1}$ are subsequently assembled into coupling matrices $\mathbf{C_1}$.

9.3 Coupling model in terms of matrices

The coupling will add off-diagonal block matrices that couple the two systems. With the chosen formulation a coupled fluid shell system may be written as,

$$\mathbf{K}_4(-i\kappa)^4 + \mathbf{K}_2(-i\kappa)^2 + \mathbf{K}_1(-i\kappa) + \mathbf{K}_0 + i\omega\mathbf{M}_1 - \omega^2\mathbf{M}_2 = \mathbf{F} \tag{9.19}$$

where the $\mathbf{K}$ matrices and the $\mathbf{M}_2$ matrix are formed of the fluid FE and plate FE models such that,

$$\mathbf{K}_j = \begin{bmatrix} \mathbf{K}_{jf} & \mathbf{0} \\ \mathbf{0} & \mathbf{K}_{jp} \end{bmatrix} \tag{9.20}$$

where indices f and p denotes fluid and plate *subsystems* respectively. The $\mathbf{M}_2$ consist of corresponding block matrices from the two sub-models . The coupling matrix $\mathbf{M}_1$ has off diagonal coupling block matrices, such that,

$$\mathbf{M}_1 = \begin{bmatrix} \mathbf{0} & \mathbf{C}_1 \\ -\mathbf{C}_1^{\mathrm{T}} & \mathbf{0} \end{bmatrix} \tag{9.21}$$

Hence, $i\omega\mathbf{M}_1$ can be seen as a gyroscopic coupling matrix.

9.4 Validation

The validation here is made for linear triangular fluid elements only. This is mostly because such elements are easy to mesh with the PDE-toolbox found in MATLAB. A fluid filled pipe modelled with fluid-shell coupled waveguide finite elements derived at KTH by Nilsson and Finnveden, [19], [1] and [20] are used here as a referenced example. These elements in turn have been validated against an axi-symmetric formulation derived by Finnveden [12].

The mesh is seen in Figure 9.2.

The parameters are chosen to resemble a 5 mm thick steel pipe filled with water. The dispersion relations are given by solving the quadratic eigenproblem,

$$\mathbf{K}_4(-i\kappa)^4 + \mathbf{K}_2(-i\kappa)^2 + \mathbf{K}_1(-i\kappa)^1 + \mathbf{K}_0 + i\omega\mathbf{M}_1 - \omega^2\mathbf{M}_2 = \mathbf{0} \tag{9.22}$$

The dispersion relations are plotted in Figure 9.3, together with those for the reference. The only difference between these two models is that the reference model includes bubble degree of freedoms for the inplane motion of the plate elements.

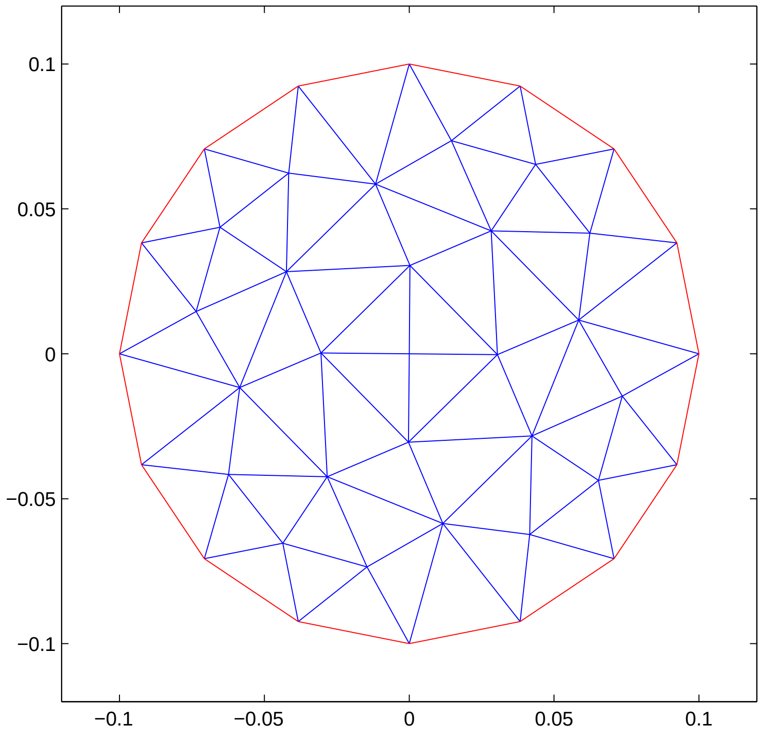

Figure 9.2: Mesh of a fluid filled pipe

The rings denote the WANDS model and, as can be seen, there is very little difference between the models.

9.5 Fluid finite element coupling to solid finite elements

The theory for coupling fluid finite elements to solids is essentially the same as the coupling to plate elements. The main difference is that the out of plane shape functions for the solid differs from the plate strip. As for the fluid elements there are three different forms of these shape functions along the wetted edge. To simplify the programming, coupling is restricted to elements of the same type, *i.e.* linear fluid elements can only be coupled to linear solid elements and likewise for quadratic and cubic elements. Since all fluid and solid elements are required to have counterclockwise local node numbering, the direction of the coupling might be simplified. The internal node is however still used in WANDS.

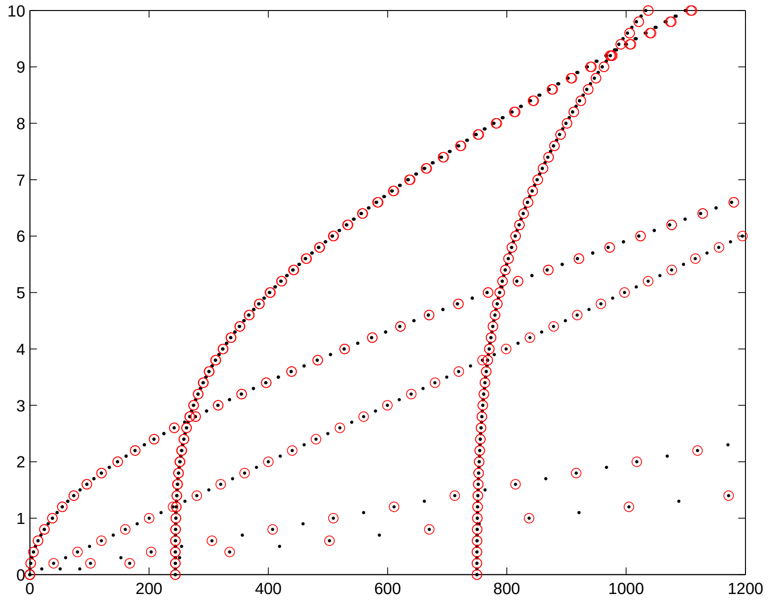

Figure 9.3: Dispersion curves for a fluid filled pipe

Chapter 10

Fluid Boundary Elements

10.1 Hamiltons principle

Consider a fluid system. Hamilton's principle for the system is written,

$$\delta L_f = \int_{t_1}^{t_2} \delta\left(U_f - T_f\right) - \delta W_{f,e} - \delta W_{f,s}\, dt = 0\,, \tag{10.1}$$

where,

U_f is the potential energy of the fluid system,

T_f is the kinetic energy of the fluid,

$\delta W_{f,e}$ is the virtual work from external sources,

$\delta W_{f,s}$ is the virtual work from the solid at the systems' shared boundary.

For reasons later to be apparent, the fluid is considered undamped, thus the virtual work from internal forces is not included in equation (10.1).

Let $t_{1,2} \rightarrow \mp\infty$ respectively and subsequently apply Parseval's identity to obtain the frequency domain relations. Due to linearity, each frequency may then be considered independently.

10.2 Energy variations and virtual work

The velocity potential Ψ, is defined such that,

$$\nabla(\Psi) = -\mathbf{v} \tag{10.2}$$

and

$$p = \rho \frac{\partial \Psi}{\partial t} \tag{10.3}$$

where $\mathbf{v}$ is the particle velocity. In the frequency domain, the variation of the potential and kinetic energies become, [1]

$$\delta U_f = \rho \int_V k^2 \delta \hat{\Psi}^* \hat{\Psi} \mathrm{dV} \tag{10.4}$$

where $k = \frac{\omega}{c}$ is the wavenumber of freely propagating waves, *omega* is the angular frequency, c is the velocity of the fluid and ρ is the fluid density.

$$\delta T_f = \rho \int_V \nabla(\delta \hat{\Psi})^{\mathrm{H}} \nabla(\hat{\Psi}) \mathrm{dV} \tag{10.5}$$

The virtual work from prescribed displacements at the boundary is defined as, see [1] (p. 38).

$$\delta W_{f,s} = -\int_S \delta p \, \mathbf{u} \cdot \mathrm{d}\mathbf{S} \tag{10.6}$$

where, $\mathbf{u}$ is the particle displacement, S is the boundary surface of the fluid and $\mathrm{d}\mathbf{S} = \mathbf{n}\mathrm{d}S$, with $\mathbf{n}$ being the unit normal vector out of the fluid domain. Substituting the velocity potential into equation (10.6), we have,

$$\delta W_{f,s} = -\rho \int_S \delta \Psi^* \frac{\partial \Psi}{\partial \mathbf{n}} \mathrm{d}S \tag{10.7}$$

The ‘external’ forces can be seen as a large number of line sources, Q_i. For simplicity each monopole source is taken individually. The total contribution from all sources can then found by considering a source at an arbitrary position. Thus,

$$\delta W_{f,e} = \int_V \delta\Psi^* Q_i \mathrm{d}V \tag{10.8}$$

where $Q_i = -\hat{Q}_i(x)\delta(\mathbf{r} - \mathbf{r}_i)$. δ is the dirac function $\mathbf{r}$ is the coordinate in the y-z plane of an arbitrary point and $\mathbf{r}_i$ is the coordinate of the line source in the y–z plane.

10.3 Boundary equation

10.3.1 Greens formula

Applying Green's formula to equation (10.5) results in,

$$\rho \int_V \nabla(\delta\hat{\Psi})^{\mathrm{H}} \nabla(\hat{\Psi})\mathrm{dV} = \rho \left(\int_{\mathrm{S}} \Psi \frac{\partial \delta\Psi^*}{\partial \mathbf{n}} - \int_{\mathrm{V}} \delta\Psi^* \triangle \Psi \mathrm{dV} \right) \tag{10.9}$$

Substituting and rearranging equations (10.1), (10.5), (10.4) and (10.9) into equation (10.1), yields,

$$\rho \left(\int_V k^2 \delta\hat{\Psi}^* \hat{\Psi} + \delta\hat{\Psi}^* \triangle \hat{\Psi} \mathrm{d}V \right) + \rho \left(\int_S \delta\hat{\Psi}^* \frac{\partial \hat{\Psi}}{\partial \mathbf{n}} - \Psi \frac{\partial \delta\hat{\Psi}^*}{\partial \mathbf{n}} \right) \tag{10.10}$$

10.3.2 Wavenumber domain

At this stage a second Fourier transformation to the wavenumber domain, with κ being the wavenumber along the x-axis, is made by letting the length of the waveguide tend to infinity and applying Parseval's identity. With the same argument as for the frequency transform, the wavenumber integral is then dropped. The result is written,

$$\rho \int_A \delta\tilde{\Psi}^* \left(\triangle_{\mathrm{2D}} \tilde{\Psi} + (k^2 - \kappa^2)\tilde{\Psi} + \tilde{Q}_i \delta(\mathbf{r} - \mathbf{r}_i) \right) \mathrm{d}A + \left(\int_\Gamma \delta\tilde{\Psi}^* \frac{\partial \tilde{\Psi}}{\partial \mathbf{n}} - \Psi \frac{\partial \delta\tilde{\Psi}^*}{\partial \mathbf{n}} \, \mathrm{d}\Gamma \right) \tag{10.11}$$

where, $\triangle_{\mathrm{2D}} = \frac{\partial^2}{\partial y^2} + \frac{\partial^2}{\partial z^2}$, A is the area of the domain and Γ is the boundary. Both integrals in (10.11) are now required to equal zero.

10.3.3 Greens functions

By requiring the first integral in equation (10.11) to equal 0 for all possible choices of $\delta\Psi^*$ we have,

$$\triangle_{2\mathrm{D}}\tilde{\Psi} + (k^2 - \kappa^2)\tilde{\Psi} = -\tilde{Q}_i\delta(\mathbf{r} - \mathbf{r}_i) \tag{10.12}$$

Wave solution

If $k^2 > \kappa^2$, the solution to equation (10.12) is generally written,

$$\tilde{\Psi} = AH_0^1(r\sqrt{k^2 - \kappa^2}) + BH_0^2(r\sqrt{k^2 - \kappa^2}) \tag{10.13}$$

for $r \neq 0$, where H_0^1 and H_0^2 are Hankel functions of order zero of the first and second kind respectively, $r = \|\mathbf{r} - \mathbf{r}_0\|$ and A and B are real constants. With the convention of time dependence $\propto e^{i\omega t}$, H_0^1 represents an incoming wave, whereas H_0^2 represents an outgoing wave. Thus $A = 0$.

The coefficient B is determined by considering the integral about the source point. For $\tilde{Q}_i = 1$ this yields, (see [Wu] Chapter3) $B = -\frac{\mathrm{i}}{4}$.

Nearfield solution

If $\kappa^2 > k^2$ we have the general solution,

$$\tilde{\Psi} = CK_0(r\sqrt{\kappa^2 - k^2}) + DI_0(r\sqrt{\kappa^2 - k^2}) \tag{10.14}$$

where K_0 and I_0 are modified Bessel functions. Since, $I_0(r) \to \infty$ as $r \to \infty$, $D = 0$. The constant C is evaluated by substituting equation (10.14) into equation (10.12) and integrating over the area in the vicinity of the source. Again set $\tilde{Q}_i = 1$, then, we have,

$$\begin{matrix}\lim \\ r \to 0\end{matrix} \int_{\Gamma_0} \frac{\partial\tilde{\Psi}}{\partial\mathbf{n}} \mathrm{d}\Gamma_0 = -1 \tag{10.15}$$

By substituting to polar co-ordinates and using the limit ([21] p 240),

$$\lim_{x \to 0} K_0(x) = -\ln(x) \tag{10.16}$$

it is found that, $C = 1/(2\pi)$. Inserting this value of C into equation (10.14) gives the Green's function for the near-field solution. By allowing complex values in K_0, this Green's function is actually valid for all arguments α, as discussed in 10.5. Therefore it is the only Green's function used in WANDS.

10.3.4 Boundary integral

With the first integral in equation (10.11) solved, the focus is turned to the second, which is also required to be zero. As for the first, area, integral, the second, boundary, integral is written as a sum of two integrals. The first of these is over the boundary of the fluid and the second over the boundary in the vicinity of the source. Thus,

$$\int_\Gamma \delta\tilde{\Psi}^* \frac{\partial\tilde{\Psi}}{\partial\mathbf{n}} - \Psi\frac{\partial\delta\tilde{\Psi}^*}{\partial\mathbf{n}}\,\mathrm{d}\Gamma = \lim_{\mathrm{r} \to 0} \int_{\Gamma_0} \delta\tilde{\Psi}^* \frac{\partial\tilde{\Psi}}{\partial\mathbf{n}} - \Psi\frac{\partial\delta\tilde{\Psi}^*}{\partial\mathbf{n}}\,\mathrm{d}\Gamma_0 + \int_\Gamma \delta\tilde{\Psi}^* \frac{\partial\tilde{\Psi}}{\partial\mathbf{n}} - \Psi\frac{\partial\delta\tilde{\Psi}^*}{\partial\mathbf{n}}\,\mathrm{d}\Gamma = 0 \tag{10.17}$$

The virtual velocity potential $\delta\Psi$ is chosen as a numerical approximation. Thus $\delta\Psi$ is expressed analytically at $\mathbf{r} = \mathbf{r}_0$. By noting this, the first integral on the right hand side may be evaluated as,

$$\lim_{r \to 0} \int_{\Gamma_0} \delta\tilde{\Psi}^* \frac{\partial\tilde{\Psi}}{\partial\mathbf{n}} - \Psi\frac{\partial\delta\tilde{\Psi}^*}{\partial\mathbf{n}}\,\mathrm{d}\Gamma_0 = \delta\Psi^*(\mathbf{r_0})\mathrm{C}(\mathbf{r_0}) \tag{10.18}$$

where,

$$C(\mathbf{r_0}) = \lim_{r \to 0} \int_{\Gamma_0} \frac{\partial\Psi_L}{\partial\mathbf{n}}\mathrm{d}\Gamma_0 \tag{10.19}$$

and Ψ_L is the solution of Laplace equation, i.e. the solution of equation (10.12) with $k^2 - \kappa^2 = 0$. Substituting equation (10.24) into equation (10.17) yields,

$$C(\mathbf{r_0})\delta\Psi^*(\mathbf{r_0}) = -\int_\Gamma \delta\tilde{\Psi}^* \frac{\partial\tilde{\Psi}}{\partial\mathbf{n}} - \Psi\frac{\partial\delta\tilde{\Psi}^*}{\partial\mathbf{n}}\ \mathrm{d}\Gamma \tag{10.20}$$

10.3.5 Wavedomain BE-model

By approximating $\delta\Psi^*$ with piecewise polynomials and evaluating equation (10.20) for each node on the boundary, a system of equations is obtained. Since there is little difference between the wavedomain BE equations and normal 2D BE equations, it is natural to base a WBE program on 2D BE software. Here a 2D BE code made by Wu [6] has been modified. The details of the code are found in Chapter 2 in [6]. In WANDS, the resulting matrix equation is written,

$$\mu\mathbf{H}\tilde{\Psi} + \mu\mathbf{G}\frac{\partial\tilde{\Psi}}{\partial\mathbf{n}} = \frac{-\mathbf{p}_{in}}{i\omega} \tag{10.21}$$

where μ is a scalar scaling coefficient introduced to improve conditioning numbers see [1] (Chapter 3). **H** and **G** are generally full non-symmetric complex valued matrices.

Equation (10.21) gives the relation between $\tilde{\Psi}$ and $\frac{\partial\tilde{\Psi}}{\partial\mathbf{n}}$, (or pressure and normal velocity).

10.3.6 Robin boundary condition

Equation (10.21) does not provide a fully determined system. In addition to equation (10.21) another relation between the boundary pressure and the velocity has to be given. This second set of conditions are due to the specifics of the boundary, rather than the fluid around it. There may either be boundary conditions specifying a coupling to another system or there may be a local boundary conditions such as a moving surface or an acoustic impedance. The latter can be described as Robin (or impedance) boundary conditions. Then for each node we have,

$$C_a\, p + C_b\, v_n = C_c \tag{10.22}$$

which may also be written as a matrix equation,

$$\mathbf{Ca}\,\mathbf{p} + \mathbf{Cb}\,\mathbf{v}_n = bf\tilde{c}c \tag{10.23}$$

Since part of the boundary may couple to other subsystems the number of boundary conditions may be less than the number of nodes in the fluid BE model. Hence equation (10.23) may not have square matrices. Also, internally in WANDS, equation (10.23) is expressed in terms of the velocity potential and it's normal derivative. The physical interpretation is however clearer from (10.22) and the coefficients C_a, C_b and C_c are given as input data to WANDS.

10.4 Difference compared to existing 2D BE software

Equations (10.11) and (10.12) show that the only difference from a 2D BE method is that two different Green's-functions must be used. For $k > \kappa$ the ordinary 2D Green–function is used, with the input argument $(kr) \rightarrow (r\sqrt{k^2 - \kappa^2})$. For $\kappa > k$ a nearfield Green–function with the argument $(r\sqrt{\kappa^2 - k^2})$ is used.

Besides the introduction of a new Green's-function for the nearfield solution, it should also be noted that Wu approximates the pressure, p and normal velocity v_n rather than the velocity potential $\delta\Psi^*$ and its normal derivative . Thus equation (10.24) is written,

$$C(\mathbf{r_0})\tilde{p}(\mathbf{r}_0) = -\int_{\Gamma} \left(i\rho\omega\tilde{v}_n\Psi + \tilde{p}\frac{\partial\tilde{\Psi}}{\partial\mathbf{n}} \right) \mathrm{d}\Gamma \tag{10.24}$$

which is exactly the same expression as in [6] page 31, but with $\tilde{p}$ and $\tilde{v}_n$ given in the wave domain.

The main difference in WANDS is that the argument into the Greens function is $\alpha = \sqrt{k^2 - \kappa^2}$ instead of k, and that the Green's function is also valid for imaginary values of α.

In [6] the (2D) Boundary Element model for a fluid is given as,

$$[\mathbf{A}]\,\hat{\mathbf{y}} = \hat{\mathbf{a}} \tag{10.25}$$

where $\mathbf{A} = \mathbf{A}(\omega)$ is the system matrix, $\hat{\mathbf{y}}$ are the unknown pressures or velocities and $\hat{\mathbf{a}}$ are the known pressures or velocities.

This is different from equation (10.21) because equation (10.25) also includes the boundary conditions. This gives smaller equations, but will be a cumbersome procedure when some of the boundary conditions are replaced by couplings to surrounding subsystems. Therefore equation (10.25) is not used in WANDS. Another, smaller difference is that WANDS includes an option of using half-infinite spaces.

10.4.1 Note about Laplace equations

By letting $r \to 0$ the 2D Laplace equation is obtained. The solution to this equation is used for calculating the coefficient $C(\mathbf{r_0})$ in Wu's BE-code. Both the wave and near–field solution tend to $-1/(2\pi)\ln(r)$ as $\kappa \to k$. Thus there is no need to change this part of the 2D code.

10.5 General Green's function

In the above derivation, the fluid is assumed undamped. For damped fluids k^2 becomes complex. In that case there is a need to find a Green's-function for any possible choice of $(k^2 - \kappa^2)$. Choose the time dependence $\propto e^{+i\omega t}$. Due to axial symmetry about the point source, for simplicity located at $r_0 = 0$, equation (10.12) is rewritten as,

$$r^2 \frac{d^2\Psi}{dr^2} + r\frac{d\Psi}{dr} + \alpha^2 r^2 \Psi = 0 \tag{10.26}$$

for any point $r \neq 0$. Note that α^2 is generally a complex number.

10.5.1 Upper half plane Green's function

$\Re(\alpha)$ may be either positive or negative. With the chosen time dependence and κ^2 real, damping requires that $\Im(\alpha^2) \geq 0$. The general solution to equation (10.26) is then,

$$\Psi = AK_0(\alpha r) + BI_0(\alpha r) \tag{10.27}$$

where $\alpha = \sqrt{\alpha^2}$. Since equation (10.26) is a second order equation, the two solutions, K_0 and I_0 span its solution space.

For real valued wavenumbers κ, α^2 is in the upper half plane or on the real axis depending on wether damping is included or not. There are several different cases for the value of α^2.

Case 1 $\alpha^2 = 0$

Case 2 $\Re(\alpha^2) = 0$ and $\Im(\alpha^2) > 0$

Case 3 $\Re(\alpha^2) > 0$ and $\Im(\alpha^2) = 0$

Case 4 $\Re(\alpha^2) > 0$ and $\Im(\alpha^2) > 0$

Case 5 $\Re(\alpha^2) < 0$ and $\Im(\alpha^2) = 0$

Case 6 $\Re(\alpha^2) < 0$ and $\Im(\alpha^2) > 0$

Case 1

Case 1 corresponds to $\kappa^2 = k^2$ and no damping, this corresponds to the coincidence frequency where the phase velocity along the line source is equal to that of the surrounding fluid. This case, theoretically, results in an infinite radiation ratio, see [13] also the field in the fluid doesn't satisfy the Sommerfeld radiation condition, see [22].

Case 2

With $\Re(\alpha^2) = 0$ and $\Im(\alpha^2) > 0$ we have, $\alpha = a + ia$ where a is real and positive. In the far–field we have, see [21](p 240)

$$K_0(\alpha r)e^{i\omega t} \propto \frac{1}{\sqrt{r}}e^{-(a+ia)r+i\omega t} = \frac{1}{\sqrt{r}}e^{-ar}e^{i(\omega t-ar)} \tag{10.28}$$

Thus $AK_0(\alpha r)$ corresponds to an outward propagating decaying wave in this case. Also in the far field,

$$I_0(\alpha r)e^{i\omega t} \propto \frac{1}{\sqrt{r}}e^{(a+ia)r+i\omega t} = \frac{1}{\sqrt{r}}e^{ar}e^{i(ar+\omega t)} \tag{10.29}$$

Thus the amplitude of $BI_0(\alpha r)$ increases in the far field and, thus B so be 0.

Case 3

With $\Re(\alpha^2) > 0$ and $\Im(\alpha^2) = 0$ we have, $\alpha = a$ with a real and positive. This corresponds to an undamped case below coincidence frequency, which is expected to behave as a nearfield. In the far field,

$$K_0(\alpha r)e^{i\omega t} \propto \frac{1}{\sqrt{r}}e^{-ar}e^{i\omega t} \tag{10.30}$$

which is a decaying solution, i.e. a near–field solution (evaluated in the far–field). Also,

$$I_0(\alpha r)e^{i\omega t} \propto \frac{1}{\sqrt{r}}e^{ar}e^{i\omega t} \tag{10.31}$$

which is a solution with an increasing amplitude, thus B must be 0 in this case.

Case 4

With, $\Re(\alpha^2) > 0$ and $\Im(\alpha^2) > 0$, $\alpha = a + ib$, where a and b are real and positive. This corresponds to a damped case below coincidence frequency. In the far field we have,

$$K_0(\alpha r)e^{i\omega t} \propto \frac{1}{\sqrt{r}}e^{-(a+ib)r+i\omega t} = \frac{1}{\sqrt{r}}e^{-ar}e^{i(\omega t-br)} \tag{10.32}$$

Thus $AK_0(\alpha r)$ corresponds to an outward propagating decaying wave in this case. Also in the far field,

$$I_0(\alpha r)e^{i\omega t} \propto \frac{1}{\sqrt{r}}e^{(a+ib)r+i\omega t} = \frac{1}{\sqrt{r}}e^{ar}e^{i(\omega t+br)} \tag{10.33}$$

Thus the amplitude of $I_0(\alpha r)$ increases in the far field and, thus B must be 0. Thus the results of Case 4 is equivalent to Case 2.

Case 5

With $\Re(\alpha^2) < 0$ and $\Im(\alpha^2) = 0$ we have, $\alpha = ia$ where a is a real and positive constant. This corresponds to the undamped solution above coincidence frequency. In the far-field,

$$K_0(\alpha r)e^{i\omega t} \propto \frac{1}{\sqrt{r}}e^{-iar+i\omega t} = \frac{1}{\sqrt{r}}e^{i(\omega t-ar)} \tag{10.34}$$

which is an outward propagating wave. Also in the far field,

$$I_0(\alpha r)e^{i\omega t} \propto \frac{1}{\sqrt{r}}e^{iar+i\omega t} = \frac{1}{\sqrt{r}}e^{i(\omega t+ar)} \tag{10.35}$$

which is an inward propagating wave. Since an inwardly propagating wave is unphysical, B is yet again 0.

Case 6

With $\Re(\alpha^2) < 0$ and $\Im(\alpha^2) > 0$ we have, $\alpha = a + ib$ where a and b are real and positive. Then, in the far field,

$$K_0(\alpha r)e^{i\omega t} \propto \frac{1}{\sqrt{r}}e^{-(a+ib)r+i\omega t} = \frac{1}{\sqrt{r}}e^{-ar}e^{i(\omega t-br)} \tag{10.36}$$

This represents an outward propagating decaying wave. Also in the far field,

$$I_0(\alpha r)e^{i\omega t} \propto \frac{1}{\sqrt{r}}e^{(a+ib)r+i\omega t} = \frac{1}{\sqrt{r}}e^{ar}e^{i(\omega t+br)} \tag{10.37}$$

which represents an increasing inward propagating wave. Thus yet again $B = 0$.

Amplitude of the Green's function

From the above reasoning it is clear that the Green's function for any physical choice of α^2 is,

$$\Psi = AK_0(\alpha r) \tag{10.38}$$

where, $\alpha = \sqrt{\alpha^2}$. To decide the unknown amplitude A, we proceed as in Section 10.3.3, (or [6] Chapter 3.1), by considering a small integral around the source.

The resulting equation, see [6] p 31, is,

$$\begin{matrix}\lim \\ r \to 0\end{matrix} \int_{\Gamma_0} \frac{\partial \Psi}{\partial r} \mathrm{d}\Gamma_0 = -1 \tag{10.39}$$

The limit,

$$\begin{matrix}\lim \\ r \to 0\end{matrix} K_0(\alpha r) \sim -\ln(\alpha r) \tag{10.40}$$

see [21] p. 240. Now, evaluating the integral of equation (10.39) results in,

$$A = \frac{1}{2\pi} \tag{10.41}$$

Hence,

$$\Psi(r) = \frac{1}{2\pi} K_0(\alpha r) \tag{10.42}$$

for any choice of $\alpha \in \mathbb{C}$.

Important note

The above derivation of a Green's function valid for any choice of α depends on the choice of time dependence. If instead of $e^{+i\omega t}$, $e^{-i\omega t}$, were chosen, Case 3, $\Re(\alpha^2) < 0$, will still result in a decaying solution for K_0. However Case 5, $\Re(\alpha^2) > 0$, will produce an outgoing wave for K_0. Thus the time dependence must be, $\propto e^{+i\omega t}$.

10.5.2 Lower half plane Green's function

The Green's function derived in the previous section is valid for any choice of $\alpha^2 = k^2 - \kappa^2$ that belongs to the upper half plane. A Green's function valid for α^2 in the lower complex half plane is given by noting that if,

$$\alpha^2 = \pm a - ib \tag{10.43}$$

where a and b are positive and real, then,

$$\alpha = \pm\sqrt{a - ib} = \pm(c - id) \tag{10.44}$$

By choosing the negative sign of the solution it can be proved that the K_0 solution in equation (10.27) must be discarded, whereas I_0 gives a physically correct solution. With $A = 0$, the coefficient $B = -\frac{1}{4}$ is found in a similar way to that given in Section 10.5.1. Hence,

$$\Psi(r) = \frac{1}{2\pi} K_0(\alpha r) \tag{10.45}$$

where $\alpha = \sqrt{\alpha^2}$ for α^2 in the upper half plane and

$$\Psi(r) = -\frac{1}{4} I_0(\alpha r) \tag{10.46}$$

where $\alpha = -\sqrt{\alpha^2}$ for α^2 in the lower half plane. For $\Im(\alpha^2) = 0$ either solution may be used. For $\alpha^2 = 0$ (coincidence) neither solution is valid.

10.6 Fluid BE validation

10.6.1 Solution for an axi–symmetric wave on a pipe

Analytical solutions

Consider a pipe with an axi-symmetric displacement. Since there is no θ dependence, the governing equation for the surrounding fluid is given by,

$$\frac{\partial^2 p}{\partial r^2} + \frac{1}{r}\frac{\partial p}{\partial r} + \frac{\partial^2 p}{\partial z^2} + k^2 p = 0 \tag{10.47}$$

where p is the pressure and r and z are the radius and axial coordinate respectively. k is the wavenumber for freely propagating waves, i.e. $k = \frac{\omega}{c}$ and c is the propagating speed in the fluid. The boundary condition for a displacement wave along the cylinder with radius, a is,

$$\frac{\partial p}{\partial r}|_{r=a} = -i\rho\omega v_r e^{-i\kappa z} \tag{10.48}$$

where ρ is the fluid density and v_r is the amplitude of the velocity of the wave. Also due to the Sommerfeld radiation condition,

$$\lim r \rightarrow \infty \quad p(r) \propto \frac{1}{\sqrt{r}} \tag{10.49}$$

By applying a Fourier transform to equation (10.47), is written,

$$\frac{\partial^2 p}{\partial r^2} + \frac{1}{r}\frac{\partial p}{\partial r} + (k^2 - \kappa^2)p = 0 \tag{10.50}$$

Propagating solution

If $k > \kappa$ the solution of equation (10.50) is,

$$p(r, \kappa) = A\, H_0^{(2)}(\alpha r) + B\, H_0^{(1)}(\alpha r) \tag{10.51}$$

where $H_0^{(1)}$ and $H_0^{(2)}$ are the first and second kind Hankel functions of zero:th order respectively and $\alpha = \sqrt{k^2 - \kappa^2}$. With the convention of time dependence $\propto \exp(i\omega t)$, $H_0^{(1)}$ represents an incoming wave, thus $B = 0$.

The Fourier transform drops the exponential dependence of the first boundary condition. Thus the first boundary condition gives the coefficient A as,

$$A = \frac{i\omega v_r}{\alpha H_a^{(2)}(\alpha a)} \tag{10.52}$$

The pressure, p, is therefore given by,

$$p(r, \kappa) = \frac{i\omega v_r}{\alpha H_a^{(2)}(\alpha a)} H_0^{(2)}(\alpha r) \tag{10.53}$$

Nearfield solution

If $\kappa > k$ the solution of equation (10.50) is,

$$p(r, \kappa) = C\, K_0(\alpha r) + D\, I_0^{(1)}(\alpha r) \tag{10.54}$$

where I_0 and K_0 are modified Bessel functions of the first and second kind and $\alpha = \sqrt{(}k^2 - \kappa^2)$. Since, $I_0(\alpha r) \to \infty$ as $r \to \infty$, $D = 0$. To find C we use the boundary condition at the cylinder surface is used to obtain,

$$C = \frac{i\rho\omega v_r}{\alpha K_a(\alpha a)} \tag{10.55}$$

Thus,

$$p = \frac{i\rho\omega v_r}{\alpha K_a(\alpha a)} K_0(\alpha r) \tag{10.56}$$

WBE solution

The propagating analytical and WBEM solutions for a cylinder with $a = 1\,m$, $f = 131.235\,Hz$, $c = 343\,m/s$ and $\kappa = 11/m$ is shown in Figure 10.1. The frequency and sound speed corresponds to $k = 2.404\,m^-1$ and the WBEM solution uses 16 nodes and 8 elements.

The nearfield solution for the same cylinder and frequency but with $\kappa = 5\,1/m$ is shown in Figure 10.2.

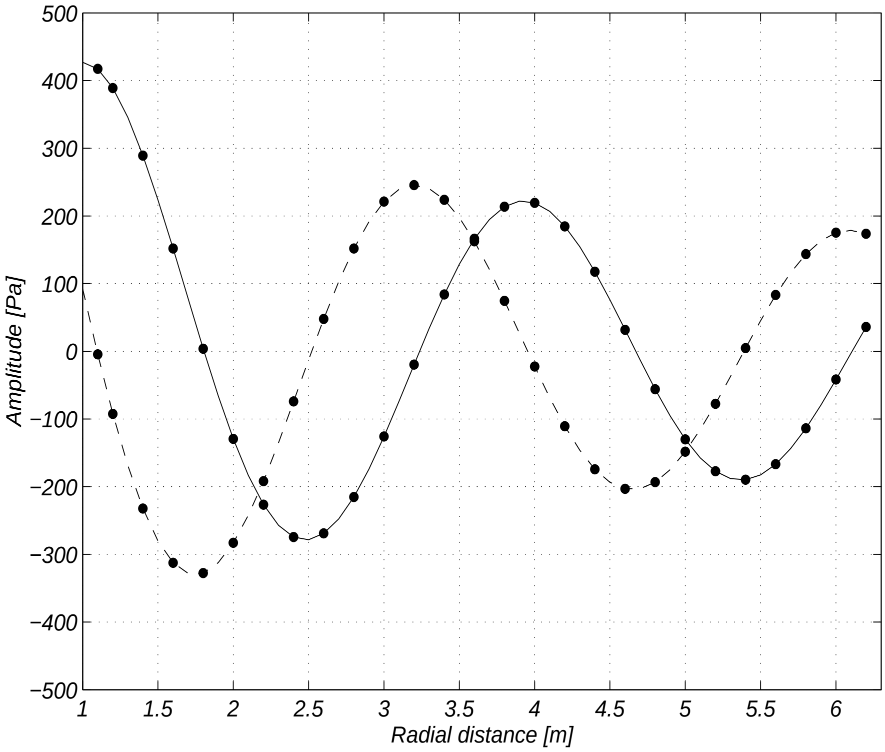

Figure 10.1: Solid lines=real part of pressure; dashed lines= imaginary part of pressure; dots=WBEM

10.6.2 Infinite duct

2D duct model

The mesh for a 2D duct is seen in Figure 10.3. The length of the duct ensures that it may be seen as infinite, given the impedances used here.

The floor, i.e. the lower part of the duct is assumed rigid. The central part of the floor, between $y = \pm X_0\,[m]$ moves with a velocity of $1\,m/s$ (with zero phase corresponding to motion into the duct). The ceiling of the duct has an impedance of $Z = \rho\,c\,(a + b\,i)$. The fluid density, $\rho = 1.21\,kg/m^3$ the fluid sound speed is $c = 343\,m/s$.

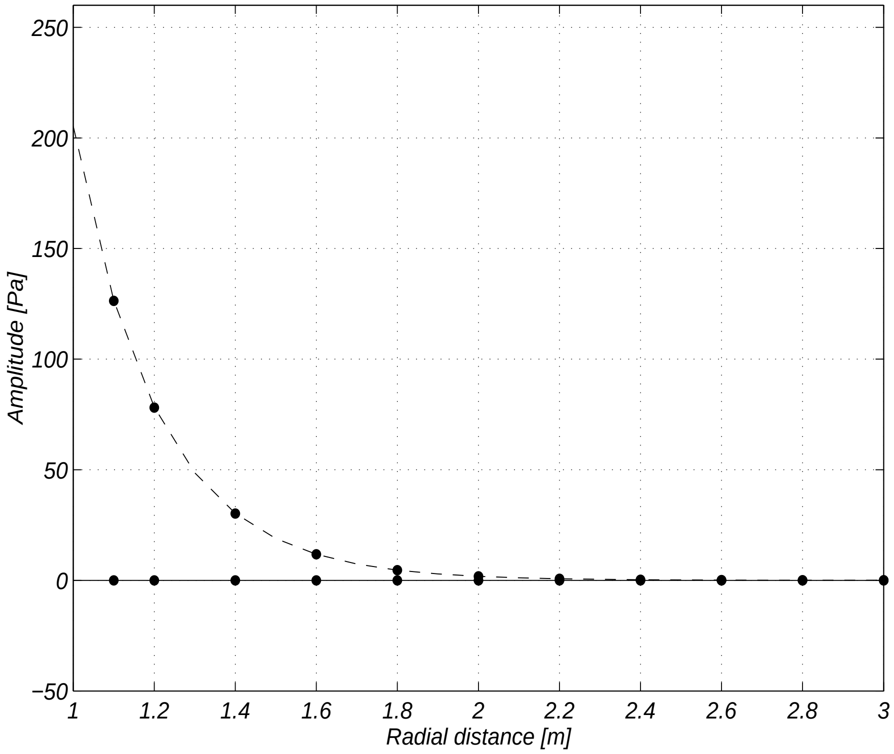

Figure 10.2: Solid lines=real part of pressure; dashed lines= imaginary part of pressure; dots=WBEM

10.6.3 WBEM duct model

The mesh for the WBEM duct is seen in Figure 10.4

The width of the duct ensures that it may be seen as 2 dimensional. The entire floor in the WBEM model is seen as hard and moving with velocity 1 m/s into the duct.

10.6.4 Comparison of 2D BEM and WBEM

For $X_0 = 3\,m$, $a = 10$ and $b = 5$, $z = 0.7\,m$ and frequency, $f = 101.04\,Hz$ the result is shown in Figure 10.5.

For longer distances, x, the solution for the WBE model decays faster than the 2D model as can be seen in Figure, 10.6.

Figure 10.6 shows the imaginary part of the solution but the real part behaves

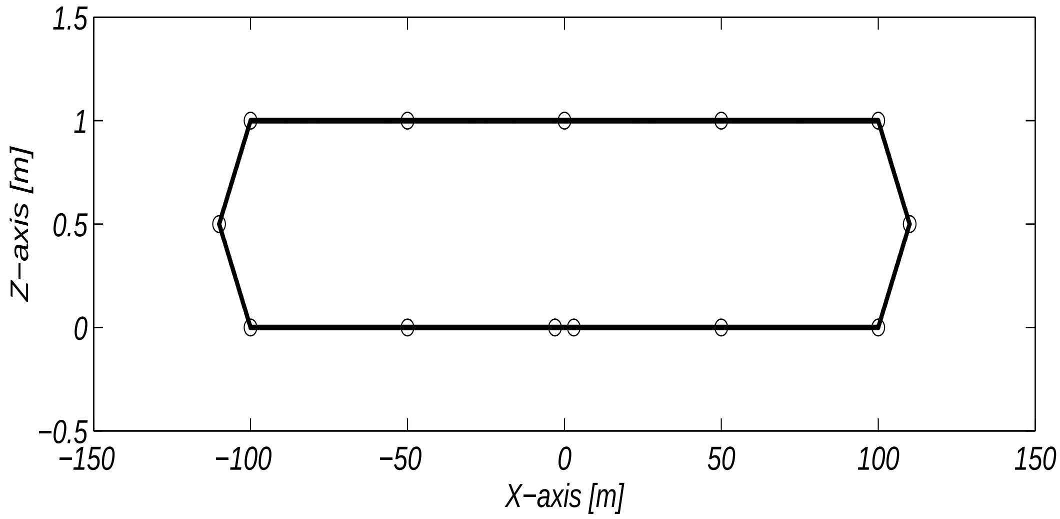

Figure 10.3: Mesh of infinite 2D duct. Note the scaling !

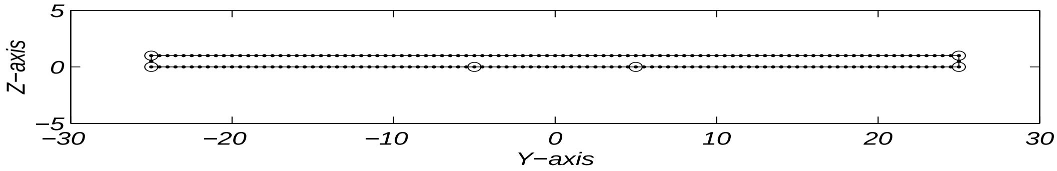

Figure 10.4: Mesh of infinite 2D duct.

similarly. This discrepancy may be corrected by letting the impedance be dependant on κ. Results for the correction $Z \to Z(3 + (k - \kappa)^4)/4$ are shown in Figure 10.7.

No general correction of this type is available. Since, in reality, impedance is usually dependant on the the angle of incidence and the WBEM method at least gives some means to correct for this angle, the discrepancy in Figure 10.6 is not a serious one.

Another example is calculated for $X_0 = 2\,m$, $z = 0.3\,m$, $f = 101.04\,Hz$, $a = 2$ and $b = 1$. This is shown in Figure 10.8.

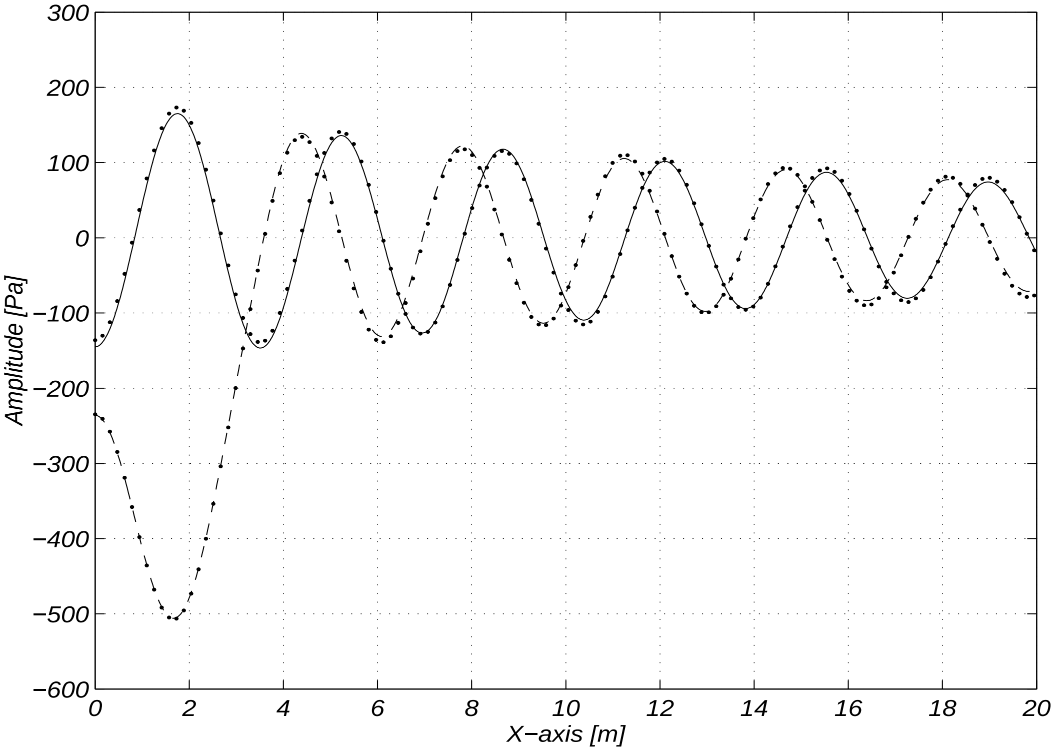

Figure 10.5: Solution for infinite duct, solid and dashed = real and imaginary parts of 2D-model solution; dots = WBE model solution

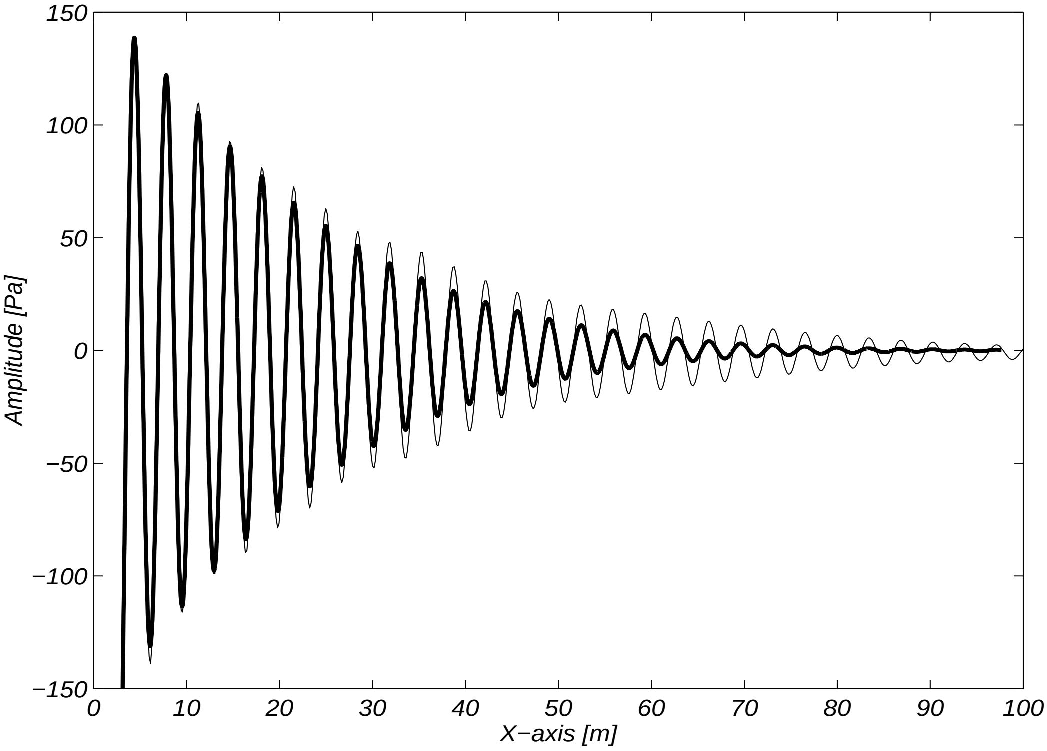

Figure 10.6: Imaginary part of solution for infinite duct; thick line = 2D model; thin line = WBEM model

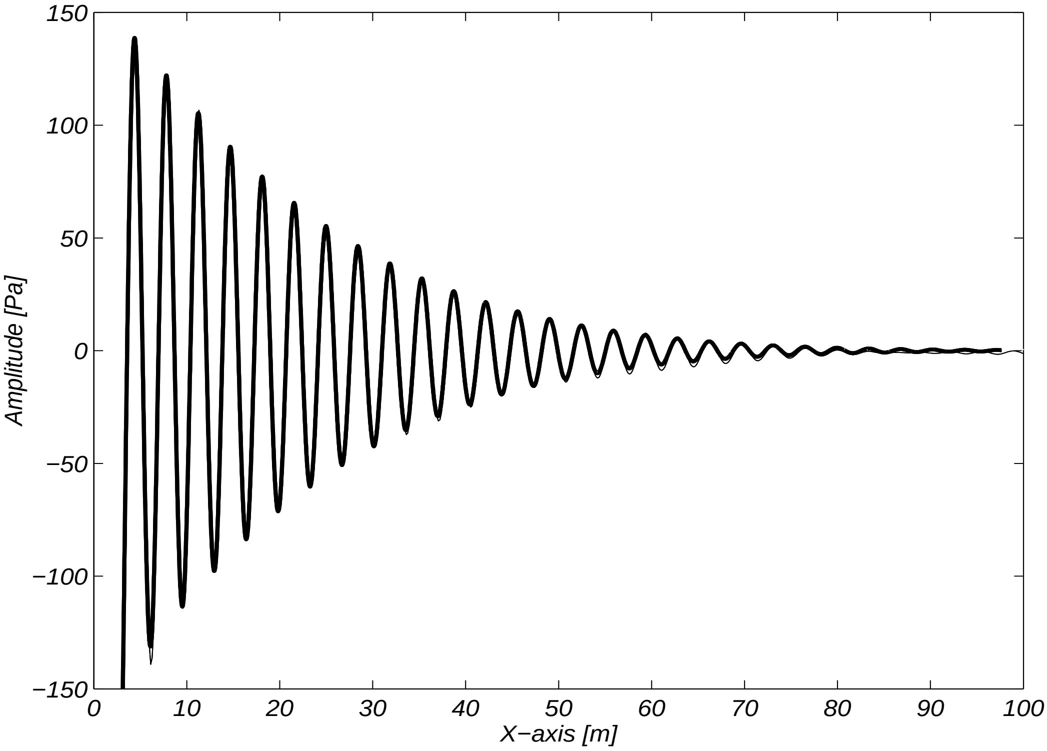

Figure 10.7: Imaginary part of solution for infinite duct; thick line = 2D model; thin line = WBEM model

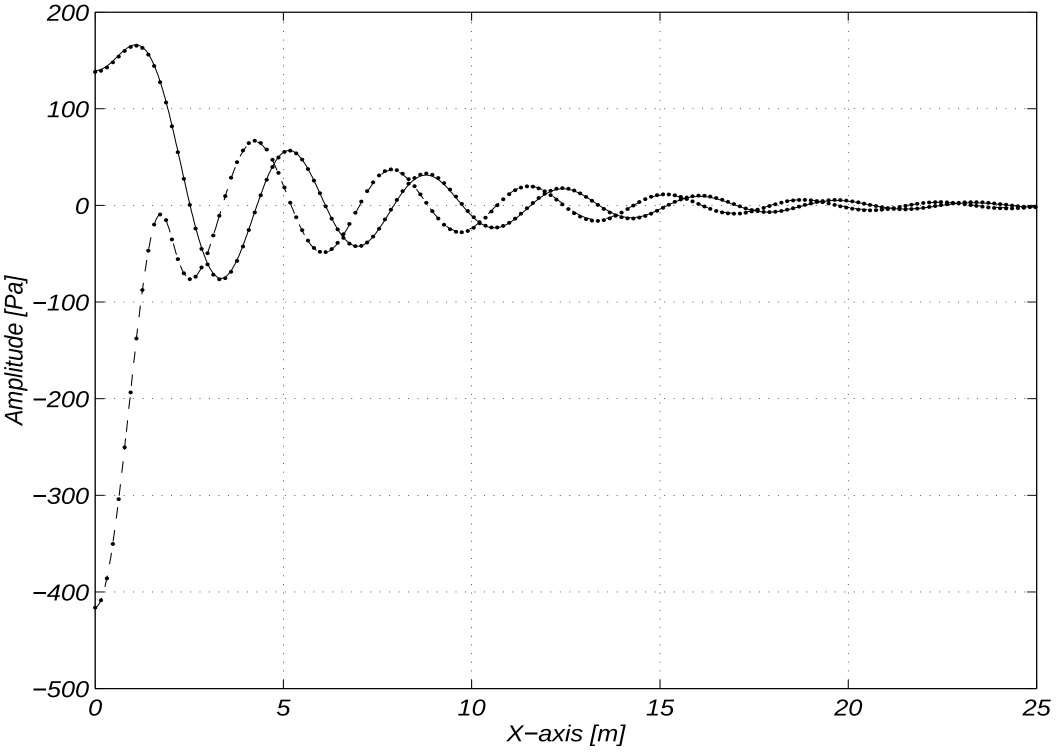

Figure 10.8: Solution for infinite duct, solid and dashed = real and imaginary parts of 2D-model solution; dots = WBE model solution

Chapter 11

FE plate and FE solid to BE fluid coupling

11.1 Introduction

The coupling between a solid or plate finite element model and a fluid boundary element is considered in this chapter. Two boundary conditions have to be fulfilled. Firstly, the displacements normal to the boundary must be equal. Secondly the virtual work from the fluid pressure acting on the solid (or plates) must be included in the finite element model. The virtual work from the finite element exerted onto to fluid is not needed, as explained in Section 11.4.

11.2 WFE-model

The derivation of waveguide finite element models for plates and solids are detailed in 5 and 4. The result may be written,

$$\int \left(\sum_{i=0}^{2} \sum_{j=0}^{2} \frac{\partial^i \delta \hat{\mathbf{U}}^{\mathrm{H}}}{\partial x^i} \mathbf{A}_{ij} \frac{\partial^j \hat{\mathbf{U}}}{\partial x^j} - \omega^2 \delta \hat{\mathbf{U}}^{\mathrm{H}} \mathbf{M} \hat{\mathbf{U}} - \delta \hat{\mathbf{U}}^{\mathrm{H}} \hat{\mathbf{F}} \right) \mathrm{dx} = 0 \tag{11.1}$$

where, $\hat{\mathbf{U}}$ is a vector of the response variables, mainly nodal displacements, and $\mathbf{A}_{ij}$ and $\mathbf{M}$ are matrices.

By letting the integration interval tend to $\mp\infty$ and applying Parrseval's identity, equation (11.1) may be written in terms of variables in the wavenumber domain, κ, denoted with the $\tilde{}$ symbol. The equation of motion becomes,

$$\int_{-\infty}^{+\infty} \left(\delta \tilde{\mathbf{U}}^{\mathrm{H}} \left(\mathbf{K}(\kappa) - \omega^2 \mathbf{M} \right) \tilde{\mathbf{U}} - \tilde{\mathbf{F}} \right) d\kappa = 0 \tag{11.2}$$

Since $\delta \tilde{\mathbf{U}}^{\mathrm{H}}$ in equation (11.3) is arbitrary and, due to linearity, solutions for different wavenumbers, κ, are independent, we have,

$$\left(\mathbf{K}(\kappa) - \omega^2 \mathbf{M} \right) \tilde{\mathbf{U}} - \tilde{\mathbf{F}}_f - \tilde{\mathbf{F}}_e = 0 \tag{11.3}$$

Where the force vector has been split up as a sum of forces from the coupled BE model, $\tilde{\mathbf{F}}_f$, and other external forces $\tilde{\mathbf{F}}_e$.

11.2.1 Calculation of force vectors

$\tilde{\mathbf{F}}$ may be calculated by considering the virtual work for each element,

$$\delta W = \int_{\Omega} \delta \tilde{\mathbf{u}}^{\mathrm{H}} \tilde{\mathbf{f}} \mathrm{d}\Omega \tag{11.4}$$

where $\delta \tilde{\mathbf{u}}^{\mathrm{H}}$ is the virtual displacement in an element, $\tilde{\mathbf{f}}$ is the the force per unit volume or area and Ω is either an area (for plate elements) or a volume (solid elements). In the most common, Gelerkin, FE approximations also used here, the virtual displacement uses the same shape functions, $\mathbf{N}$, that approximate the sought displacements. Thus the virtual work on each element may be written,

$$\delta W = \int_x \delta \tilde{\mathbf{u}}^{\mathrm{H}} \int_A \mathbf{N}^{\mathrm{T}} \tilde{f} \, \mathrm{dA} \, \mathrm{dx} = \int_x \delta \tilde{\mathbf{u}}^{\mathrm{H}} \tilde{\mathbf{f}} \, \mathrm{d}x \tag{11.5}$$

Assembling the element virtual works according to equation (11.5) yields,

$$\delta W = \int \delta \tilde{\mathbf{U}}^{\mathrm{H}} \tilde{\mathbf{F}} \mathrm{dx} \tag{11.6}$$

which is the result used in equation (11.1).

11.3 WBE-model

A Wavedomain Boundary Element (WBE) model for the fluid is derived in Chapter 10. When the boundary conditions are not included, the result may be written as,

$$\Big[\ \mathbf{H}\ \Big]\,\tilde{\mathbf{p}} - \Big[\ \mathbf{G}\ \Big]\,\tilde{\mathbf{v}}_n = \tilde{\mathbf{p}}_i \tag{11.7}$$

where, $[\mathbf{H}]$ and $[\mathbf{G}]$ and are matrices depending on the argument $\sqrt{(k^2-\kappa^2)}$. $\tilde{\mathbf{p}}$ and $\tilde{\mathbf{v}}_n$ are the pressures and normal velocities at the shared boundary and $\tilde{\mathbf{p}}_i$ is the boundary pressure due to incoming waves. (see [6] Ch 2 eq 47)

11.4 Boundary conditions

Only boundary conditions along the length of the system are considered here and not those at its end. For each system there are two types of boundary conditions, Dirichlet (or Essential) and Neuman (or Natural).

The Dirichlet solid–fluid boundary conditions are the displacements along the wetted surface. The displacements for the two systems must match, thus,

$$i\omega\tilde{u}_\perp = \tilde{v}_n \tag{11.8}$$

where, $\tilde{u}_\perp$ is the displacement of the solid normal to the surface and into the solid and $\tilde{\mathbf{v}}_n$ is the particle velocity of the fluid normal to the surface.

Neuman boundary conditions are due to the virtual work on the respective model from the other system.

For the solid model the virtual work is due to a virtual displacement and the force from the 'actual' fluid pressure acting on the surface. Thus, for each element along the surface, the virtual work from the fluid is given by,

$$\int \delta\tilde{u}_\perp^{\mathrm{H}}\tilde{p}\,d\Gamma \tag{11.9}$$

where, $\delta\tilde{u}_\perp$ is the virtual displacement normal to the surface and out of the fluid.

For the boundary element model the virtual work is due to the 'virtual pressure', i.e. the first variation of the pressure multiplied by the displacement of the solid into the fluid. This term is already included in the boundary element formulation as,

$$\Psi \frac{\partial \delta \tilde{\Psi}^*}{\partial \mathbf{n}} \tag{11.10}$$

where $\delta\tilde{\Psi}^*$ is the Green's function of the system, see Chapter 10.

11.4.1 The Dirichlet Boundary Conditions

At the shared boundary the normal displacement of the WFE model must equal the normal displacement of the WBE model. The velocity $\mathbf{v}_n$ of the WBE model is defined to be positive for velocities out of the fluid domain, ([6] p 31 + p32).

Also here the time dependance is $\propto e^{i\omega t}$

With these conventions we have,

$$i\omega\tilde{\mathbf{u}}_\perp = \tilde{\mathbf{v}}_n \tag{11.11}$$

where, $\mathbf{u}_\perp$ is the normal displacement of the WFE model into the solid. These displacements are given as a subset of all response variables, $\mathbf{U}$, so that,

$$i\omega\mathbf{C}_2\tilde{\mathbf{U}} = \mathbf{I}_2\tilde{\mathbf{v}}_n \tag{11.12}$$

where $\mathbf{C}_2$ is a transformation matrix transforming FE-displacements $\tilde{\mathbf{U}}$ to the equivalent normal displacements at the boundary. $\mathbf{I}_2$ is a matrix that is unitary if all normal velocities where coupled to the finite element model.

A more detailed derivation of $\mathbf{C}_2$ for different elements is made in Section 11.7. Also note that the assembling of $\mathbf{C}_2$ differs from assembling finite element matrices. This is because the contribution to a nodal displacement from different elements should be averaged rather than added.

11.4.2 The Neumann Boundary Condition

The virtual work from the fluid on the solid must be positive for a displacement resulting from a pressure increase. Thus the displacement should be defined as positive into the solid. The virtual work, $\tilde{\delta W}_{s,f}$, from the fluid to the solid in the wavenumber domain is written as,

$$\tilde{\delta W}_{s,f} = \int_{\Gamma} \delta\tilde{u}^* p \ \mathrm{d}\Gamma \tag{11.13}$$

where Γ is the shared boundary between the solid and fluid domains and δu is the virtual displacement into the solid. The integral of equation (11.13) should be evaluated for each segment along the boundary. Both $\widetilde{\delta u}^*$ and $\tilde{p}$ are approximated by piecewise polynomials. Thus for each segment (boundary element) along the shared boundary,

$$\delta\tilde{\mathbf{u}}^{\mathrm{H}} \int_{\Gamma} \mathbf{N}_{\mathbf{u}}^{\mathrm{T}} \mathbf{N}_{\mathbf{f}} \,\mathrm{d}\Gamma \,\tilde{\mathbf{p}}_{\mathrm{ele}} \tag{11.14}$$

The integral in equation (11.14) forms a coupling matrix between the finite element and the boundary element. If all these elements are assembled we have,

$$\tilde{\delta W}_{s,f} = \delta\tilde{\mathbf{U}}^{\mathrm{H}} \left[\mathbf{C}_1\right] \tilde{\mathbf{p}} \tag{11.15}$$

Hence the force from the fluid onto the plate or solid FE model is given by,

$$\left[\mathbf{C}_1\right] \tilde{\mathbf{p}} \tag{11.16}$$

A more detailed derivation of $\mathbf{C}_1$ for different elements is made in Section 11.6. This matrix is however very similar to that used for the force of a fluid FE model onto a plate or solid FE model.

11.5 Combined equations

In total there are at least three equations that have to be fulfilled. First the FE-model must be fulfilled. This equation now also includes the forces from the fluid acting on the solid FE model.

$$\left[\mathbf{K}(\kappa) - \omega^2\mathbf{M}\right]\tilde{\mathbf{U}} - [\mathbf{C}_1]\,\tilde{\mathbf{p}} = \tilde{\mathbf{F}} \tag{11.17}$$

The second equation that must be fulfilled is the BE model,

$$\left[\;\mathbf{H}\;\right]\tilde{\mathbf{p}} - \left[\;\mathbf{G}\;\right]\tilde{\mathbf{v}}_n = \tilde{\mathbf{p}}_i\,. \tag{11.18}$$

The third equation is the boundary conditions that specifies equal velocity of the two systems,

$$i\omega\,[\mathbf{C}]_2\,\tilde{\mathbf{U}} - \mathbf{I}_2\tilde{\mathbf{v}} = \mathbf{0}\,. \tag{11.19}$$

A fourth equation is the Robin boundary conditions, that may have to be used for boundary element nodes that are not coupled to the FE model, see Chapter 10.

By introducing the velocity potential according to Chapter 8, such that,

$$\nabla(\Psi) = -\mu\tilde{\mathbf{v}} \tag{11.20}$$

and

$$p = i\omega\mu\rho\tilde{\Psi} \tag{11.21}$$

the combined system may be written as,

$$\begin{bmatrix} \mu\mathbf{G}_{new} & \mu\mathbf{H} & \mathbf{0} \\ \mathbf{0} & -i\omega\rho\mu\mathbf{C}_1 & \left(\mathbf{K}(\kappa) - \omega^2\mathbf{M}\right) \\ \mu\left(\mathbf{I}_2\right) & \mathbf{0} & -\mathbf{C}_2 \end{bmatrix} \begin{bmatrix} \frac{\partial\tilde{\boldsymbol{\Psi}}}{\partial\mathbf{n}} \\ \tilde{\boldsymbol{\Psi}} \\ \tilde{\mathbf{U}} \end{bmatrix} = \begin{bmatrix} \frac{\tilde{\mathbf{p}}_i}{i\omega\rho} \\ \tilde{\mathbf{F}} \\ \mathbf{cc} \end{bmatrix} \tag{11.22}$$

where, $\mathbf{G}_{new} = \frac{1}{i\omega\rho}\mathbf{G}$.

Note If the Robin boundary conditions are needed for some part of the boundary this will add a fourth row to equation (11.22). The two last ‘blocks rows’ should however together have precisely the number of rows that the BE model has nodes.

Note In the original calculation, see Chapter 3 in [6], there is a multiplication of $i\omega\rho$ involved in the calculation of $\mathbf{G}$, so the $\mathbf{G}$ matrix that is defined here is in fact a simplification compared to [6]. (A direct use of the code in [6] would give a BE model that depends on both of the two arguments ω and κ, rather than just $\alpha(\omega, \kappa)$).

11.6 Derivation of Neuman coupling matrix

The $\mathbf{C}_1$ matrix in Section 11.4.2 is derived in some more detail in this section.

For each element the virtual work from the fluid on the plate is given by,

$$\delta W = \int_\Gamma \delta\tilde{u}_\perp^* \tilde{p} \mathrm{d}\,\Gamma \tag{11.23}$$

The out of plane displacement, $u_\perp$, for a plate element is approximated as,

$$u_\perp = w = \mathbf{N}(\xi)\tilde{\mathbf{u}} \tag{11.24}$$

where, $\mathbf{N}(\xi)$ and $\tilde{\mathbf{u}}$ are given by,

$$\mathbf{N}_b(y) = [N_{1b} \quad N_{2b} \quad N_{1b} \quad N_{2b}] = \begin{bmatrix} \frac{1}{4}(2 - 3\xi + \xi^3) \\ \frac{L}{8}(1 - \xi - \xi^2 + \xi^3) \quad \frac{1}{4}(2 + 3\xi - \xi^3) \\ \frac{L}{8}(-1 - \xi + \xi^2 + \xi^3) \end{bmatrix}^{\mathrm{T}} \tag{11.25}$$

and

$$\delta\tilde{\mathbf{u}}^{\mathrm{H}} = \begin{bmatrix} \delta\tilde{w}_1^* \\ \delta\tilde{\phi}_1^* \\ \delta\tilde{w}_2^* \\ \delta\tilde{\phi}_2^* \end{bmatrix} \tag{11.26}$$

11.6.1 Sign of displacement into the FE–domain

To make sure that the local displacements are positive into the FE–domain, consider the expression,

$$\mathrm{int}_{\mathrm{flag}} = \mathrm{sign}(\tilde{\mathrm{r}}_{\mathrm{e}} \times \tilde{\mathrm{r}}_{\mathrm{i}}) \bullet \tilde{\mathrm{e}}_{\mathrm{x}}\,. \tag{11.27}$$

where the all vectors are defined in Figure 11.1.

The $\mathrm{int}_{\mathrm{flag}} = +1$ if the out–of–plane displacement is positive into the FE–domain and $\mathrm{int}_{\mathrm{flag}} = -1$ if they are positive into the fluid. Thus by multiplying the displacements with $\mathrm{int}_{\mathrm{flag}}$ they are ensured to be positive into the FE–domain.

Thus,

$$\mathrm{int}_{\mathrm{flag}} \cdot \delta\mathrm{u}_{\perp} \tag{11.28}$$

is always positive into the FE–domain.

11.6.2 Transformation from global to local displacement

The global degrees of freedom of a plate model are given in the global x, y and z directions and the rotation ϕ. To retrieve the displacement normal to an element, a transformation from the global system coordinate system to the, plate elements, local coordinate system is employed. By also including, $\mathrm{int}_{\mathrm{flag}}$, defined above, the transformed displacements are assured to be into the FE-domain. Hence,

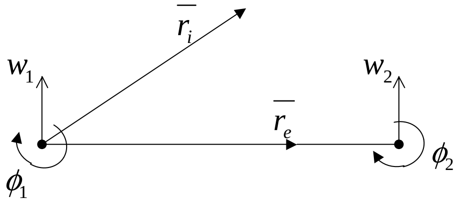

Figure 11.1: Making displacements positive into the FE-domain

$$\begin{bmatrix} \tilde{w}_{1\,loc} \\ \tilde{\phi}_{1\,loc} \\ \tilde{w}_{2\,loc} \\ \tilde{\phi}_{2\,loc} \end{bmatrix} = \mathrm{int}_{\mathrm{flag}} \begin{bmatrix} -\sin(\varphi) & \cos(\varphi) & 0 & 0 & 0 & 0 \\ 0 & 0 & 1 & 0 & 0 & 0 \\ 0 & 0 & 0 & -\sin(\varphi) & \cos(\varphi) & 0 \\ 0 & 0 & 0 & 0 & 0 & 1 \end{bmatrix} \begin{bmatrix} \tilde{v}_1 \\ \tilde{w}_1 \\ \tilde{\phi}_1 \\ \tilde{v}_2 \\ \tilde{w}_2 \\ \tilde{\phi}_2 \end{bmatrix} \tag{11.29}$$

The pressure of the boundary element model does not need any transformation since it is a scalar.

For an edge of a solid element with cubic interpolation functions, there are four nodes on the edges. Assume that all of the edge nodes lie equally spaced on a straight line. The transformation from global to local coordinates then given,

$$\begin{bmatrix} \tilde{w}_{1\,loc} \\ \tilde{w}_{2\,loc} \\ \tilde{w}_{3\,loc} \\ \tilde{w}_{4\,loc} \end{bmatrix} = \mathrm{int}_{\mathrm{flag}} \begin{bmatrix} -s\varphi & c\varphi & 0 & 0 & 0 & 0 & 0 & 0 \\ 0 & 0 & -s\varphi & c\varphi & 0 & 0 & 0 & 0 \\ 0 & 0 & 0 & 0 & -s\varphi & c\varphi & 0 & 0 \\ 0 & 0 & 0 & 0 & 0 & 0 & -s\varphi & c\varphi \end{bmatrix} \begin{bmatrix} \tilde{v}_1 \\ \tilde{w}_1 \\ \tilde{v}_2 \\ \tilde{w}_2 \\ \tilde{v}_3 \\ \tilde{w}_3 \\ \tilde{v}_4 \\ \tilde{w}_4 \end{bmatrix} \tag{11.30}$$

where $s\varphi = \sin(\varphi)$ and $c\varphi = \cos(\varphi)$ has been introduced to save some space. For linear and quadratic interpolating functions only the 2 by 4 and 3 by 6 upper left part of the transformation matrix are needed.

11.6.3 Integration of element coupling

Evaluating equation (11.23) for a single element of width $2a$ now gives,

$$\delta W = \int_{-a}^{+a} \delta\tilde{\mathbf{u}}_{loc}^{\mathrm{H}} \mathbf{N}_b(x,a)\mathbf{N}_p(x)\tilde{\mathbf{p}}\,\mathrm{d}x = \delta\tilde{\mathbf{u}}^{\mathrm{H}}\,[\mathbf{T}]\;a\int_{-1}^{+1} \mathbf{N}_b(\xi,a)\mathbf{N}_p(\xi)\,\mathrm{d}\xi\,\tilde{\mathbf{p}} \quad (11.31)$$

where,

$$\delta\tilde{\mathbf{u}}^{\mathrm{H}} = \begin{bmatrix} \delta\tilde{v}_1^* & \delta\tilde{w}_1^* & \delta\tilde{\phi}_1^* & \delta\tilde{v}_2^* & \delta\tilde{w}_2^* & \delta\tilde{\phi}_2^* \end{bmatrix} \quad (11.32)$$

and the transformation matrix $[\mathbf{T}]$ is the matrix given in equation, (11.29).

By assuming that the nodes of the boundary element are equally spaced and lye on a straight line, the above integral may be evaluated analytically. The results for the plate's out-of-plane shape functions and different interpolating boundary element functions has been calculated with `MAPLE`. The results for linear, quadratic and cubic fluid shape functions are,

$$a\int_{-1}^{+1} \mathbf{N}_b(\xi,a)\mathbf{N}_p(\xi)\mathrm{d}\xi = \begin{bmatrix} \frac{7}{10} & \frac{3}{10} \\ \frac{a}{5} & \frac{2\,a}{15} \\ \frac{3}{10} & \frac{7}{10} \\ -\frac{2\,a}{15} & -\frac{a}{5} \end{bmatrix} \quad (11.33)$$

$$a\int_{-1}^{+1} \mathbf{N}_b(\xi,a)\mathbf{N}_p(\xi)\mathrm{d}\xi = \begin{bmatrix} \frac{11}{30} & \frac{2}{3} & \frac{-1}{30} \\ \frac{a}{15} & \frac{4\,a}{15} & 0 \\ \frac{-1}{30} & \frac{2}{3} & \frac{11}{30} \\ 0 & -\frac{4\,a}{15} & -\frac{a}{15} \end{bmatrix} \quad (11.34)$$

and

$$a\int_{-1}^{+1}\mathbf{N}_b(\xi,a)\mathbf{N}_p(\xi)\mathrm{d}\xi = \begin{bmatrix} \frac{4}{35} & \frac{93}{280} & \frac{3}{70} & \frac{3}{280} \\ \frac{a}{70} & \frac{3\,a}{28} & \frac{3\,a}{70} & \frac{a}{420} \\ \frac{3}{280} & \frac{3}{70} & \frac{93}{280} & \frac{4}{35} \\ -\frac{a}{420} & -\frac{3\,a}{70} & -\frac{3\,a}{28} & -\frac{a}{70} \end{bmatrix} \tag{11.35}$$

for the respective case.

For coupling between solid finite elements and fluid boundary elements only elements with the same type of interpolation are implemented in WANDS. Other coupling types and curved boundaries may be implemented in the future. For cubic–cubic coupling on a straight line with equally spaced nodes the integral in equation (11.31) the interpolation functions both for the boundary element and for the edge of the solid finite element are given in [6]. The evaluation of the 'cubic-cubic' integral results in,

$$\begin{bmatrix} \frac{4}{105} & \frac{33}{1120} & \frac{-3}{280} & \frac{19}{3360} \\ \frac{33}{1120} & \frac{27}{140} & \frac{-27}{1120} & \frac{-3}{280} \\ \frac{-3}{280} & \frac{-27}{1120} & \frac{27}{140} & \frac{33}{1120} \\ \frac{19}{3360} & \frac{-3}{280} & \frac{33}{1120} & \frac{4}{105} \end{bmatrix} \tag{11.36}$$

The quadratic-quadratic coupling results in,

$$\begin{bmatrix} \frac{4}{15} & \frac{2}{15} & \frac{-1}{15} \\ \frac{2}{15} & \frac{16}{15} & \frac{2}{15} \\ \frac{-1}{15} & \frac{2}{15} & \frac{4}{15} \end{bmatrix} \tag{11.37}$$

The linear-linear coupling results in,

$$\begin{bmatrix} \frac{2}{3} & \frac{1}{3} \\ \frac{1}{3} & \frac{2}{3} \end{bmatrix} \tag{11.38}$$

11.6.4 assembling

The assembling of different coupling element matrices into a global coupling matrix are made as in a normal FE–software.

11.7 Derivation of Dirichlet coupling matrix

11.7.1 Boundary conditions for each element

Consider a plate finite element coupled to a linear boundary element. The essential (or Dirichlet) boundary condition is that,

$$i\omega\tilde{u}_{\perp} = \tilde{v}_n \tag{11.39}$$

Given that $\tilde{v}_n$ is defined as normal velocity positive into the solid, $(i\omega\tilde{u}_{\perp})$ must also be defined positive into the solid. By using int_{flag} as defined in equation, (11.27) the relation for coupling a linear boundary element to a plate finite element may be written,

$$\begin{bmatrix} \tilde{v}_{1n} \\ \tilde{v}_{2n} \end{bmatrix} = i\omega \begin{bmatrix} 1 & 0 & 0 & 0 \\ 0 & 0 & 1 & 0 \end{bmatrix} \begin{bmatrix} \tilde{w}_{1loc} \\ \tilde{\phi}_{1loc} \\ \tilde{w}_{2loc} \\ \tilde{\phi}_{2loc} \end{bmatrix} \tag{11.40}$$

where the local node displacements are given as in equation (11.29). For a quadratic boundary element we must evaluate the interpolation function of the plate element at the mid coordinate, this gives,

$$\begin{bmatrix} \tilde{v}_{1n} \\ \tilde{v}_{2n} \\ \tilde{v}_{3n} \end{bmatrix} = i\omega \begin{bmatrix} 1 & 0 & 0 & 0 \\ \frac{2}{4} & \frac{a}{4} & \frac{2}{4} & \frac{-a}{4} \\ 0 & 0 & 1 & 0 \end{bmatrix} \begin{bmatrix} \tilde{w}_{1loc} \\ \tilde{\phi}_{1loc} \\ \tilde{w}_{2loc} \\ \tilde{\phi}_{2loc} \end{bmatrix} \tag{11.41}$$

and for a cubic boundary element, e.g. a four–noded element, we have,

$$\begin{bmatrix} \tilde{v}_{1n} \\ \tilde{v}_{2n} \\ \tilde{v}_{3n} \\ \tilde{v}_{4n} \end{bmatrix} = i\omega \begin{bmatrix} 1 & 0 & 0 & 0 \\ \frac{80}{27} & \frac{32a}{27} & \frac{28}{27} & \frac{-16a}{27} \\ \frac{80}{27} & \frac{32a}{27} & \frac{28}{27} & \frac{-16a}{27} \\ 0 & 0 & 1 & 0 \end{bmatrix} \begin{bmatrix} \tilde{w}_{1loc} \\ \tilde{\phi}_{1loc} \\ \tilde{w}_{2loc} \\ \tilde{\phi}_{2loc} \end{bmatrix} \tag{11.42}$$

For a solid finite element coupled to a boundary element with the same type of interpolation the matrices above are replaced with identity matrices. Naming the above matrices $[\mathbf{BC_{mat}}]$ the coupling matrix $[\mathbf{C_2}]$ for each element may be written,

$$\tilde{\mathbf{v}}_n = i\omega[\mathbf{BC_{mat}}][\mathbf{T}]\tilde{\mathbf{u}} \tag{11.43}$$

11.7.2 Assembling

The assembling of Dirichlet boundary conditions from different elements cannot be made by just adding the matrix components. This is because these represents displacements and thus for a node shared between two elements the imposed displacements would be twice that of a neighbouring node that is not shared. Instead the average displacement from each element must be imposed. This is effectively a parallel coupling of the displacements. Thus, at a shared node,

$$c_{ij} = \frac{c_{ij1} \cdot c_{ij2}}{c_{ij1} + c_{ij2}} \tag{11.44}$$

where c_{ij} is the assembled matrix and, c_{ij1} and c_{ij2} are the components from coupling of the respective elements.

Chapter 12

Solid BE model

12.1 General

The solid BE model is made by subroutines created by X.Sheng [23] and [4]. These subroutines gives the relation between '*traction*' vectors and displacements at the boundary. The 'traction' vectors are forces per unit area acting on the boundary, hence the normal component of a traction vector is a pressure.

The matrix equation, see [4], is written,

$$[\mathbf{H}_{solid}]\tilde{\mathbf{u}} = [\mathbf{G}_{solid}]\tilde{\mathbf{t}} + \mathbf{b} \tag{12.1}$$

where, $\hat{\mathbf{u}}$ is a vector of the displacement at the boundary and $\hat{\mathbf{t}}$ is a vector of the traction forces on the boundary. The vector $\mathbf{b}$ denotes body forces but these have not been implemented in WANDS.

Note!

Equation (12.1) is different from the corresponding fluid BE equation in the same way that a solid FE equation differs from a fluid FE equation. Hence, $[\mathbf{H}]$ is always the matrix in front of the 'primary' variable. For a fluid this is the pressure whereas for the solid it is the displacement. The 'secondary' variable is in both cases that which is proportional to a spatial derivative to the primary variable. For the solid this is the traction vector.

However to comply with the order in which the fluid BE model is written, the assembly into the system matrix is made so that the traction vector comes first. Hence,

$$\begin{bmatrix} -\mathbf{G}_{solid} & \mathbf{H}_{solid} & \dots \\ \dots & & \end{bmatrix} \begin{bmatrix} \hat{\mathbf{t}} \\ \hat{\mathbf{u}} \\ \dots \end{bmatrix} \tag{12.2}$$

There are some other differences between the solid and the fluid BE models.

- There are three (essential) boundary conditions that need to be given for each node.
- Only quadratic elements are implemented for the solid BE models.
- The solid BE model always has some damping included in the material. This means that there is no need to implement the 'CHIEF' points used for the fluid BE.
- There are no field or power calculations implemented in the solid BE model.
- There is however an edge element option in the solid BE formulation.

The local coordinate system of the solid BE-model is shown in Figure 12.1

x is the first direction vector, **s** is the second and **n** is the third. The boundary is indicated with a dashed line

12.2 Boundary conditions

In addition to the boundary element equation (12.1) (without body forces), essential (Dirichlet or Robin) boundary conditions are also needed. These are generally written as,

$$C_A u_i + C_B t_i = C_C \tag{12.3}$$

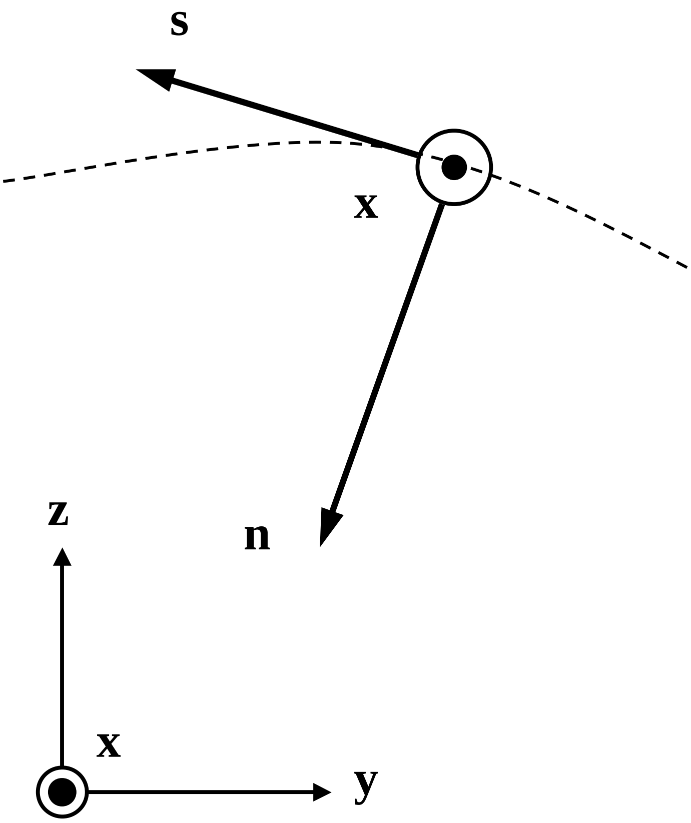

Figure 12.1: Coordinate system of solid boundary element compared to global coordinate system.

where u_i is the displacement in the i:th direction $1 = x$, $2 = s$, $3 = n$ and similarly for the traction t_i in the i:th direction. These boundary conditions are then written into the system matrix, similarly to the boundary conditions for the fluid BE model. Internally in the system matrix in WANDS, $\mathbf{C}_B$ is to the left of $\mathbf{C}_A$, since the traction components are numbered lower that the displacements, see equation (12.2).

12.3 Validation

A simple validation example has been made where the displacements in a solid FE model are compared with those in a solid BE model. Since the BE models have already been used in Sheng's software [4] and [23], this very simple model is the only one considered.

The example was also used to clarify the coordinate directions used by Sheng.

The FE mesh is seen in Figure 12.2,

The results of a simple BE model are compared with the solution for this model. The axis in figure 12.2 are given in metres and the material is aluminium, but with an unusually high loss factor of $\eta = 0.1$. The validation is for an almost static case with $\omega = 20\,Hz$ and $\kappa = 1\,m^{-1}$. A downward force is applied at the top centre node of the FE mesh. The magnitude of this force is 0.05 N, which approximately corresponds to a pressure of 1/3 N/m applied to the three mid nodes of the BE model.

The bottom nodes of the FE model are restrained.

The BE model is just a straight line from $y = 12$ to $y = 8$ metres. The reason for letting the boundary elements run from a higher value of y to a lower, is that this corresponds to a BE model below the line. Hence if $\mathbf{x}$ is the unit vector in the x-direction and s is the unit vector in the direction along the boundary element, then $\mathbf{n} = \mathbf{x} \times \mathbf{s}$ is the unit vector pointing into the solid domain.

The displacements in the x-direction is plotted in Figure 12.3

The displacements in the s-direction, *i.e.* in the negative y-direction, are plotted in Figure 12.4.

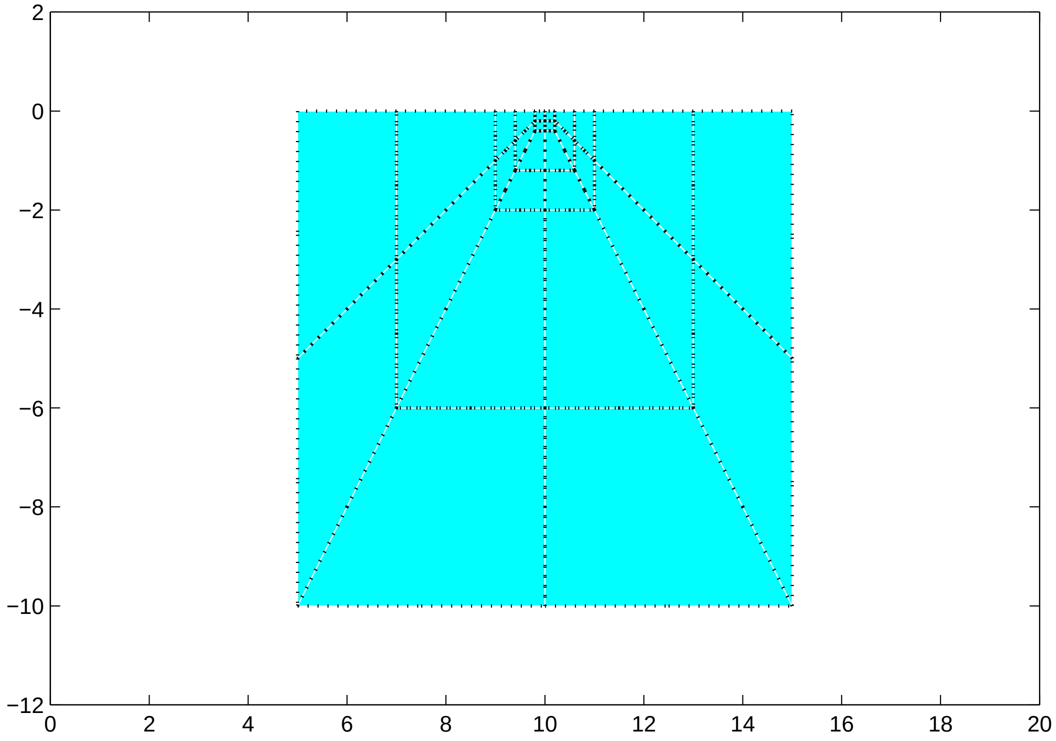

Figure 12.2: Simple FE model for validation of solid BE.

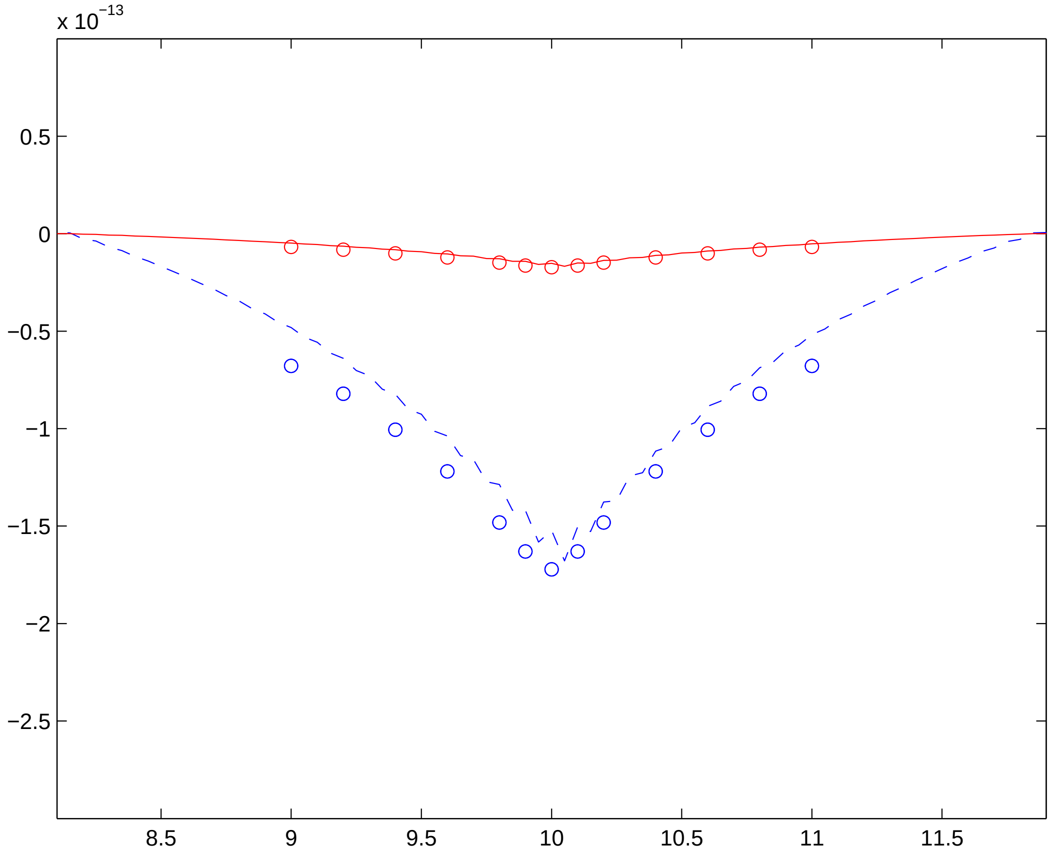

Figure 12.3: Displacement in the x-direction.

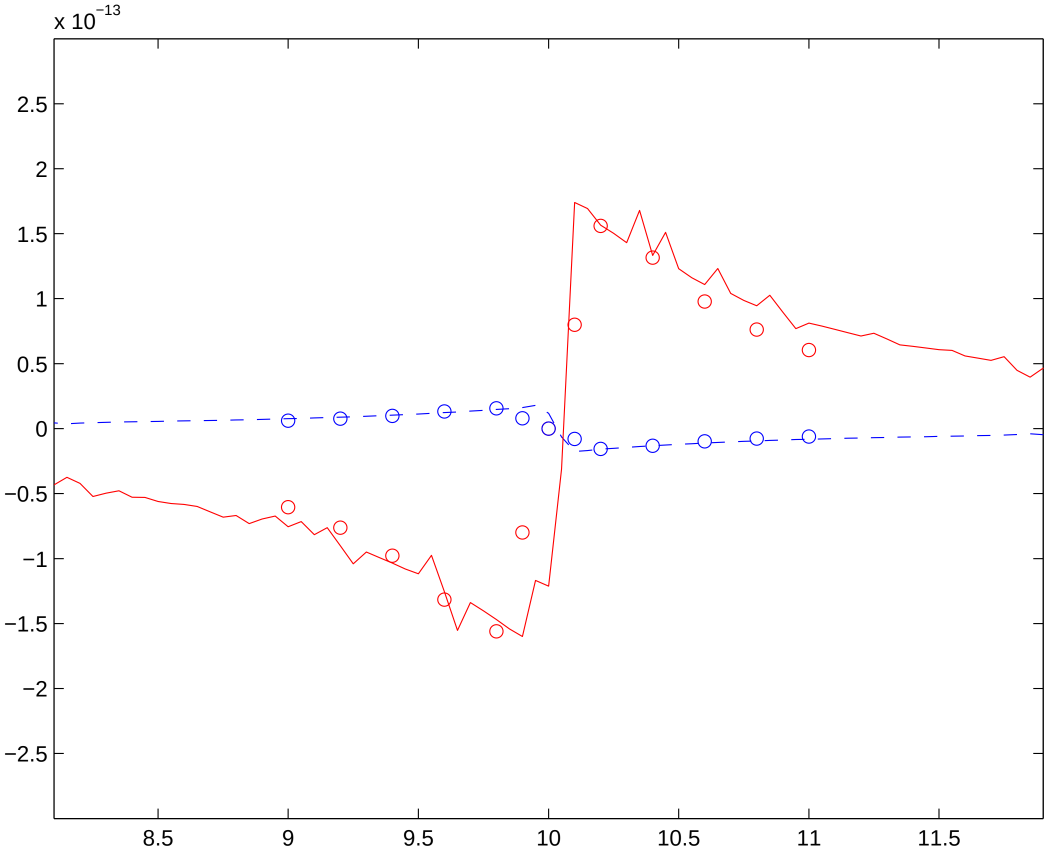

Figure 12.4: Displacement in the x-direction.

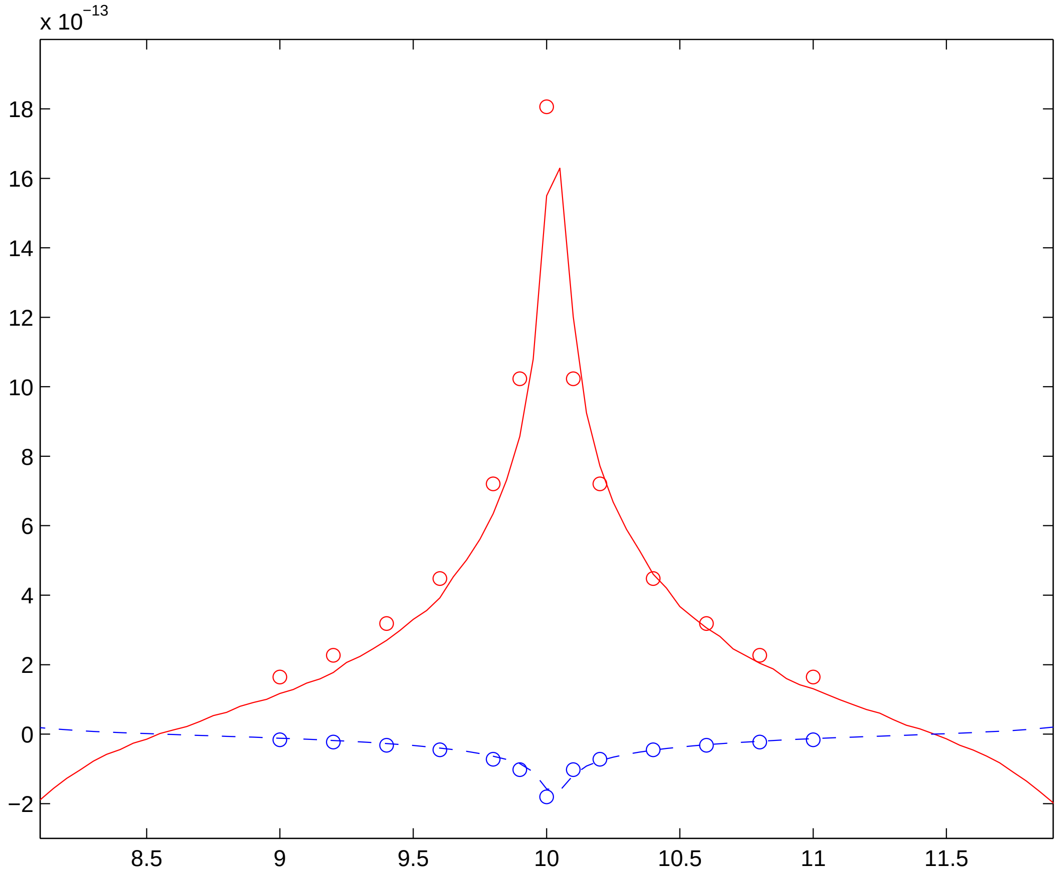

Figure 12.5: Displacement in the x-direction.

The displacements in the n-direction, *i.e.* in the negative z-direction, are plotted in Figure 12.5.

The solid lines in these figures are the real part of the displacement and the dashed lines corresponds to the imaginary parts. The circles corresponds to the FE model.

Note!

As already mentioned, the force in the FE model corresponds to pressures in the BE model, which may explain the less sharp displacements in the BE model. The edge nodes of the BE model have very large displacements, which are not shown here. These displacements might become more normal if the 'edge element' option is included. The slightly rough displacements of the BE model, especially in the x-direction, might be due to either some numerical problems or some minor error in the code. The largest displacement (in the z-direction) is however fairly smooth and further investigation is not within the scope of this work. The condition number of the system matrix for the BE model is $7 \cdot 10^3$ which is well within any double precision accuracy.

Chapter 13

Solid BE to Plate FE and Solid FE coupling

Coupling of a solid boundary element to a plate or solid finite element model is very similar to the coupling of a fluid boundary element to the same types of finite elements.

Hence the coupling consists of two parts.

13.1 Virtual work on FE model

The first part describes the forces from the boundary element model onto the plate or solid finite elements. The main difference compared to the fluid boundary element coupling is that there are three directions of the forces along the boundary elements that need to be coupled to the finite elements. In principle this is done as for the coupling of fluid boundary elements. Thus, over one element we have the virtual work in the frequency domain,

$$\delta W = \int \delta \mathbf{t}^{\mathrm{H}} \mathbf{u} \, ds \tag{13.1}$$

where,

$$\mathbf{t} = \left[\begin{array}{ccc} t_x & t_s & t_n \end{array} \right] \tag{13.2}$$

are the traction vectors in the local coordinate system along the boundary element and

$$\mathbf{u} = \left[\begin{array}{ccc} u_x & u_s & u_n \end{array} \right] \tag{13.3}$$

are the corresponding displacements at the edge of the finite element. The traction vector in the **n** direction is the pressure onto the solid boundary element.

To be able to calculate these components of the virtual works we may note that both the displacements and the traction can be described by shape functions $\mathbf{N}_{be}(s)$ and $\mathbf{N}_{fe}(s)$ that describe these along the coupled edge. The shape functions for the boundary elements are quadratic, and for simplicity they are considered to be straight here. Hence,

$$t_i = \mathbf{N}_{be}(s)\hat{\mathbf{t}}_i \tag{13.4}$$

where subindex $i = x, s, n$ and

$$\mathbf{N}_{be}(\xi) = \left[\begin{array}{ccc} \frac{1}{2}\xi(\xi-1) & (\xi+1)(\xi-1) & \frac{1}{2}\xi(\xi+1) \end{array} \right] \tag{13.5}$$

and $\xi = s/a$ where a is the half width of the element.

In WANDS solid boundary elements are only coupled to solid finite elements that also are quadratic. For plate elements the inplane displacements, i.e. the x and s displacements are linear whereas the out of plane motion is cubic. The virtual work from the traction vector in the i-direction may thus be written,

$$\delta W_i = \delta\hat{\mathbf{t}}_i^{\mathrm{H}} \int \mathbf{N}_{be}(s)^T \mathbf{N}_{fe}(s)\, ds \hat{\mathbf{u}}_i \tag{13.6}$$

the virtual work in the other directions are similar. The total virtual work on the finite element could be written as one equation. Here, however, it is simply seen as the sum over the indices i and after dropping the $\delta\hat{\mathbf{t}}_i^{\mathrm{H}}$ term (in accordance with how it is made for other couplings) the entries for each direction are assembled into the coupling matrix. For the s and n directions a transformation matrix must also be applied. Hence,

$$\hat{\mathbf{u}}_s = \mathbf{T}\hat{\mathbf{u}} \tag{13.7}$$

where $\mathbf{u}$ here includes all nodal degrees of freedom along the edge of the finite element.

As discussed in Chapter 10 the virtual work, or Neuman boundary condition, is already included in the boundary element model.

13.2 Essential boundary conditions

The essential boundary conditions are simply that the displacements at each pair of coupled nodes must be the same. For each element his gives an equation of the type,

$$\mathbf{I}\mathbf{u}_{\mathbf{be}} - \mathbf{T}\mathbf{u}_{\mathbf{fe}} = \mathbf{0} \tag{13.8}$$

For instance to couple the out of plane motion of a plate with the out of plane motion of a solid boundary element, the displacements of the nodes of the plate element must first be given in the local coordinate system of the boundary element. Since the plate element is assumed to be angled as the boundary element, we have

$$\begin{bmatrix} w_1' \\ \phi_1' \\ w_2' \\ \phi_2' \end{bmatrix} = \begin{bmatrix} -\sin\alpha & \cos\alpha & 0 & 0 & 0 & 0 \\ 0 & 0 & 1 & 0 & 0 & 0 \\ 0 & 0 & 0 & -\sin\alpha & \cos\alpha & 0 \\ 0 & 0 & 0 & 0 & 0 & 1 \end{bmatrix} \begin{bmatrix} v_1 \\ w_1 \\ \phi_1 \\ v_2 \\ w_2 \\ \phi_2 \end{bmatrix} \tag{13.9}$$

where the primed system is that angled in the same way as the boundary element and the unprimed is the global coordinate system. The mid node displacement of the boundary element should be coupled to the displacement at the middle of the plate element. This displacement is given by the out of plane displacements and rotations of the two plate nodes, by evaluating the shapefunctions at $s = 0$. The result is,

$$\begin{bmatrix} w_{1B} \\ w_{2B} \\ w_{3B} \end{bmatrix} = \begin{bmatrix} 1 & 0 & 0 & 0 \\ \frac{1}{2} & \frac{a}{4} & \frac{1}{2} & \frac{a}{4} \\ 0 & 0 & 0 & 1 \end{bmatrix} \begin{bmatrix} w'_1 \\ \phi'_1 \\ w'_2 \\ \phi'_2 \end{bmatrix} \tag{13.10}$$

where the subindex B denotes displacement corresponding to the boundary element and a is the half width of the plate.

Chapter 14

Software structure

The general structure of the WANDS software is described here. The main program can be seen as consisting of three parts. These are firstly a subroutine called GEN_READ that reads essential generic data for the system. Secondly a part that creates different data structures and creates the sub matrices used to form the system matrix. Finally a part that assembles and solves the system and writes the calculated results.

14.0.1 GEN READ

The first part is the GEN_READ subroutine which reads the system data from the input file. The system data is the data in the input file that begins with the word `*INSYS:`. Primarily this information defines which different submodels are to be found in the rest of the input. In the `*INSYS:` data blocks each submodel is given a 'tag'. These tags are exported to the main program where they are used as inputs to the subroutines that constructs the different block matrices for the system.

The data that is read also provides information on the frequency and wavenumber ranges that should be used as well as specifying what data should be written to output files.

14.1 Submodel routines

When the *INSYS: blocks are read, the number of different submodel types have been decided and 'tagged'. This means that the matrices that are used to form the complete system have been decided and the program now starts to search for the data needed to form each of these matrices. As can be seen from the earlier discussions in this manual, the block matrices for the FE submodels and the coupling submodels are found by multiplying a number of submodel matrices by wavenumbers, frequencies and sometimes a scaling factor. For instance, for a solid FE model, the dynamic stiffness matrix becomes

$$\mathbf{D}_s = \left[\mathbf{K_2}(-i\kappa)^2 + \mathbf{K_1}(-i\kappa) + \mathbf{K_0} - \omega^2\mathbf{M_2}\right] \tag{14.1}$$

Hence the matrices $\mathbf{K_2}$, $\mathbf{K_1}$,$\mathbf{K_0}$ and $\mathbf{M}$ must be formed first and then used repeatedly to create different dynamic stiffness matrices $\mathbf{D}_s$ for different values of the wavenumber κ and the frequency ω.

The code the mainprogram calls to create solid FE matrices is,

```
c-----------------------------------------------------------------------
c   SET FE SOLID MATRICES
    DO 60 s_count=1,SIZE%fes_mods



        WRITEDATA%FES(s_count)%WR   =   SYSDATA%FE_SOLID(s_count)%WR
        TAG(1)      =   SYSDATA%FE_SOLID(s_count)%tag
        TAGLENG(1)  =   SYSDATA%FE_SOLID(s_count)%tagleng

        ! write matrices if WR is true

        CALL FE_SOLID(filein,folder,SOLID_MATS(s_count),
     *                 tag(1),tagleng(1), WRITEDATA%FES(s_count))
```

```
60  ENDDO

c---------------------------------------------------------------------------
```

The loop is made over all solid FE models, so when `s_count`=2, the second solid FE model matrices are formed. `filein` is the file that the data should be read from. `folder` is the folder to which data should be written, the data written at this stage are the matrices e.g. **M** and also some data that relate degrees of freedom with node numbers etc. `SOLID_MATS(s_count)` is a structure that contains the matrices that are exported to the main program. `tag(1)` is the tag for the `s_count`, submodel and `tagleng` is just the length of this string. `WRITEDATA%FES(s_count)` specifies if the solid FE matrices should be written.

In contrast, for BE models the matrices relating forces and displacements are formed by integrating Bessel functions whose arguments are given by the wavenumber and frequency. Since this generally must be made for each considered wavenumber and frequency, these matrices are formed when the system matrix is formed. Only the data needed, such as geometrical and material data are extracted in the subroutine used in this second part of the main program.

The following sections describe briefly each of the submodel routines called.

14.1.1 FE_PLATE

Creates the matrices for one plate FE model. This routine calls two other routines. The first DATA_INPUT_PLATE reads the data for the specific submodel. The second FEM_2_5D_plate actually creates the matrices. The latter subroutine is called twice, once for the stiffness matrices and once for the damping matrices.

14.1.2 FE_SOLID

Creates the matrices for one solid FE model. This routine calls two other routines. The first DATA_INPUT_SOL reads the data for the specific submodel. The second

FEM_2_5D_SOL actually creates the matrices. The latter subroutine is called twice, once for the stiffness and the mass matrices and once for the damping matrices.

14.1.3 FE_FLUID

Creates the matrices for one fluid FE model. This routine calls two other routines. The first DATA_INPUT_FLU reads the data for the specific submodel. The second FE_2_5D_FLU actually creates the matrices. The latter subroutine is called twice, once for the 'stiffness' and 'mass' matrices and once for the damping matrices.

14.1.4 FEPFES_COUP

This subroutine creates the coupling matrices for coupling between a plate and a solid FE model. This subroutine needs data from each of the plate model, the solid model and the coupling model. It calls DATA_INPUT_PLATE and DATA_INPUT_SOL to get the input data for the respective plate and solid submodels. Then it calls DATA_INPUT_SP to get the coupling data. Finally the coupling matrices are created by the SOL_PLATE subroutine.

14.1.5 FEPFEF_MAIN

This subroutine creates the the coupling between a plate finite element model and a fluid finite element model. FEPFEF_MAIN calls four major subroutines. DATA_INPUT_PLATE and DATA_INPUT_FLU have already been used for reading the plate and fluid submodels data when these where created, but they are reused in FEPFEF_MAIN. The coupling specific data is read by the subroutine, DATA_INPUT_PFF and a coupling matrix $M1_{ur}$ is formed by the subroutine FEPFEF_COUP. Since the coupling formulation is gyroscopic, this matrix is used both to describe the work done by the fluid on the plate and that done by the plate on the fluid. As an option, the $M1_{ur}$ coupling matrix is written to the file `M1_urTAG.out` file.

14.1.6 FESFEF_MAIN

This subroutine creates the coupling between solid and fluid finite elements. It is very similar to the subroutine that couples plate elements to fluid finite elements.

14.1.7 COUP_MAIN_PF

This subroutine creates the coupling between one plate FE model and one fluid BE model. It calls COUPDATA to get the coupling specific data. Then it calls PLATEDATA which reads data for the plate from the **topology output file**. Then it calls BEMDATA, which reads the data needed for the fluid BE model.SET_C1 creates the C1 matrix and SET_C2 creates the C2 and I2 matrices.

14.1.8 COUP_MAIN_SF

This subroutine creates the coupling between one solid FE model and one fluid BE model. It calls COUPDATA_SF to get the coupling specific data. Then it calls SOLIDDATA which reads data for the solid from the **topology output file**, since the node numbering changes between input data and output data when the solid FE model is created. Finally it calls BEMDATA, which reads the data needed for the fluid BE model. SET_C1_SF creates the C1 matrix and SET_C2_SF creates the C2 and I2 matrices.

14.1.9 BEFBEF_COUP

Creates the coupling matrices between two fluid BE submodels.

14.1.10 BE_INP2

This subroutine prepares all data needed to form BE H and G matrices. The actual formation of these matrices is not made in the main program (MAINPROG2) but made in a solution routine. The reason is that there is no explicit dependency of the frequency and wavenumber

14.1.11 BESBES_COUP

This subroutine creates coupling between two solid boundary elements. It calls the subroutine BEMDATA_BSBS which reads the specific coupling data. It also use the subroutine BES_prep twice to read the solid BE data for the solid BE domains to be coupled. The coupling itself is just matrices that sets the specified adjacent displacements and tractions equal, this is done in the subroutine SET_BSBS_MAT

14.1.12 BESBEF_COUP

This subroutine does coupling between a solid BE domain and a fluid BE domain. It calls BES_prep and BEMDATA_TOP to get the data for the two models to be coupled. Then the data for the coupling is read by BEMDATA_BSBF. The coupling matrices are subsequently formed by, SET_BSBF_MAT after which they are written to the output files.

14.2 DLOOP

The third section in the WANDS mainprogram is the solution method, DLOOP. This is performs a double loop over all frequencies and wavenumber under consideration. Also some postprocessing, such as radiated power, is calculated within DLOOP.

14.2.1 DLOOP_SOL record data

DLOOP_SOL is called as a subroutine which uses the data structures of the different submodels. Hence the amount of data fed into DLOOP_SOL is quite substantial. The DLOOP_SOL routine is called as,

```
      CALL DLOOP_SOL(SYSDATA,SIZE,FLUID_MATS,PLATE_MATS,SOLID_MATS,BEF_MATS,
     *BEF_DATA,BES_MATS, BES_DATA,COUP_MATS_PF, COUP_MATS_SF,
     *COUP_MATS_PS,COUP_MATS_PFF,COUP_MATS_SFF,COUP_MATS_BFBF,
     *COUP_MATS_BSBS,COUP_MATS_BSBF,COUP_MATS_FSBS,COUP_MATS_FPBS,
     *WRITEDATA, folder)
```

SYSDATA is a record that contains all the tags for the different submodels. SIZE is a record that just gives the number of submodels there are of each type. FLUID_MATS is a record that contains the finite element matrices for the fluid submodels.

As an example, FLUID_MATS(2)%K0%ent(13) is the 13:th entry in the $\mathbf{K}_0$ matrix of the second fluid finite element. This entry has the row and column indices given by, FLUID_MATS(2)%K0%row(13) and FLUID_MATS(2)%K0%col(13).

Similar data is given for plate and solid FE models as, PLATE_MATS and SOLID_MATS

For a fluid BE domain the matrices that relate the velocity potential and its normal derivative through the boundary integral are yet to be calculated. However boundary condition for boundaries not coupled to other models may also be present. These boundary conditions are reshaped into matrix equation in the BE_INP2 subroutine and these equations are given as inputs to the DLOOP subroutine by the

BEF_MATS record. BES_MATS gives the corresponding matrices for the solid BE submodels.

BEF_DATA and BES_DATA contains the data needed to form the boundary integral matrices, i.e. the $\mathbf{H}$ and $\mathbf{G}$ matrices.

The coupling matrices between different types of submodels are given in the records,

COUP_MATS_PF	for plate FE to fluid BE coupling
COUP_MATS_SF	for solid FE to fluid BE coupling
COUP_MATS_PS	for plate FE to solid FE coupling
COUP_MATS_SFF	for solid FE to fluid FE coupling
COUP_MATS_PFF	for plate FE to fluid FE coupling
COUP_MATS_BFBF	for fluid BE to fluid BE coupling
COUP_MATS_BSBS	for solid BE to solid BE coupling
COUP_MATS_BSBF	for solid BE to fluid BE coupling
COUP_MATS_FSBS	for solid FE to solid BE coupling
COUP_MATS_FPBS	for plate FE to solid BE coupling

Finally the WRITEDATA record is also given as input, this record contains some information on which outputs should be written.

14.2.2 DLOOP SOL subroutine structure

Inside the DLOOP_SOL subroutine there are several other subroutines called. The most important of these are as follows.

SET_SYSIND. This subroutine sets the indices in the global system matrix for the corners of each BE and FE matrix.

SET_SYSPOINT. This routine compares the tags that the coupling matrices points at with the BE and FE matrix submodels, so that the coupling is associated with a model number rather than just a tag name.

SET_COUPIND. This routine sets the indices of the different coupling matrices.

After these basic routines have been called, the loops over the frequencies and wavenumbers start. The outer loop is that over the frequencies, whereas the inner loop is over the wavenumbers that are associated with this specific frequency. First the fluid BE models [**H**] and [**G**] matrices are formed directly into the system matrix and the boundary condition matrices that are already formed are written into the system matrix. Then the solid BE models are written into the system matrix in a similar way. The subroutines that do this are,

BEF_FORM and BES_FORM for the fluid and solid BE models respectively.

After this all other matrices are written into the system matrix by using the,

SYSFORM subroutine.

The system is solved by using the,

SYS_SOLVE subroutine which uses two different routines downloaded from the NAG library. (One routine is for square matrices and the other is for the overdetermined system that arise from some fluid BE models)

Finally some postprocessing is made (such as calculating radiated power from fluid BE models). This is done in the SYS_POST_PROC routine, that also writes some directly calculated results to an output file.

14.3 Data structures

14.3.1 Background and definitions

WANDS is written strictly as a code that passes data in and out of subroutines. Hence there are no 'common' blocks of shared information between different routines.

There is some data that is read from the TOPOLOGY.out file, i.e. that are read from an already written output. This is used when coupling a solid FE model to a fluid or solid BE model.

Passing data between subroutines is usually recommended. In WANDS it has the specific advantage that the programming becomes easier and more robust. It also means that additional solution methods or submodel types become more easy to include in the software.

The major drawback is that there is substantial amount of data that needs to be passed between different subroutines. To make the overview easier to understand the data is therefore grouped in different records, each of these records may contain different types of data such as matrices, vectors and integers. The data a record may contain is defined by the records structure. The structure associated with a specific record is given in the beginning of the subroutine, i.e.

```
TYPE(FE_MATS_SPARSE), DIMENSION(:), ALLOCATABLE ::  PLATE_MATS
```

means that the record PLATE_MATS is of the structure type FE_MATS_SPARSE. This particular command line is copied from the mainprogram. Since there may be several plate FE models PLATE_MATS is here defined as an array. The number of entries in this array will be the same as the number of different FE plate submodels. However, since this is not known until the *INSYS: blocks of the input file has been read, the record is defined as allocatable. This means that the size of the array is given later in the program.

The plate matrices for FE plate submodels are constructed one at a time. Hence, in the FE_PLATE subroutine the matrices are given in the record,

```
TYPE(FE_MATS_SPARSE)     :: PLATE_MATS_S
```

The structures are defined in the STRUCTURES module and in the SOL_STRUCTURES module both of which are found in the FORTRAN files with same names. As an example the FE_MATS_SPARSE structure, used in the example above, is defined as,

```
c---------------------------------------------------------
c     FE MATRICES IN SPARSE FORMAT

        TYPE FE_MATS_SPARSE

        SEQUENCE
        TYPE(SPARSE_MAT_C)  :: K4
        TYPE(SPARSE_MAT_C)  :: K2
        TYPE(SPARSE_MAT_C)  :: K1
        TYPE(SPARSE_MAT_C)  :: K0
        TYPE(SPARSE_MAT_C)  :: M



        TYPE(SPARSE_VEC_C)  :: F    ! force vector
        integer matsize
        integer Kindex(2,2)

c       MEANS:
c       Kindex(1,1)=rowstart
c       Kindex(1,2)=rowend
c       Kindex(2,1)=colstart
c       Kindex(2,2)=colend

        integer*1 dummy(4*dimsp+12)



        END TYPE

c-------------------------------------------------------
```

As can be seen, this structure uses another structure called `SPARSE_MAT_C`, which is defined as,

```
    TYPE SPARSE_MAT_C   ! Generic type for storing complex sparse matrices
    SEQUENCE
    complex*16 ent(dimsp), dummy(2)         ! real and imaginary part of entry
    integer row(dimsp), col(dimsp)      ! row and column index
    integer matsize(2)                      ! size on matrix rows and columns

    END TYPE
```

Note!

The meaning of this has already been explained in section 14.2. However there has been a quite considerable problem with this structure. As can be seen the dimension of the SPARSE_MAT_C structure, i.e. the number of entries allowed in an FE matrix, is set by the dimsp parameter, which in turn is set at the top of the STRUCTURES module. If dimsp is to large the 'image' size of the compiled code will exceed that allowed in Windows. Of course one may increase dimsp if some other array is decreased, but it has been found that the array (matrix) sizes given by dimsp are the most significant for the image size.

This problem has now been solved by using allocatable arrays and sparse matrix formats for all larger matrices. However, this meant that the stack size of the compiler had to be increased instead. The limit of the number of degrees of freedom that can be used in the current version of WANDS is determined by the maximum array size. For a two dimensional, complex valued, double precision array the limit is 8192 by 8192.

By compiling for a 64 bit system, it might be possible to increase this size. To rewrite the code to use a sparse system matrix and sparse solvers, probably involves much work.

If the image size problem reoccurs the program can be split into a main executable *.exe file and one or several *.dll files.

14.3.2 Solution structures

In the DLOOP_SOL subroutine the different submodels are assembled into a larger system matrix. This process means that the different matrices are put in the right place. For the program and programmer to keep these ordered a record SYSIND for the indices of the FE and BE submodels has been created. For the coupling submodels a different record, COUPIND, has been created. The structures for both of these records are found in the SOL_STRUCTURES module in the file with the same name. Since these structures will be used if any new submodel types are included in WANDS, it may be useful to explain how they work.

1	1	$[\mathbf{HG}]$ matrix indices for solid BE model
1	2	$[\mathbf{HG}]$ matrix indices for fluid BE model
1	3	$[\mathbf{C_a C_b}]$ matrix indices for solid BE model
1	4	$[\mathbf{C_a C_b}]$ matrix indices for fluid BE model
2	1	$[\mathbf{K}(\kappa) - \omega^2\mathbf{M}]$ matrix index for plate FE
2	2	$[\mathbf{K}(\kappa) - \omega^2\mathbf{M}]$ matrix index for solid FE
2	3	$[\mathbf{K}(\kappa) - \omega^2\mathbf{M}]$ matrix index for fluid FE

Table 14.1: Index structure notation

SYSIND

`SYSIND` is a record of type `INDEX0`. `INDEX0` contains a record, `SUB`, which is of type `INDEX1`. `INDEX1` contains a record, also called `SUB`, which is of type `INDEX2`. `INDEX2` contains a record, also called `SUB`, which is of type `INDEX3`.

Finally `INDEX3` contains the row and column indices that the corners of the submodel matrix will have when it is assembled into the system matrix. This is given as `G_INDX(l,m,n)`.

The index for any FE or BE matrix is thus given by,

`SYSIND%SUB(i)%SUB(j)%SUB(k)%G_INDX(l,m,n)`

`i=1` denotes that the indices are for a BE domain, whereas `i=2` denotes that they are for an FE domain.

`j` denotes different things depending on whether a BE or FE domain is considered. The meaning of `i` and `j` is summarised in Table 14.1

`k` the number of the submodel of this type.

`l,m` is the corner of the matrix, the four corners are denoted as,

- `l,m`=`1,1` is the upper left corner of the matrix.
- `l,m`=`1,2` is the upper right corner of the matrix.
- `l,m`=`2,1` is the lower left corner of the matrix.

BEF_BEF	Fluid BE to Fluid BE
BES_BES	Solid BE to Solid BE
BES_BEF	Solid BE to Fluid BE
FEP_FES	Plate FE to Solid FE
FEP_FEF	Plate FE to Fluid FE
FES_FEF	Solid FE to Fluid FE
FEP_BEF	Plate FE to Fluid BE
FES_BEF	Solid FE to Fluid BE
FES_BES	Solid FE to Solid BE
FEP_BES	Plate FE to Solid BE

Table 14.2: Coupling index structure notation

- l,m=2,2 is the lower right corner of the matrix.

n=1 denotes the value of the row at this corner and n=2 denotes the column.

Example

SYSIND%SUB(1)%SUB(3)%SUB(2)%G_INDX(1,1,2)

is the column index of the upper left corner of the second solid BE models boundary condition matrices, $[\mathbf{C_a C_b}]$.

COUPIND

The coupling matrices are assembled after the BE and FE models have been assembled into the system matrix. To aid this a record COUPIND is created.

COUPIND is a record of type C_INDEX1. C_INDEX1 contains several records of type C_INDEX2. C_INDEX2 contains a record, SUB, of the type INDEX3, (also used in SYSIND)

The records used in C_INDEX1 are

The following SUB record is used to number the different coupling elements. This can be made in different ways and the specific order of the coupling submodel type can be read in the COUPIND_SUBS.for or SYSFORM_SUBS.for files.

Example

```
COUPIND%FEP_FES(1)%SUB(2)%G_INDX(1,2,1)
```

is the row index of the upper right corner of the second coupling matrix of the first plate to solid coupling model. The second coupling matrix, here means the $\mathbf{C}_1^{\mathrm{T}}$ matrix, which together with the $\mathbf{C}_2^{\mathrm{T}}$ matrix defines that a combination of displacements in the two models are equal.

References

[1] Nilsson C-M. *Waveguide Finite Elements Applied on a Car Tyre.* PhD thesis, Royal Institute of Technology, Aeronautical and Vehicle Engineering /MWL, 2004. TRITA-AVE 2004:21, ISBN 91-7283-798-5, http://media.lib.kth.se/dissengrefhit.asp?dissnr=3812.

[2] Nilsson C-M. Jones C.J.C. D.J. Thompson. A waveguide finite element and boundary element approach to calculating the sound radiated by tram rails. *Submitted to the Journal of Sound and Vibration.*

[3] Nilsson C-M. Jones C.J.C. A coupled waveguide finite and boundary element method for calculating the sound transmission through complex panel structures. *Proceedings of the XI International Conference on Recent Advances in Structural Dynamics*, 2006.

[4] Sheng X. Jones C.J.C. Thompson D.J. Modelling ground vibration from rail traffic using the discrete wavenumber finite and boundary element methods. ISVR Technical Memorandum No:899, 2002.

[5] Cook R.D. Malkus D.S. Plesha M.E. *Concepts and applications of finite element analysis.* Wiley, cop, third edition, 1988.

[6] Wu T.W. *Boundary element acoustics: fundamentals and computer codes.* 2000.

[7] Strang G. *Introduction to applied mathematics.* Wellesley–Cambridge Press, cop, 1986.

[8] Petyt M. *Introduction to finite element vibration analysis.* Cambridge university press, 1990.

[9] Birgersson F., Finnveden S., and Nilsson C-M. A spectral super element for modelling of plate vibrations: part 1, general theory. *Accepted for publication in the Journal of Sound and Vibration, subject to minor revisions.*

[10] Fried I. Accuracy and condition of curved (isoparametric) finite elements. *Journal of Sound and Vibration*, 43(3), 1973.

[11] Alaami B. Waves in prismatic guides of arbitrary cross section. *Journal of Applied Mechanics*, (December):1067–1071, 1973.

[12] Finnveden S. Spectral finite element analysis of the vibration of straight fluid-filled pipes with flanges. *Journal of Sound and Vibration*, 199(1):125–154, 1996.

[13] Cremer L. and Heckl M. *Structure Borne Sound : Structural Vibrations and Sound Radiation at Audio Frequencies.* Springer Verlag, 1988.

[14] Megson T.H.G. *Structural and Stress analysis.* Elsevier, 1996.

[15] Vlasov V.Z. *Beams,plates & shells.* 1966.

[16] Allman D.J. A compatible triangular element including vertex rotations for plane elasticity analysis. *Computers & Structures*, 19(1-2):1–8, 1984.

[17] Abel J.F. An algorithm for multipoint constraints in finite element analysis. *Int. J. Num. Meth. Engng*, 14(3):464–467, 1979.

[18] Temkin S. *Elements of Acoustics.* John Wiley, sons, 1981.

[19] Orrenius U. and Finnveden S. Calculation of wave propagation in rib–stiffened plate structures. *Journal of Sound and Vibration*, 198(2):203–224, 1996.

[20] Nilsson C.M. and Finnveden. S. Waves in thin-walled fluid-filled ducts with arbitrary cross sections.

[21] Råde L. and Westergren B. *Beta mathematics handbook.* Studentlitteratur and Chartwell–Bratt Ltd, 1990.

[22] Kirkup S. *The Boundary Element Method in Acoustics.* 1998.

[23] Sheng X. Jones C.J.C. Thompson D.J. Computer programs for the discrete wavenumber finite/boundary element model for ground vibration and noise from railway tunnels. ISVR Technical Memorandum No:915, 2003.